Spring 2018

# A multiple scattering method to study the cable harness inside a vehicle shell

Yansheng Wang



Department: Electrical and Computer Engineering

# A MULTIPLE SCATTERING METHOD TO STUDY THE CABLE HARNESS INSIDE A VEHICLE SHELL

by

YANSHENG WANG

A DISSERTATION

Presented to the Graduate Faculty of the

MISSOURI UNIVERSITY OF SCIENCE AND TECHNOLOGY

In Partial Fulfillment of the Requirements for the Degree

DOCTOR OF PHILOSOPHY

in

ELECTRICAL ENGINEERING

May 2018

Approved by

Jun Fan, Advisor
James L. Drewniak
David J. Pommerenke
Daryl G. Beetner
Ji Chen

## PUBLICATION DISSERTATION OPTION

This dissertation consists of the following three articles which have been submitted for publication, or will be submitted for publication as follows:

Paper I: Pages 6-31, "Evaluating Field Interactions Between Multiple Wires and the Nearby Surface Enabled by a Generalized MTL Approach," have been published on IEEE Transaction on Electromagnetic Compatibility, vol. 60, no. 4, pp. 971-980, Aug. 2018.

Paper II: Pages 32-57, "A Generalized Multiple-Scattering Method for Modeling a Cable Harness with Ground Connections to a Nearby Metal Surface," have been accepted by IEEE Transaction on Electromagnetic Compatibility.

Paper III: Pages 58-83, "Evaluating the Crosstalk Current and the Total Radiated Power of an Arbitrary Cable Harness Using the Generalized MTL Method," are intended for submission to IEEE Transaction on Electromagnetic Compatibility.

# ABSTRACT

This dissertation contains three major parts. In the first part, a generalized multi-conductor transmission line (GMTL) method is proposed to model a cable harness. In the GMTL method, all wires of the cable harness take the infinity as the reference. In such a way, the GMTL method takes into account not only the transmission-line mode but also the antenna-mode current on the cable harness. Further, by employing the GMTL method and the mixed-potential integral equations (MPIE) method in a multiple scattering (MS) procedure, it enables an efficient and accurate approach to evaluate the current distribution on a cable harness with a nearby metal surface. Notice that the cable harness is not grounded to the metal surface in this part. In the second part, a hybrid algorithm called the generalized multiple scattering (GMS) method is proposed to efficiently and accurately calculate the current distribution on a cable harness which has several ground connections to a nearby metal surface. This is a simplified case to mimic a cable harness routed inside a vehicle shell. The GMS method uses the GMTL method for the cable harness part and the MPIE method for the rest of the structure including the metal surface and the grounding wires. Neither the GMTL nor the MPIE method alone takes into account the mutual interactions between the cable harness and the rest of the structure. Therefore, an iterative scheme is arranged in the GMS method to compensate the abovementioned interactions. These interactions occur via not only field couplings, but also current conducting through the grounding points on the cable harness. In the third part, the GMTL method is reformulated to cover both straight and bent cable harnesses. The extraction of the per-unit-length inductance and capacitance is also simplified compared to the extraction method described in the first part. Besides, the steepest descent method is utilized to compute the radiation of a cable harness based on the obtained current through the GMTL method. The capability and limitations of the GMTL method are also carefully examined.

# ACKNOWLEDGMENTS

First and foremost, I would like to express my sincere gratitude to my advisor, Prof. Jun Fan, for the continuous support of my Ph.D. study and related research, for his patience, motivation, and immense knowledge. His guidance helped me in all the time of research and writing of this dissertation. I could not have imagined a better advisor and mentor for my Ph.D. study.

Besides my advisor, I would like to thank the rest of my dissertation committee: Prof. Drewniak, Prof. Pommerenke, Prof. Beetner, and Prof. Chen, for their insightful comments and encouragement, but also for the hard questions which incented me to widen my research from various perspectives.

I gratefully acknowledge the funding sources that made my Ph.D work possible. I was mainly funded by the Ford Motor Company and the National Science Foundation (NSF) under Grants No. IIP-1440110.

My sincere thanks also go to the whole EMC group and other friends at the Missouri S&T. I am grateful for the time spent with them.

Last but not the least, I would like to thank my family: my wife, my parents, my sisters, and my brothers, for supporting me spiritually throughout my life in general.

# TABLE OF CONTENTS

Page

# LIST OF ILLUSTRATIONS

PAPER III

# LIST OF TABLES

SECTION

# 1. INTRODUCTION

This dissertation presents the study of an accurate and efficient method to model a cable harness routed inside a vehicle shell. This section introduces the background of the study, the state-of-the-art research of the cable harness modeling, and the major contents and contributions of each paper included in this dissertation.

## 1.1. BACKGROUND

Cable harnesses are commonly found in modern transportation systems such as automobiles [Liu et al., 2017], high-speed trains [Zhang et al., 2017a], aircrafts [Bagci et al., 2007] and etc. A cable harness is an assembly of electrical wires which transmit signals and electrical power. It serves as the interconnects among various electronic modules and therefore play a crucial role in determining the electromagnetic compatibility (EMC), electromagnetic interference (EMI) [Cao et al., 2017c, Cao and et al., 2017, Maghlakelidze et al., 2018], signal integrity (SI) [Chen et al., 2017, 2018, Jiang et al., 2016, Jin et al., 2016, Xu et al., 2017, Zhang et al., 2017b], and power integrity (PI) [Cao et al., 2016h, 2017b, Hardin et al., Huang et al., 2016, Zhao et al., 2016, 2017a,b] performance of the system.

The modeling of a cable harness along with the vehicle body is important for vehicle EMI design since vehicle harness can act both as a source of radiation [Cao et al., 2018b, Han et al., 2012, Jin et al., 2014, Patnaik and et al., 2017, Shen and et al, Shen et al., 2016a,b, 2017a, Shinde and et al., Wang and et al., 2015, Wu et al., 2016, Yan et al., 2014] and the victim of undesired coupling [Oganezova et al., 2016, Shen et al., 2014, 2015]. The radiation from antenna-mode current on the cable harness can illuminate the vehicle

body and further radiate into outer environment as electromagnetic (EM) pollution [Huang and et al, 2018b, Huang and Fan, Huang et al., 2017b, 2018, Hwang and Huang, 2017, Shen et al., 2017b, Wang et al., 2017b, 2018c,d,e]. Additionally, external fields coupled to the cable harness via the vehicle body can introduce EMI problems that are prevented through constrains on packaging, harness routing and shielding requirements to meet strict EMC/EMI requirements [Cao et al., 2018a]. Detecting these issues [Yan et al., 2018, 2016, 2017] in the early stages of vehicle design through vehicle-harness co-simulation can reduce design cost and help achieve compliance with EMC/EMI requirements without a need for a redesign.

## 1.2. LITERATURE REIVEW

Full-wave methods like finite difference time domain (FDTD) method, finite element method (FEM), method of moments (MoM) [Huang and et al, 2018a, Huang et al., 2017a, Wang et al., 2016a, Zhang et al., 2017a], and partial element quivalent circuit (PEEC) method [Cao et al., 2014, 2015a,b, 2016b,c,d,e,f,g,i, Nitsch et al., 2009, Tao et al., 2017, Yang et al., 2017a,b], can be used for field computation with high accuracy. However, depending on the complexity of the EM problem at hand high computational cost of using full-wave methods may be deterrent in using these methods for field calculation. Co-simulation of cable harness with vehicle body is a complex EM problem since cables in a vehicle harness are generally routed close to conductive surfaces. Therefore, when using MoM, for instance, to solve fields for cable harnesses inside a vehicle body, the metal surface underneath the cables has to be characterized by finely discretized mesh regions, which introduces a large computational burden. Besides, a cable harness usually consists of hundreds of wires which adds to the complexity of the problem leading to computationally expensive simulations when solving harness with full-wave methods. In general, full-wave methods result in long simulation run time and are also limited by the computation resources available to the user.

A hybrid solution method combining multi-conductor transmission line (MTL) theory with the full-wave method has been proposed in the literature [Badzagua et al., 2010, Chobanyan et al., 2009, Topchishvili et al., 2004] as a solution to overcome this difficulty. Different versions of this hybrid solution method have been implemented in multiple commercially available EM tools [EMCoS, Systems, Technology], where either a radiation or an immunity problem is considered. In the hybrid method, the cable harness was handled by the MTL theory and the nearby metal surface was solved by MoM. However, this hybrid solver failed to consider the interactions between the cable harness and the metal surface. To account for the abovementioned interactions, iterative approaches were introduced in [Bayram and Volakis, 2005, Liu et al., 2017, Sabath and Garbe, 2003]. However, these iterative approaches suffered from some limitations. In [Sabath and Garbe, 2003], the antenna-mode currents were missed from the total currents induced on the wire structure. In [Bayram and Volakis, 2005], the developed solver was based on a circumscribed assumption that the electric potential was equal on the same conducting surface, which was true only for electrically small structures. In [Liu et al., 2017], the proposed method overcame the two abovementioned drawbacks, but its capability was limited to two-wire structures which did not have ground connections to the nearby metal surface.

Limitations of the abovementioned hybrid solvers lie in the essential defects of the employed TL solver. To overcome the limitations, a new TL solver is required. Over the past decades, several TL based methods were developed. [Nitsch and Tkachenko, 2010, 2004] derived the full-wave TL theory that could be applied to a set of thin wires. [Chiariello et al., 2008] described a generalized TL model to study the high-frequency mixed-mode propagation along electrical interconnects. [Tkatchenko et al., 1995] applied a recursive procedure based on the perturbation theory to evaluate the electric currents and potentials on a single wire above a perfect conducting ground. The derivation in [Cooray et al.] accounted for the effects of finitely conducting ground on a single wire. [Lugrin et al., 2015] presented an approach to model the multi-conductor transmission line (MTL) with

arbitrary terminations. This approach was still applicable even if the TL approximation conditions no longer held. However, all these proposed methods assume an infinitely large ground plane beneath the wires, which prevents these methods from practical applications since the reference plane beneath the wires inside a modern transportation system, is usually of irregular shape, limited size, and arbitrary discontinuities such as slots, holes, wedges, etc. The methods discussed in [Liu et al., 2017, Maffucci et al., 2004, 2005, Vukicevic et al., 2006] were not restricted by the reference plane. Nevertheless, these papers only derived TL parameters between two conductors. These derivations are not applicable in real situations where multiple wires exist.

## 1.3. CONTENTS AND CONTRIBUTIONS

The outlines and contributions of this dissertation are summarized.

In the first paper, a GMTL method is proposed to analyze the current distribution on a cable harness, i.e. a multi-wire structure. This GMTL method makes the transmission line (TL) like formulation independent of the geometry of the reference plane and the number of wires. A multiple scattering (MS) approach is adopted to analyze a cable harness close to a metal surface. Notice that the cable harness is not grounded to the metal surface. In the MS approach, the cable harness is solved using the GMTL method, and the metal surface is handled by the Mixed-potential integral equations (MPIE) method. Neither the GMTL method nor the MPIE method alone takes into account the mutual interactions between the cable harness and the metal surface. Therefore, an iterative process is arranged in the MS approach to compensate the above-mentioned interactions.

In the second paper, a generalized multiple scattering (GMS) method is proposed to analyze the current distribution on a cable harness with ground connections to a nearby metal surface. Similar to the previous MS approach, the cable harness is solved using the GMTL method, the metal surface and the grounding wires are handled by the MPIE method, and an iterative process is arranged to compensate the interactions between the cable harness

and the rest of the structure. However, the previous MS approach only accounts for the mutual interactions via field couplings. In the newly proposed GMS method, not only the field couplings but also the currents conducting through the grounding points on the cable harness are considered in the mutual interactions.

In the third paper, a general formulation of the GMTL method is proposed to cover both straight and bent cable harnesses. In the radiation problems, the obtained currents on a cable harness are decomposed into left-going and right-going waves based on the least-square method. Further, the steepest descent method is adopted to efficiently and accurately calculate the total radiated power (TRP) from the cable harness. The capability and limitations of the GMTL method and the necessity of the recursive corrections are carefully examined.

# PAPER

## I. EVALUATING FIELD INTERACTIONS BETWEEN MULTIPLE WIRES AND THE NEARBY SURFACE ENABLED BY A GENERALIZED MTL APPROACH

Yansheng Wang, Dazhao Liu, Ying S. Cao, Richard Kautz, Nevin Altunyurt,

Sandeep Chandra, and Jun Fan

**ABSTRACT**

Interactions between a cable harness containing multiple wires and the nearby metal surface can be evaluated by full-wave methods. Though these methods can calculate the interactions with great accuracy, they have long simulation times and large memory requirements when dealing with complex wire structures. The multiple scattering (MS) approach by treating the cable harness and the surface separately using different algorithms has been proven to be superior to the full-wave methods when evaluating these interactions. However, the cable harness solver in the previous MS approach is restricted to two-wire structures since the per-unit-length (pul) inductance (L) and capacitance (C) are derived based on the antenna and differential modes assumption between two wires. In this paper, a generalized multi-conductor transmission line (GMTL) approach is proposed to overcome the two-wire limitation. In the GMTL approach, all wires take the infinity as the reference. The extraction of the pul L and C for the cable harness is not limited by the number of wires. Thus, the GMTL approach can conveniently model multiple wire structures. The application of the GMTL approach to the multiple wires enables the MS approach to accurately evaluate the interactions between the cable harness and the metal surface.

**Keywords:** Cable harness, Method of moments (MoM), multiple scattering (MS), multi-conductor transmission line (MTL), SPICE.

# 1. INTRODUCTION

Cable harnesses consisting of multiple wires play a crucial role in determining the EMC performance of a system, such as a vehicle, a high-speed train, or an aircraft [Bagci et al., 2007]. The modeling of a cable harness together with the nearby metal surface is necessary to predict the emissions from the harness during the design process, since the radiation from antenna-mode currents on the cable harness can illuminate the metal surface and further radiate into outer environment as electromagnetic (EM) pollution.

The most straightforward way to study the radiation from a cable harness with a nearby metal surface is to run full-wave simulations based on numerical methods such as the finite difference time domain (FDTD), finite element method (FEM), method of moments (MoM), and parital element equivalent circuit (PEEC) method [Cao et al., 2015, 2017, Nitsch et al., 2009]. Correspondingly, the available commercial full-wave simulation software includes CST MW, HFSS, and EMC studio. However, all these full-wave approaches require generating a large number of mesh cells either in a finite computation domain as in FDTD and FEM or on the surface and the multiple wires as in MoM and PEEC. Co-simulation of the cable harness and the metal surface leads to a large computational burden, especially when the cable harness part dominates in the amount of the generated mesh cells. For the meshing of this geometry, it is inevitable to discretize the relatively complex ground surface using mesh cells; whereas multiple wires which take the form of typical transmission lines (TL), are not required to be meshed explicitly. Following the idea, hybrid algorithms combining the multi-conductor transmission line (MTL) theory with full-wave methods have been proposed in the literature [Badzagua et al., 2010, Chobanyan et al., 2009, Topchishvili et al., 2004]. Different versions of hybrid solution methods have been implemented in multiple commercially available EM tools [EMCoS, Systems, Technology].

To solve a radiation problem in the currently available version of the previously mentioned hybrid solvers, the currents on the multiple wires are first calculated by the MTL analysis. These currents are then considered as the impressed sources to illuminate the

surface structure in the full-wave field solver. Next, the scattered fields from the metal surface can be calculated in the absence of the cable harness by the full-wave solvers. It should be noted that these solvers neglect the effects of the scattered fields from the metal surface on the multiple wires. To account for these effects, iterative approaches were applied in [Bayram and Volakis, 2005, Sabath and Garbe, 2003]. However, the total currents illuminated on the wire structure in [Sabath and Garbe, 2003] did not include the antenna-mode currents. In [Bayram and Volakis, 2005], it implied that the surrounding surface structure should be translationally uniform along the cable harness. Though limitations may apply in those papers, the idea of iteration was adopted in this work to take into account the mutual interaction between the cable harness and the metal surface.

In this study, a hybrid solver was developed to solve the current distribution on multiple wires with a nearby metal surface. The metal surface was modeled and solved based on the MoM formulation, which is the most convenient method to study the open space problems such as the radiation problem. The multiple wires were modeled and solved by a TL like theory, which is more efficient than the MoM formulation. The TL like theory is referred to as the generalized multiple-conductor transmission line (GMTL) approach in this paper.

Before the introduction to the GMTL approach, several previous studies were reviewed. [Nitsch and Tkachenko, 2010, 2004] derived the full-wave TL theory that could be applied to a set of thin wires. [Chiariello et al., 2008] described a generalized TL model to study the high-frequency mixed-mode propagation along electrical interconnects. [Tkatchenko et al., 1995] applied a recursive procedure based on the perturbation theory to evaluate the currents and potentials on a single wire above a perfect conducting ground. The derivation in [Cooray et al.] accounted for the effects of finitely conducting ground on a single wire. [Lugrin et al., 2015] presented an approach to model the MTL with arbitrary terminations. This approach is still applicable even if the TL approximation conditions no longer hold. However, all these proposed methods assume an infinitely large ground

plane beneath the wires, which prevents these methods from practical applications since the reference plane beneath the wires inside a vehicle, train or aircraft, is usually of irregular shape, limited size, and arbitrary discontinuities such as slots, holes, wedges, etc. The methods discussed in [Liu et al., 2017, Maffucci et al., 2004, 2005, Vukicevic et al., 2006] were not restricted by the reference plane. Nevertheless, these papers only derived TL parameters between two conductors. These derivations are not applicable in real situations where multiple wires exist.

Therefore, a new approach that can analyze multiple wires and is not restricted by the geometry of the reference plane is desired. To resolve the issue, the traditional TL theory is extended to the GMTL approach in this paper. The traditional TL theory is commonly applied in the scenarios where $N$ parallel conductors are referenced to a nearby metal surface. The extracted quasistatic per-unit-length (pul) RLGC parameters are valid only when TL conditions hold. Therefore, the calculated currents only take into account the TL-mode currents among the $N$ conductors and the nearby surface. To include the antenna-mode currents, assume that the reference metal surface is moved an infinite distance away from the $N$ conductors, i.e, the currents on the $N$ conductors take the infinity as reference, which actually defines the antenna-mode currents. Thus, in this situation, in addition to the traditional TL-mode currents between the $N$ conductors, the antenna-mode currents between the $N$ conductors and infinity are introduced. This lays the foundation of the GMTL approach to handle multiple wires.

Next, to account for the mutual interactions between the multiple wires (called the GMTL region hereinafter) and the nearby metal surface (called the MoM region hereinafter), an iterative approach similar to the fashion described in [Liu et al., 2017] is adopted in this work to account for the multiple reflections between the GMTL and MoM regions. The iteration method is called the multiple scattering (MS) approach in this paper.

To summarize, compared to the previous work, this paper introduces the GMTL approach to analyze the current distribution on the multiple wire structure. This method makes the TL like formulation independent of the geometry of the reference plane and the number of wires. Besides, because of the application of the GMTL approach for the wire part, this work extends the MS approach to correctly evaluate the interactions between the cable harness consisting of multiple wires and the nearby metal surface with arbitrary shape, orientation, and size.

The paper is organized as follows. In Section II, the MoM solver is briefly introduced. In Section III, Agrawal's scattered voltage form is first introduced, then the extraction method for pul inductance (L) and capacitance (C) is provided for a single wire and is further extended for multiple wires, and finally a recursive correction approach is given to obtain the exact currents on wires. In Section IV, the flowchart of the MS approach combining the GMTL and the MPIE solvers is explained in detail. In Section V, a numerical example is provided to validate the MS approach. Conclusions are presented in Section VI.

## 2. THE MPIE SOLVER

MoM is widely employed to study radiation problems. In this study, one common formulation of MoM, the mixed-potential integral equations (MPIE) formulation [Fan et al., 2001, Liu, 2013, Wang et al., 2016, Zhang et al., 2017], is applied to create a full-wave solver. The derivation for MPIE is well-known and thus is omitted in this paper. For more details, the reader is referred to [Liu, 2013]. There are two usages for the constructed MPIE solver. First, in the MS approach the MPIE solver is employed to compute the induced electric current densities on the surface when illuminated by incident field and further to calculate the scattered field onto the multiple wires. Second, in order to validate the MS approach, the MPIE solver is used to solve the current distribution for the whole structure including the multiple wires and the nearby surface.

## 3. THE GMTL APPROACH

In this section, the Agrawal's scattered voltage form is first introduced. Then the extraction method for pul L and C is provided for a single wire and is further extended for multiple wires. Finally, a recursive correction approach is given to obtain the exact currents on wires. A test case is used to benchmark the proposed GMTL approach.

### 3.1. The Scattered Voltage Representation of the TL Excited by External Fields.

The scattered voltage representation for the response of a terminated two-wire TL excited by a nonuniform electromagnetic field as shown in Fig. 1 was developed by Agrawal *et al*. in 1980s [Agrawal et al., 1980]. This representation utilizes only the tangential component of the excitation E-field to compute the induced voltage source for the TL.

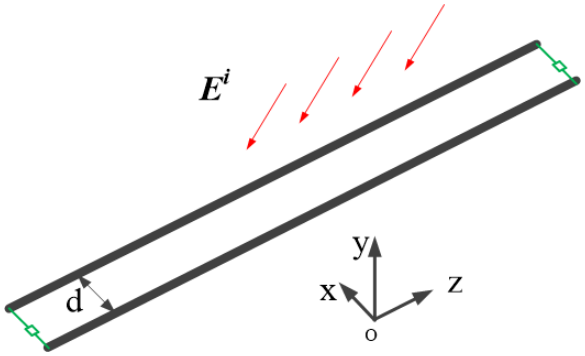


Figure 1. A two-wire structure illuminated by incident E-field.

Rather than the total voltage representation [Taylor et al., 1965] and the scattered current representation [Rachidi, 1993], it is more convenient to apply Agrawal's representation in this study since the tangential component of the excitation E-field can be easily obtained. As described in Section I, the incident E-field onto the wires during the MS procedures is due to the electric current density on the metal surface close to the wires. Given the electric current density on the metal surface, it is straightforward to compute the incident E-field at the location of the wires, which further excites the wire structures.

As shown in Fig. 1, assuming a lossless two-wire structure along the $z$-direction, the modified Telegrapher's equations according to Agrawal's representation are

$$\begin{cases} \frac{dV^s(z)}{dz} + j\omega L I^t(z) = E_z^i(d, y, z) - E_z^i(0, y, z) \\ \\ \frac{dI^t(z)}{dz} + j\omega C V^s(z) = 0 \end{cases} \tag{1}$$

where $\omega$ is the angular frequency, $L$ and $C$ are the pul inductance and capacitance between the two wires, $V^s(z)$ and $I^t(z)$ are the induced voltage and current at the location $z$, $E_z^i(d, y, z)$ and $E_z^i(0, y, z)$ are the z-components of the incident E-field on the two wires, and $d$ is the wire separation.

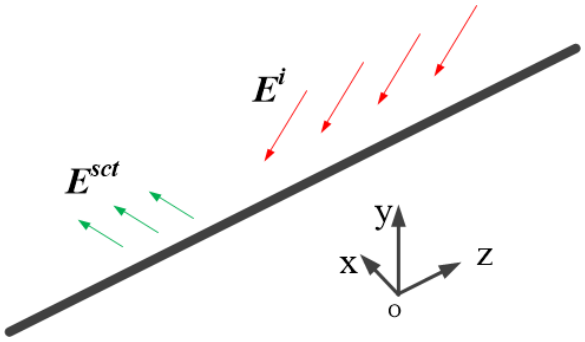


Figure 2. A single wire illuminated by incident E-field.

**3.2. Extraction of the pul L and C for a Single Wire.** As shown in Fig. 2, for a thin wire along the $z$-axis in MoM, the scattered E-field is

$$\vec{E}^{sct} = -j\omega\vec{A}(\vec{z}) - \nabla\phi(\vec{z}), \tag{2}$$

where the vector magnetic potential $\vec{A}(\vec{z})$ and the scalar electric potential $\phi(\vec{z})$ are

$$\vec{A}(\vec{z}) = \frac{\mu}{4\pi}\int_0^l I(\vec{z}')\vec{e}_z g(\vec{z}, \vec{z}')dz', \tag{3}$$

$$\phi(\vec{z}) = \frac{1}{4\pi\varepsilon}\int_0^l \rho(\vec{z}')g(\vec{z}, \vec{z}')dz', \tag{4}$$

the free-space Green's function $g(z, z')$, the electric charge density $\rho(\vec{z})$ are

$$g(z, z') = \frac{\exp\left(-jk\sqrt{(z-z')^2 + a^2}\right)}{\sqrt{(z-z')^2 + a^2}}, \tag{5}$$

$$\rho(\vec{z}) = -\frac{1}{j\omega}\frac{dI}{dz}, \tag{6}$$

$l$ is the wire length, $a$ is the wire radius, $\vec{e}_z$ is the unit vector along the $z$-direction, and $z$ and $z'$ indicate the observation and the source locations, respectively.

Applying the PEC boundary condition on the thin wire leads to

$$\vec{E}_z^{sct} = \left[-j\omega\vec{A}(\vec{z}) - \nabla\phi(\vec{z})\right]_z = -\vec{E}_z^i \tag{7}$$

Substituting (3) into (7), substituting (6) into (4), and referring to the scattered voltage representation introduced in Part A of this section, the following equations can be obtained

$$\begin{cases} \frac{d\phi(z)}{dz} + j\omega\frac{\mu}{4\pi}\int_0^l I(z')g(z, z')dz' = E_z^i(0, 0, z) \\ \\ \phi(z) + \frac{1}{j\omega}\frac{1}{4\pi\varepsilon}\int_0^l \frac{dI(z')}{dz'}g(z, z')dz' = 0 \end{cases} \tag{8}$$

Recall the equation that

$$\int_{-b}^{b} f(z')\,\delta(z-z')dz' = f(z)\int_{-b}^{b}\delta(z-z')dz', \tag{9}$$

where $z, z' \in [-b, b]$, and $\delta(z-z')$ is the Dirac Delta function. Since the free-space Green's function will rapidly change to an extremely large value when $z'$ is approaching $z$, it can roughly be treated as a Dirac Delta function. Thus, comparing (8) to (9), $I(z')$ and $\frac{dI(z')}{dz'}$ are taken out of the integrals in (8) and changed to $I(z)$ and $\frac{dI(z)}{dz}$. Rigorously speaking, $I(z')$

and $\frac{dI(z')}{dz'}$ cannot be taken out of the integral. Therefore, some errors are introduced in this step. However, these errors can be corrected recursively, which will be covered in Part D of this section. After some manipulations, the following equations are obtained:

$$\begin{cases} \frac{d\phi(z)}{dz} + j\omega L I(z) = E_z^i(0,0,z) \\ \\ \frac{dI(z)}{dz} + j\omega C \phi(z) = 0 \end{cases} \tag{10}$$

where the pul $L$ and $C$ are

$$L(z) = \frac{\mu}{4\pi} \int_0^l g(z,z')dz', \tag{11}$$

$$C(z) = \frac{4\pi\varepsilon}{\int_0^l g(z,z')dz'}. \tag{12}$$

Notice that the pul $L$ and $C$ have a z-dependence. This is unlike the constant value provided

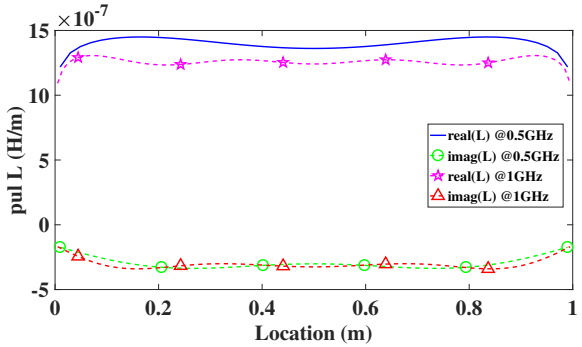


(a)

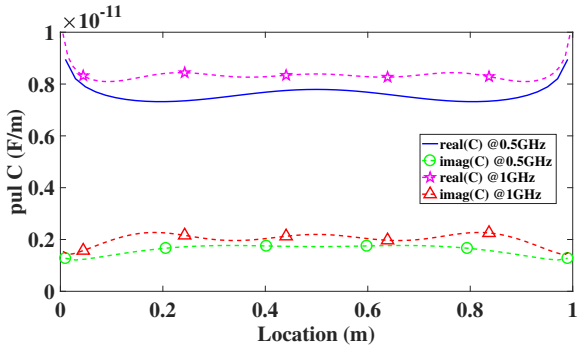


(b)

Figure 3. The pul (a) $L$ and (b) $C$ for a single one-meter-long wire.

in the traditional TL theory. To better illustrate the phenomena, the pul $L$ and $C$ computed at 0.5 and 1 GHz for a single wire of one meter long are shown in Fig. 3.

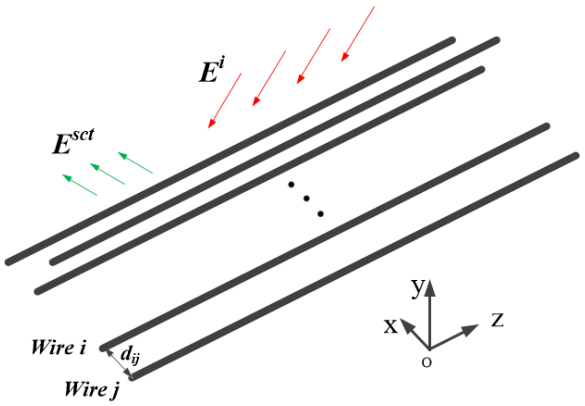


Figure 4. A multi-wire structure illuminated by incident E-field.

**3.3. Extension to the GMTL Equations.** The obtained equations in the case of a single wire can be extended to the case of $N$ wires. As shown in Fig. 4, assume all wires are along $z$-direction. The matrix format of the GMTL equations reads

$$\begin{cases} \frac{d\bar{\phi}(z)}{dz} + j\omega\overline{\overline{L}}(z)\bar{I}(z) = \overline{E}^i_z(x,y,z) \\ \\ \frac{d\bar{I}(z)}{dz} + j\omega\overline{\overline{C}}(z)\bar{\phi}(z) = \bar{0} \end{cases} \tag{13}$$

where the electric potential $\phi(z)$, the current $I(z)$, and the $z$-component of the incident electric field $E^i_z(x,y,z)$ in vector format are represented as

$$\bar{\phi}(z) = \begin{bmatrix} \phi_1(z) \\ \phi_2(z) \\ \vdots \\ \phi_N(z) \end{bmatrix}, \tag{14}$$

$$\overline{I}(z) = \begin{bmatrix} I_1(z) \\ I_2(z) \\ \vdots \\ I_N(z) \end{bmatrix}, \tag{15}$$

$$\overline{E}^i_z(x,y,z) = \begin{bmatrix} E^i_{z,1}(x,y,z) \\ E^i_{z,2}(x,y,z) \\ \vdots \\ E^i_{z,N}(x,y,z) \end{bmatrix}, \tag{16}$$

the pul inductance and capacitance among wires in matrix format are defined as

$$\overline{\overline{L}}(z) = \begin{bmatrix} L_{11}(z) & L_{12}(z) & \cdots & L_{1N}(z) \\ L_{21}(z) & L_{22}(z) & \cdots & L_{2N}(z) \\ \vdots & \vdots & \ddots & \vdots \\ L_{N1}(z) & L_{N2}(z) & \cdots & L_{NN}(z) \end{bmatrix}, \tag{17}$$

$$\overline{\overline{C}}(z) = \begin{bmatrix} C_{11}(z) & C_{12}(z) & \cdots & C_{1N}(z) \\ C_{21}(z) & C_{22}(z) & \cdots & C_{2N}(z) \\ \vdots & \vdots & \ddots & \vdots \\ C_{N1}(z) & C_{N2}(z) & \cdots & C_{NN}(z) \end{bmatrix}, \tag{18}$$

and the elements $L_{ij}(z)$ and $C_{ij}(z)$, $i, j = 1, 2, \cdots, N$, can be obtained by (19) and (20), respectively.

$$L_{ij}(z) = \frac{\mu}{4\pi} \int_0^L g_{ij}(z, z')dz', \tag{19}$$

$$C_{ij}(z) = \frac{4\pi\varepsilon}{\int_0^L g_{ij}(z, z')dz'}, \tag{20}$$

where

$$g_{ij}(z, z') = \frac{\exp\left(-jk\sqrt{(z-z')^2 + d_{ij}^2}\right)}{\sqrt{(z-z')^2 + d_{ij}^2}} \tag{21}$$

and

$$d_{ij} = \begin{cases} a_i, i = j \\ \\ s_{ij}, i \neq j \end{cases} \tag{22}$$

$a_i$ is the radius of the $i$th wire and $s_{ij}$ is the center-to-center separation between the $i$th and the $j$th wire.

**3.4. Achieving the Exact Currents by Recursive Correction.** As mentioned in Part B of this section, some errors are brought in when evaluating (8) by moving $I(z')$ and $\frac{dI(z')}{dz'}$ out of the integrals. These errors can be corrected by a recursive process as described below. The derivation is based on the GMTL equations.

The exact wire currents are computed using (23), which is the matrix representation of (8) for multiple wires.

$$\begin{cases} \frac{d\overline{\phi}(z)}{dz} + j\omega\frac{\mu}{4\pi}\int_0^L \overline{\overline{g}}(z,z')\overline{I}(z')dz' = \overline{E}_z^i(x,y,z) \\ \\ \overline{\phi}(z) + \frac{1}{j\omega}\frac{1}{4\pi\varepsilon}\int_0^L \overline{\overline{g}}(z,z')\frac{d\overline{I}(z')}{dz'}dz' = \overline{0} \end{cases} \tag{23}$$

Add $j\omega\overline{\overline{L}}(z)\overline{I}(z)$ and $\frac{1}{j\omega}\overline{\overline{C}}^{-1}(z)\frac{d\overline{I}(z)}{dz}$ to both sides of the first and the second equation of (23), respectively. After simple manipulations, (23) can be written as

$$\begin{cases} \frac{d\overline{\phi}(z)}{dz} + j\omega\overline{\overline{L}}(z)\overline{I}(z) = \overline{E}_z^i(x,y,z) + j\omega D_1\left\{\overline{I}(z)\right\} \\ \\ \frac{d\overline{I}(z)}{dz} + j\omega\overline{\overline{C}}(z)\overline{\phi}(z) = D_2\left\{\overline{I}(z)\right\} \end{cases} \tag{24}$$

where

$$D_1\left\{\overline{I}(z)\right\} = \overline{\overline{L}}(z)\overline{I}(z) - \frac{\mu}{4\pi}\int_0^L \overline{\overline{g}}(z,z')\overline{I}(z')dz' \tag{25}$$

$$D_2\left\{\overline{I}(z)\right\} = \frac{d\overline{I}(z)}{dz} - \overline{\overline{C}}(z)\frac{1}{4\pi\varepsilon}\int_0^L \overline{\overline{g}}(z,z')\frac{d\overline{I}(z')}{dz'}dz' \tag{26}$$

The solutions to (23) are series expansions based on the perturbation theory [Tkatchenko et al., 1995]

$$\begin{aligned}\overline{\phi}(z) &= \overline{\phi}_{(0)}(z) + \overline{\phi}_{(1)}(z) + \overline{\phi}_{(2)}(z) + \cdots \\ \overline{I}(z) &= \overline{I}_{(0)}(z) + \overline{I}_{(1)}(z) + \overline{I}_{(2)}(z) + \cdots\end{aligned} \tag{27}$$

The beginning ($n = 0$) results $\overline{\phi}_{(0)}(z)$ and $\overline{I}_{(0)}(z)$ can be obtained via the following equations.

$$\begin{cases} \frac{d}{dz}\overline{\phi}_{(0)}(z) + j\omega\overline{\overline{L}}\,(z)\,\overline{I}_{(0)}\,(z) = \overline{\overline{E}}^{i}_{z}(x, y, z) \\ \\ \frac{d}{dz}\overline{I}_{(0)}(z) + j\omega\overline{\overline{C}}\,(z)\,\overline{\phi}_{(0)}(z) = \overline{0} \end{cases} \tag{28}$$

The subsequent ($n \geq 1$) current and scattered voltage perturbations are then obtained by

$$\begin{cases} \frac{d}{dz}\overline{\phi}_{(n)}(z) + j\omega\overline{\overline{L}}\,(z)\,\overline{I}_{(n)}\,(z) = j\omega D_1\left\{\overline{I}_{(n-1)}(z)\right\} \\ \\ \frac{d}{dz}\overline{I}_{(n)}\,(z) + j\omega\overline{\overline{C}}\,(z)\,\overline{\phi}_{(n)}(z) = D_2\left\{\overline{I}_{(n-1)}(z)\right\} \end{cases} \tag{29}$$

A SPICE solver with modified nodal analysis (MNA) is adopted in this work to solve (28) and (29), which is referred to as the recursive GMTL solver in this paper. The multiple wire structure is first divided into many small segments. Each segment is represented by lumped circuit elements in a T-shaped topology as shown in Fig. 5. In such a topology, $\overline{I}(z')$ and $\frac{d}{dz'}\overline{I}(z')$ which are defined in the center of the segment can be approximated using the following equations.

$$\overline{I}(z') = \frac{\overline{I}_2(z') + \overline{I}_1(z')}{2} \tag{30}$$

$$\frac{d}{dz'}\overline{I}(z') = \frac{\overline{I}_2(z') - \overline{I}_1(z')}{\Delta z'/2} \tag{31}$$

where $\bar{I}_1(z')$ and $\bar{I}_2(z')$ are the currents flowing through the left and the right voltage sources, respectively. Their elements, $I_1(z)$ and $I_2(z)$, are shown in Fig. 5. Notice that only the self terms of the inductance and capacitance are illustrated in the Fig. 5. The mutual terms among different wires are neglected to keep the figure brief. For details on how to convert (28) and (29) to MNA circuits, readers are referred to [Cheever, Mandache and Topan, 2006].

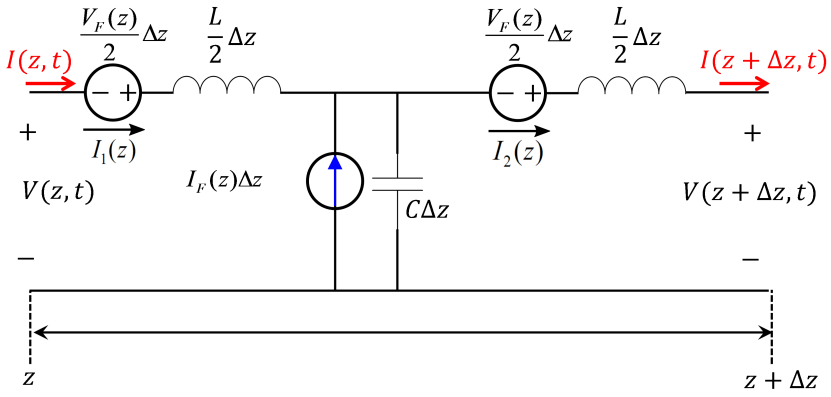


Figure 5. T-shaped lumped circuit representation for each wire segment.

**3.5. Test Case Validation.** As illustrated in Fig. 6, a test case containing five wires along the $z$-direction is implemented to study the excited currents on the wires. The cross-sectional distribution of the wires is provided in Fig. 6 (b). The length and the radius of all the wires are 1 m and 0.1 mm, respectively. Detailed termination information is shown in Fig. 6 (a). According to Fig. 6 (a), Wire 1, 2, and 3 are connected via lumped circuit elements at both ends. A lumped current source of 1 $A$ at 0.5 GHz is applied between Wire 1 and 2 to excite the wire structure. Thus, conduction currents dominate the total currents on Wire 1, 2, and 3. Wire 4 and 5 are not connected to the first three wires. The currents induced on these two wires are mainly due to the field couplings from the other three wires.

The recursive GMTL solver is applied to solve the excited currents on the wire structure. The MPIE solver is utilized to validate the computed currents. Without the loss of generality, currents obtained on Wire 1 and 4 are compared in Fig. 7. As shown in Fig. 7,

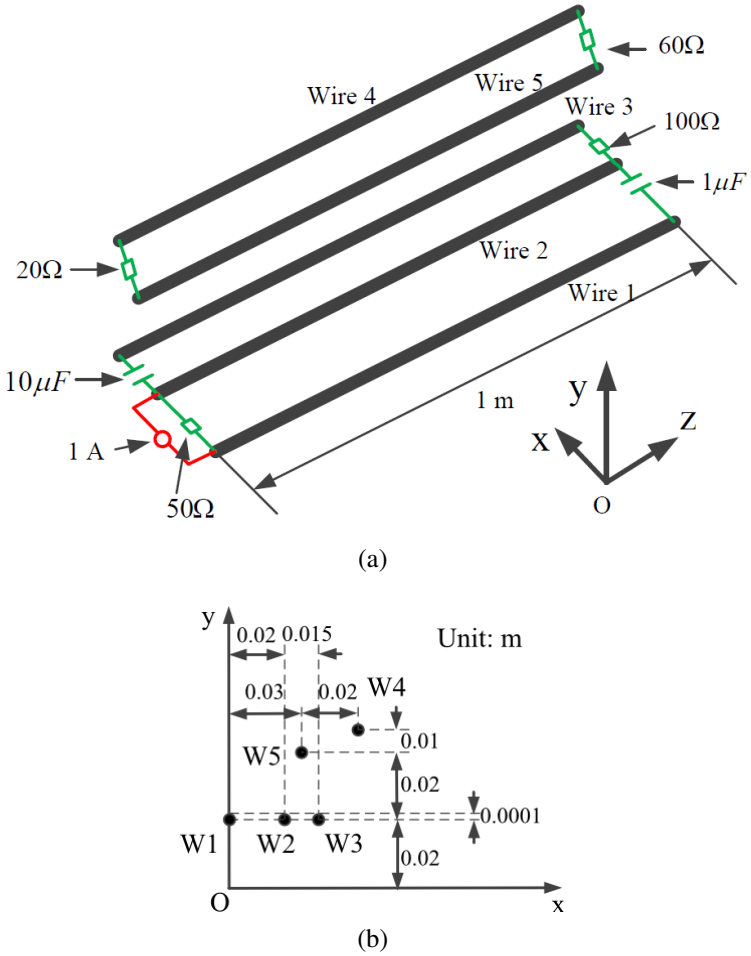


Figure 6. A test case for the recursive GMTL solver: (a) 3D view with detailed information about terminations and excitations, (b) the cross-sectional view.

the beginning current on Wire 1 (Recursion = 0) agrees well with the MPIE calculation since it is dominated by the conduction current. The current on Wire 4 which is mainly caused by field couplings converges after three recursions. All the converged currents match well with the reference results by the MPIE solver, which validates the accuracy of the recursive GMTL solver.

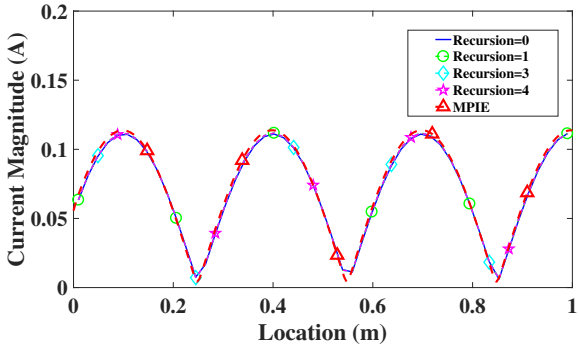


(a)

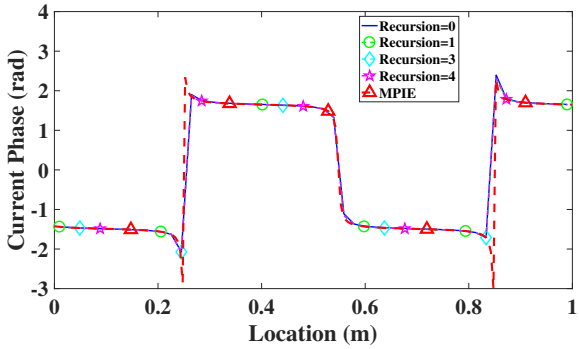


(b)

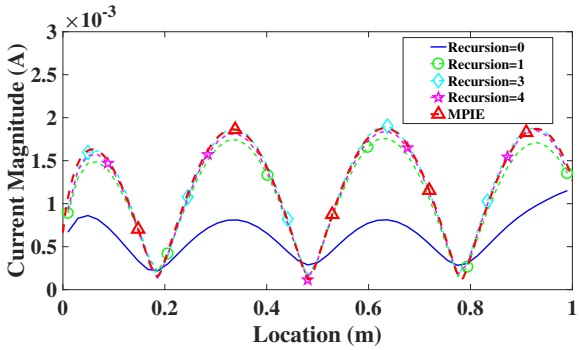


(c)

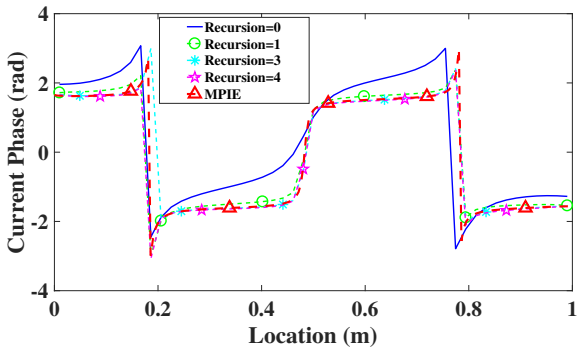


(d)

Figure 7. The obtained currents on Wire 1: (a) Magnitude and (b) phase; the obtained currents on Wire 4: (c) magnitude and (d) phase.

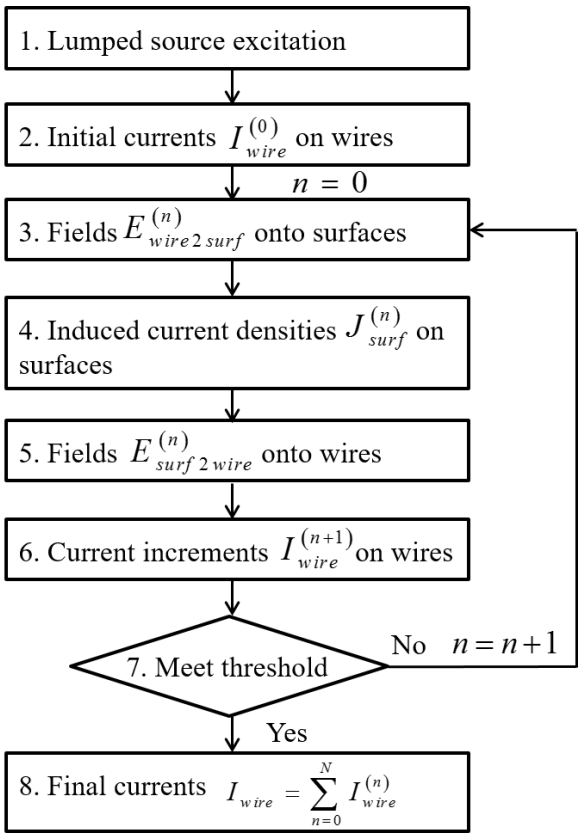


Figure 8. Flowchart of the MS approach.

## 4. FLOWCHART OF THE MS METHOD COMBINING THE GMTL AND THE MPIE

The co-simulation of the multiple wires and the nearby surface involves two parts: the wire part and the surface part. The wire part is modeled based on the GMTL approach while the surface part is modeled using the MPIE formulation. The MS method is applied to iteratively account for the mutual effects between the wire and the surface parts.

The flowchart of the adopted MS method is shown in Fig. 8. Detailed descriptions for each step are listed below.

Step 1 (GMTL solver): Excite the wire structure using a lumped source.

Step 2 (GMTL solver): Calculate the initial currents on wires $I_{wire}^{(n)}$, where n = 0. Notice that $I_{wire}^{(n)}$ is the converged currents after the recursion process as described in (29).

Step 3: Calculate the incident E-field $E^{(n)}_{wire2surf}$ onto the nearby surface, where n = 0. The computation is based on (2)-(6) with dependence changed to 3-D location $r$ and $r'$ and the currents $I^{(n)}_{wire}$ obtained in the previous step are applied.

Step 4 (MPIE solver): Calculate the induced electric current density $J^{(n)}_{surf}$ on the surface due to $E^{(n)}_{wire2surf}$ in the previous step, where n = 0.

Step 5: Calculate the scattered E-field $E^{(n)}_{surf2wire}$ at the wire location, where n = 0. The computation is similar as Step 3 and the current density $J^{(n)}_{surf}$ obtained in the previous step is applied.

Step 6 (GMTL solver): Calculate the induced current increments on wires $I^{(n+1)}_{wire}$ due to $E^{(n)}_{surf2wire}$ in the previous step, where n = 0. Step 3 to 6 constitute one iteration (scattering).

Step 7: Check the threshold. The total current after the 1st iteration is $I_{wire} = I^{(0)}_{wire}+I^{(1)}_{wire}$. To make it more general, the total current after the $N$th iteration is $I_{wire} = \sum_{n=0}^{N} I^{(n)}_{wire}$. If the maximal current increment on each wire is less than a certain level (e.g 5%) of the peak value of the total current on the same wire, the MS process stops and continues to Step 8. Otherwise, the MS process goes on to Step 3 and set n = n+1. Notice that the current increments on wires are applied to compute $E^{(n)}_{wire2surf}$ in the following scattering process.

Step 8: The final converged currents on wires are $I_{wire} = \sum_{n=0}^{N} I^{(n)}_{wire}$.

## 5. NUMERICAL VALIDATION

To validate the current calculation for multiple wires with a nearby surface based on the MS approach, a test case is created as shown in Fig. 9 with detailed geometry information. The test case contains four wires and a slotted surface beneath the wire structure. The cross-sectional distribution of the wires is illustrated in Fig. 9 (b). The

wire excitation and terminations are illustrated in Fig. 9 (a). As can be seen in the figure, Wire 1 and 2 are connected, in which case conduction currents donimate; Wire 3 and 4 are connected, in which case currents are mainly caused by field couplings.

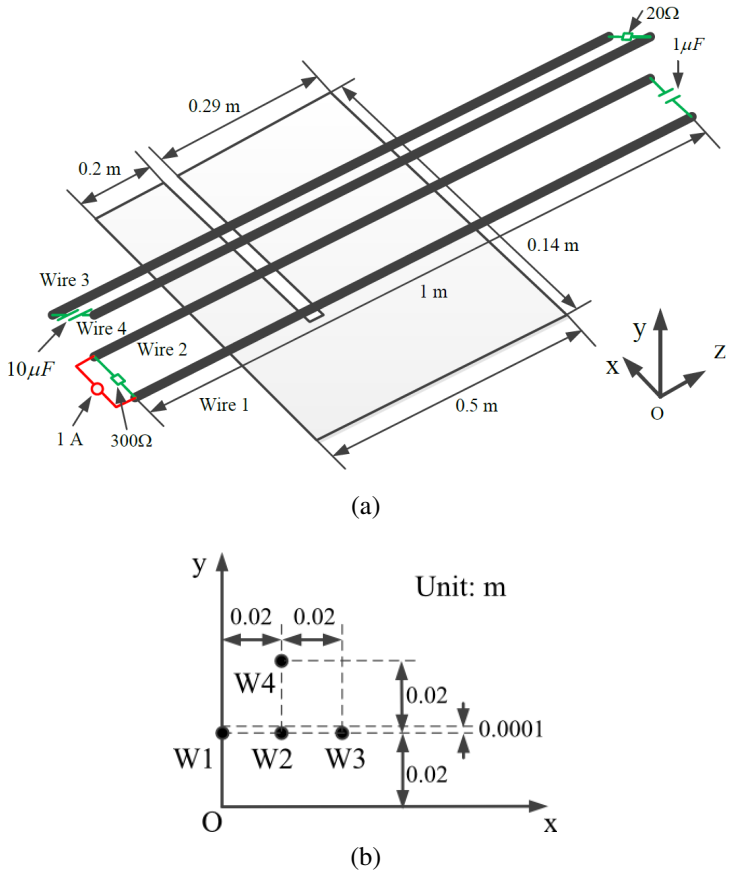


Figure 9. A test case for the MS approach: (a) 3D view with detailed information about terminations and excitations, (b) the cross-sectional view.

Following the MS approach as described in Fig. 8, the excited currents on wires can be obtained. Without the loss of generality, currents on Wire 1 and 4 are compared in Fig. 10 at 1 GHz. For Wire 1 where the conduction currents dominate, the initial currents when iteration equals to zero are already close to the reference results calculated by the MPIE solver with pseudo segments. It can be observed from Fig. 10 (a) and (b) that the computed currents on Wire 1 converge after one iteration. For Wire 4, the initial currents merely resemble the reference results. However, they converge after three iterations as shown in Fig. 10 (c) and (d). And the converged currents match well with the reference results. Even

though the maximal magnitude of the crosstalk currents on Wire 4 is less than $1/10$ of the maximal currents on Wire 1, the crosstalk on Wire 4 can still be accurately evaluated by the MS approach. Notice that the currents on Wire 1 are insensitive to the nearby surface during the MS process while the currents on Wire 4 are to the opposite. The current increment on Wire 4 is mainly due to the scattered fields from the metal surface. This phenomenon reveals how the nearby surface affects the current distribution on wires. The number of wire segments and surface cells used in the MS and the MPIE methods are listed in Table 1. Less wire segments are required in the MS method to achieve similar accuracy compared to the MPIE method. The reduction in wire segments will be more phenomenal in cases with more complex wire strucutres.

Table 1. Wire segments and surface cells used in the MS and MPIE.

| | Wire segments | Surface cells |
|---|---|---|
| MS | 400 | 88 |
| MPIE | 840 | 88 |

Besides, current vs. frequency at the center points of Wire 1 and 4 are compared in Fig. 11. The obtained currents by the MS approach correlate well with the reference results. In Fig. 11 (a), clear resonant periods can be observed since conduction currents dominate on Wire 1 and 2. However, no clear period can be found in Fig. 11 (c). This is because currents on Wire 3 and 4 are mainly caused by the scattered fields from the metal surface. It should be noted that some frequency points (0.15, 0.3, 0.45, 0.6, 0.75, and 0.9 GHz) are skipped in Fig. 11, since the GMTL method doesn't converge at these frequency points leading to inaccurate results. These frequency points correspond to the natural resonant frequencies of the wires. In other words, when the wire length is multiple integer of half wavelength, the GMTL method will fail [Bayram and Volakis, 2005]. To resolve the issue in the future work, additional loss terms may be added either lumpedly at the ends of the wires [Middelstaedt et al., 2016] or distributedly along the wires [Chabane et al., 2017].

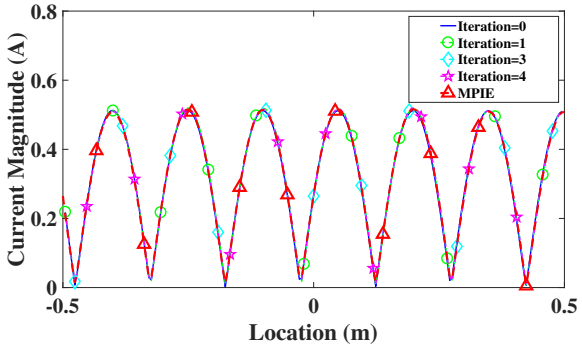


(a)

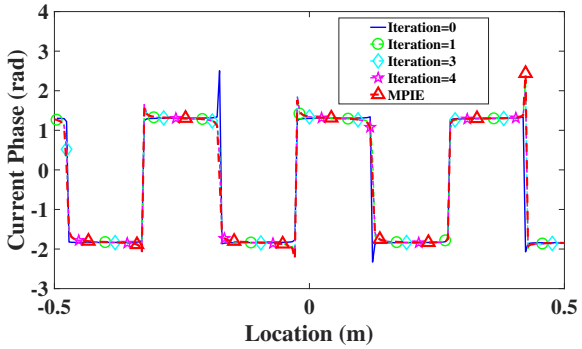


(b)

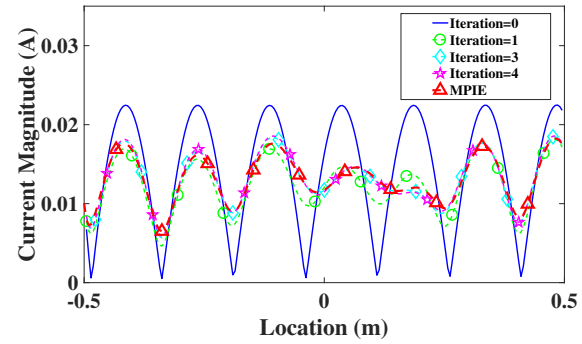


(c)

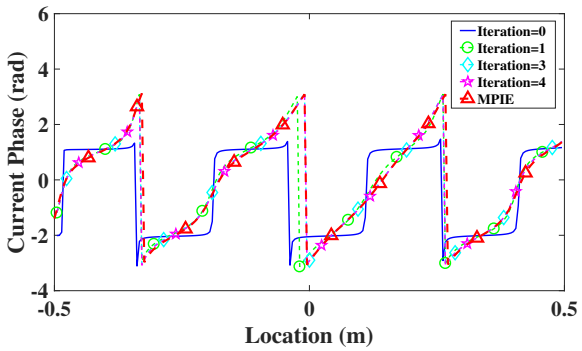


(d)

Figure 10. At 1 GHz, (a) Magnitude and (b) phase of the currents on Wire 1, (c) magnitude and (d) phase of the currents on Wire 4.

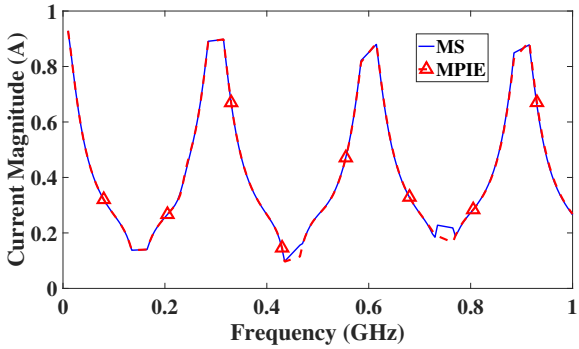


(a)

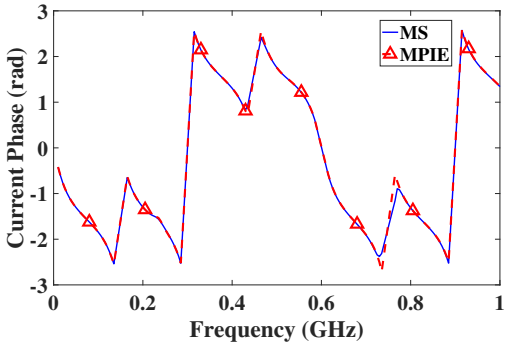


(b)

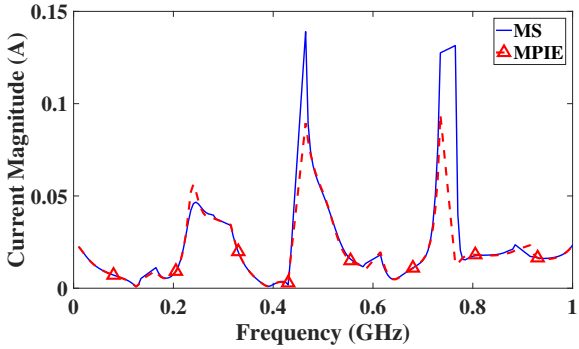


(c)

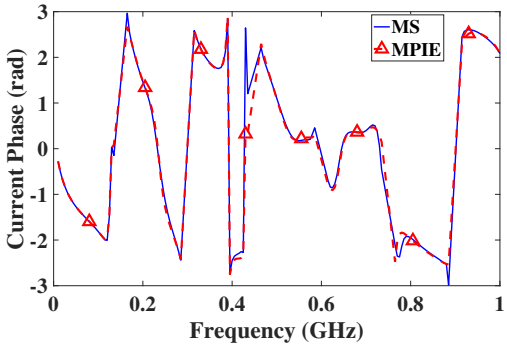


(d)

Figure 11. From 10 MHz to 1 GHz, (a) Magnitude and (b) phase of the currents at the center of Wire 1, (c) magnitude and (d) phase of the currents at the center of Wire 4.

## 6. CONCLUSIONS

In this paper, co-simulation of a cable harness consisting of multiple wires and a nearby metal surface was carried out in two parts: the multiple wire part and the surface part. The multiple wire part was modeled by the GMTL approach and solved recursively. A test case demonstrates the accuracy of the recursive GMTL solver. The surface part was handled by the MPIE solver. To account for the mutual interactions between the multiple wires and the metal surface, the MS approach was employed. In the studied test case where four wires are set above a slotted surface, only three scatterings are required before all wire currents converge. And the converged currents match well with the reference results. These test cases validate the proposed recursive GMTL solver and the further MS approach for the co-simulation. Although not specically demonstrated, the MS approach can be applied to cases with more complicated surface structures, since the surface part is purely solved by the mature algorithm of MoM.

The GMTL is an extension of the traditional TL theory. Some limitations in the traditional TL theory may still be applicable in the GMTL approach. As mentioned in [Bayram and Volakis, 2005], the TL theory fails at wire resonances if TLs are left open without terminations. This limitation is also true for the GMTL approach. Efforts can be made to resolve the issue. Regarding the upper frequency limitation, it would be safe to apply the GMTL approach if the separation of wires is less than 1/10 of a wavelength, as is advised in the traditional TL theory. However, this requires future investigation.

Besides, the proposed GMTL approach can only be used to analyze multiple straight thin wires. Further work can be expended to apply the GMTL approach to bend, curved, and arbitrarily oriented wires. For thick wire cases where non-uniform current distribution and proximity effects should be considered, the modal decomposition method [Jin, 2017, Jin et al., 2018] can be used for pul $L$ and $C$ extraction.

Last by not the least, since a cable harness is usually terminated to the nearby surface at one or more locations through vertical grounding wires, for the future work, the MS approach should include the effects introduced by the grounding wires.

## REFERENCES

A. K. Agrawal, H. J. Price, and S. H. Gurbaxani. Transient response of multiconductor transmission lines excited by a nonuniform electromagnetic field. *IEEE Trans. Electromagn. Compat.*, EMC-22(2):119–129, May 1980.

I. Badzagua, H. Chobanyan, G. Chikovani, I. Oganezova, E. Yavolovskaya, T. Injgia, A. Gheonjian, and R. Jobava. Effective computational techniques for EMC analysis of cable harness. *Proceedings of the 2010 International Seminar/Workshop on Direct and Inverse Problems of Electromagnetic and Acoustic Wave Theory*, pages 96–102, Sep. 2010.

H. Bagci, A.E. Yilmaz, J. Jin, and E. Michielssen. Fast and rigorous analysis of EMC/EMI phenomena on electrically large and complex cable-loaded structures. *IEEE Trans. Electromagn. Compat.*, 49(2):361–381, May 2007.

Y. Bayram and J. L. Volakis. A generalized MoM-SPICE iterative technique for field coupling to multiconductor transmission lines in presence of complex structures. *IEEE Trans. Electromagn. Compat.*, 47(2):234–246, May 2005.

Y. S. Cao, L. Jiang, and A. E. Ruehli. Distributive radiation and transfer characterization based on the PEEC method. *IEEE Trans. Electromagn. Compat.*, 57(4):734–742, Aug. 2015.

Y. S. Cao, Y. Wang, L. Jiang, A. E. Ruehli, J. Fan, and J. Drewniak. Quantifying EMI: a methodology for determining and quantifying radiating for practical design guidelines. *IEEE Trans. Electromag. Compat.*, 59(5):1424–1432, Oct. 2017.

S. Chabane, P. Besnier, and M. Klingler. A modified enhanced transmission line theory applied to multiconductor transmission lines. *IEEE Trans. Electromagn. Compat.*, 59(2):518–528, Apr. 2017.

Cheever. All of cheever's MNA pages condensed into one. *[Online]: http://www.swarthmore.edu/NatSci/echeeve1/Ref/mna/MNA_All.html*.

A. G. Chiariello, A. Maffucci, G. Miano, F. Villone, and W. Zamboni. A transmission-line model for full-wave analysis of mixed-mode propagation. *IEEE Trans. Adv. Packag.*, 31(2):275–284, May 2008.

H. Chobanyan, I. Badzagua, T. Injgia, A. Gheonjian, and R. Jobava. Application of hybrid MOM/MTL method to simulation of interaction between cable harness and antennas. *Proceedings of the 2009 International Seminar/Workshop on Direct and Inverse Problems of Electromagnetic and Acoustic Wave Theory*, pages 33–38, Sep. 2009.

V. Cooray, F. Rachidi, and M. Rubinstein. Formulation of the field-to-transmission line coupling equations in terms of scalar and vector potentials. *IEEE Trans. Electromagn. Compat.*, (99):1–6.

EMCoS. EMC studio, version 8.2. *[Online]. Available: http://www.emcos.com*.

J. Fan, H. Shi, A. Orlandi, J. L. Knighten, and J. L. Drewniak. Modeling DC power-bus structures with vertical discontinuities using a circuit extraction approach based on a mixed-potential integral equation formulation. *IEEE Trans. Adv. Packag.*, 24(2): 143–157, May 2001.

S. Jin. Modal based bga modeling in high-speed package. *Ph.D. dissertation, MST, Rolla, MO*, 2017.

S. Jin, D. Liu, B. Chen, K. Qiu, J. Lin, R. Brooks, and J. Fan. Analytical equivalent circuit modeling for BGA in high-speed package. *IEEE Trans. Electromagn. Compat.*, 60 (1):68–76, Feb. 2018.

D. Liu. Common mode current estimation for cable bundle inside a vehicle. *Ph.D. dissertation, MST, Rolla, MO*, 2013.

D. Liu, Y. Wang, R. W. Kautz, N. Altunyurt, S. Chandra, and J. Fan. Accurate evaluation of field interactions between cable harness and vehicle body by a multiple scattering method. *IEEE Trans. Electromagn. Compat.*, 59(2):383–393, Apr. 2017.

G. Lugrin, S. V. Tkachenko, F. Rachidi, M. Rubinstein, and R. Cherkaoui. High-frequency electromagnetic coupling to multiconductor transmission lines of finite length. *IEEE Trans. Electromagn. Compat.*, 57(6):1714–1723, Dec. 2015.

A. Maffucci, G. Miano, and F. Villone. An enhanced transmission line model for conducting wires. *IEEE Trans. Electromagn. Compat.*, 46(4):512–528, Nov. 2004.

A. Maffucci, G. Miano, and F. Villone. An enhanced transmission line model for conductors with arbitrary cross sections. *IEEE Trans. Adv. Packag.*, 28(2):174–188, May 2005.

L. Mandache and D. Topan. New treatment of the multiple mutually coupled inductors to improve the modified nodal analysis in harmonic regime. *51st Internationales Wissenschaftliches Kolloquium*, Sep. 2006.

F. Middelstaedt, S. V. Tkachenko, R. Rambousky, and R. Vick. High-frequency electromagnetic field coupling to a long, finite wire with vertical risers above ground. *IEEE Trans. Electromagn. Compat.*, 58(4):1169–1175, Aug. 2016.

J. Nitsch, F. Gronwald, and G. Wollenberg. *Radiating Nonuniform Transmissionline Systems and the Partial Element Equivalent Circuit Method*. John Wiley & Sons, Ltd., 2009.

J. B. Nitsch and S. V. Tkachenko. High-frequency multiconductor transmission-line theory. *Found. Phys.*, 40(9):1231–1252, 2010.

J.B. Nitsch and S.V. Tkachenko. Complex-valued transmission-line parameters and their relation to the radiation resistance. *IEEE Trans. Electromagn. Compat.*, 46(3): 477–487, Aug. 2004.

F. Rachidi. Formulation of the field-to-transmission line coupling equations in terms of magnetic excitation fields. *IEEE Trans. Electromagn. Compat.*, 35(3):404–407, Aug. 1993.

F. Sabath and H. Garbe. Radiation analysis of PCB layout using a hybrid mom-mtl method. *IEEE Trans. Electromagn. Compat.*, 45(2):424–435, May 2003.

EM Software & Systems. FEKO.

C. Taylor, R. Satterwhite, and C. Harrison Jr. The response of a terminated two-wire transmission line excited by a nonuniform electromagnetic field. *IEEE Trans. Antennas Propag.*, 13(6):987–989, Nov. 1965.

Computer Simulation Technology. CST CABLE STUDIO, 2017. *[Online]. Available: http://www.cst.com*.

S.V. Tkatchenko, F. Rachidi, and M. Ianoz. Electromagnetic field coupling to a line of finite length: theory and fast iterative solutions in frequency and time domains. *IEEE Trans. Electromagn. Compat.*, 37(4):509–518, Nov. 1995.

D. Topchishvili, R. Jobava, F. Bogdanov, B. Chikhradze, and S. Frei. A hybrid MTL/MoM approach for investigation of radiation problems in EMC. *Proceedings of the 9th International Seminar/Workshop on Direct and Inverse Problems of Electromagnetic and Acoustic Wave Theory*, pages 65–68, Oct. 2004.

A. Vukicevic, F. Rachidi, M. Rubinstein, and S. V. Tkachenko. On the evaluation of antenna-mode currents along transmission lines. *IEEE Trans. Electromagn. Compat.*, 48(4): 693–700, Nov. 2006.

Y. Wang, R. Kautz, N. Altunyurt, and J. Fan. An equivalent circuit model for the wire-to-surface junction based on method of moments. *Proc. 2016 IEEE Int. Conf. Wireless Inf. Technol. Syst. Appl. Comput. Electromagn.*, pages 1–2, 2016.

D. Zhang, Y. Wen, Y. Wang, D. Liu, X. He, and J. Fan. Coupling analysis for wires in a cable tray using circuit extraction based on mixed-potential integral equation formulation. *IEEE Trans. Electromagn. Compat.*, 59(3):862–872, June 2017.

# II. A GENERALIZED MULTIPLE-SCATTERING METHOD FOR MODELING A CABLE HARNESS WITH GROUND CONNECTIONS TO A NEARBY METAL SURFACE

Yansheng Wang, Ying S. Cao, Dazhao Liu, Richard Kautz, Nevin Altunyurt, and Jun Fan

## ABSTRACT

This paper proposes a generalized multiple-scattering (GMS) method to evaluate the current distribution on a cable harness with ground connections to a nearby metal surface. The GMS method is a hybrid method combining the transmission line theory and the method of moments. The GMS method uses the generalized multi-conductor transmission line (GMTL) solver for the cable harness part and the mixed-potential integral equations (MPIE) solver for the rest of the structure including the metal surface and the grounding wires. Neither the GMTL nor the MPIE solver alone takes into account the mutual interactions between the cable harness and the rest of the structure. Therefore, an iterative scheme is arranged in the GMS method to compensate the abovementioned interactions. These interactions occur via not only field couplings, but also current conducting through the grounding points on the cable harness. A numerical test case is provided to benchmark the proposed GMS method.

**Keywords:** Cable harness, method of moments (MoM), multiple scattering (MS), multi-conductor transmission line (MTL), radiation.

## 1. INTRODUCTION

Cable harnesses serving as the interconnects among various modules play a crucial role in determining the electromagnetic compatibility (EMC) performance of a system such as a vehicle, high-speed train, or aircraft [Bagci et al., 2007]. A cable harness is an assembly of electrical wires which transmit signals or electrical power. The modeling

of a cable harness with the nearby metal surface structure is significant during the design process since the radiation from antenna-mode currents on the cable harness can illuminate the metal surface and further radiate into the outer environment as electromagnetic (EM) pollution.

To efficiently calculate the current distribution on a cable harness, a hybrid solver combining the multi-conductor transmission line (MTL) theory with the method of moments (MoM) was proposed in previous works [Badzagua et al., 2010, Chobanyan et al., 2009, Topchishvili et al., 2004]. In the hybrid method, the cable harness was handled by the MTL theory and the nearby metal surface was solved by MoM. However, this hybrid solver failed to consider the interactions between the cable harness and the metal surface. To account for the abovementioned interactions, iterative approaches were introduced in [Bayram and Volakis, 2005, Liu et al., 2017, Sabath and Garbe, 2003, Wang et al., 2018]. However, these iterative approaches suffered from some limitations. In [Sabath and Garbe, 2003], the antenna-mode currents were missed from the total currents induced on the wire structure. In [Bayram and Volakis, 2005], the developed solver was based on a circumscribed assumption that the electric potential was equal on the same conducting surface, which was true only for electrically small structures. In [Liu et al., 2017, Wang et al., 2018], the proposed method overcame the two abovementioned drawbacks, but its capability was limited to structures where the cable harness did not have ground connections to the nearby metal surface.

In this study, a hybrid solver evolving from the one in [Wang et al., 2018] is developed to solve the current distribution on a cable harness with ground connections to a nearby metal surface. Without the loss of generality, an example of a cable harness with ground connections to a nearby metal surface is illustrated in Fig. 1 (a). In this figure, the cable harness contains three wires and has two ground connections to the metal surface. The cable harness is usually terminated at both ends. For simplicity, terminations of the cable harness are not illustrated in this and all the following figures. As shown in Fig. 1 (b), the above structure is treated as a combination of the signal path (SP) and the return path

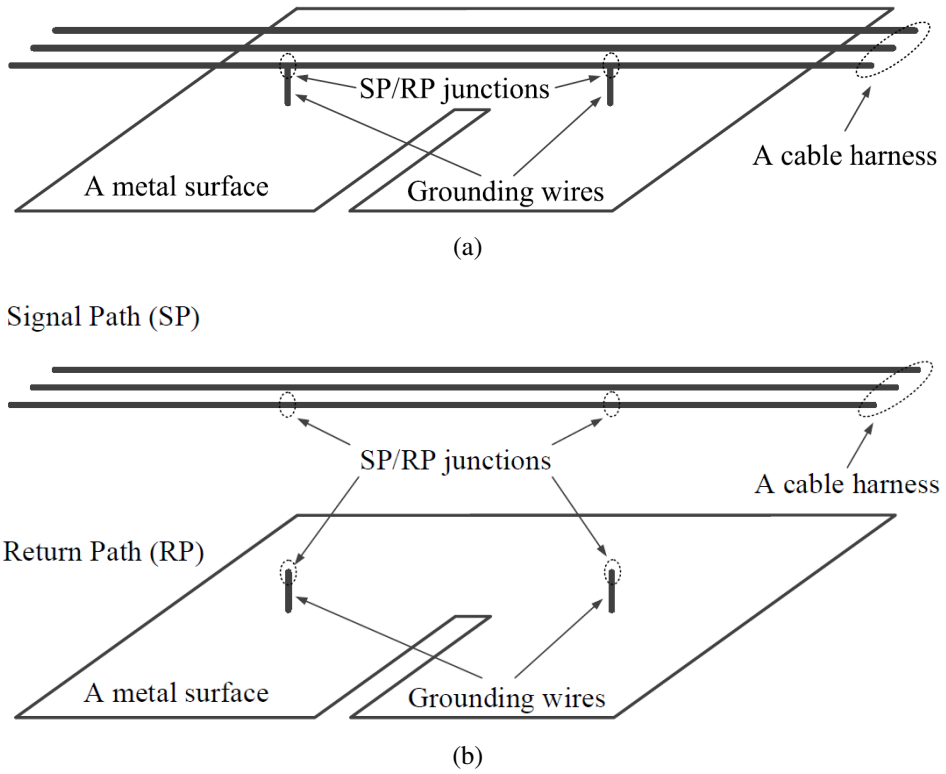


Figure 1. A cable harness consisting of three wires has two ground connections to a nearby metal surface: (a) the physical structure, and (b) the logical separation of the above structure in the proposed algorithm, i.e. a combination of the SP and RP by splitting the structure at the SP/RP junctions.

(RP) by the proposed hybrid solver in this paper. The above structure is divided into the SP and the RP at the SP/RP junctions. An SP/RP junction is a point where the SP connects to the RP. The RP consists of the metal surface together with the grounding wires. It is modeled and solved based on MoM, specifically the mixed-potential integral equations (MPIE) formulation [Fan et al., 2001, Liu, 2013, Wang et al., 2016, Zhang et al., 2017]. The SP is formed by the cable harness, which is modeled and solved in the generalized multi-conductor transmission line (GMTL) solver [Wang et al., 2018]. The GMTL solver takes the infinity as the reference, which earns two advantages in practical applications. First, unlike in [Chiariello et al., 2008, Lugrin et al., 2015, Nitsch and Tkachenko, 2010, 2004, Tkatchenko et al., 1995] where an infinitely large ground plane was assumed beneath

the cable harness, the current calculation based on the GMTL solver is independent of the nearby plane; i.e., the plane close the cable harness can be of arbitrary shape, orientation, and size. Second, going beyond the work in [Liu et al., 2017] and [Maffucci et al., 2004, 2005, Vukicevic et al., 2006] where the transmission line (TL) parameters were only derived between two wires, the GMTL solver handles multiple wires. Notice that neither the MPIE nor the GMTL solver alone considers the mutual interactions between the SP and the RP. To account for the abovementioned interactions, the idea of iteration from [Bayram and Volakis, 2005, Liu et al., 2017, Sabath and Garbe, 2003, Wang et al., 2018] is adopted in this work. However, different from the multiple-scattering (MS) method reported in [Bayram and Volakis, 2005, Liu et al., 2017, Sabath and Garbe, 2003, Wang et al., 2018] where the cable harness interacted with the nearby surface only through field couplings, the proposed generalized MS (GMS) method takes into account the mutual interactions via not only the field couplings, but also the current conducting through the SP/RP junctions.

To summarize, a GMS method is proposed to analyze the current distribution on a cable harness with ground connections to a nearby metal surface. The proposed method not only inherits the advantages of the MS method in [Wang et al., 2018], but also generalizes its capability to evaluate the interactions between the SP and the RP via both field couplings and current conducting through the SP/RP junctions.

The paper is organized as follows. In Section II, some key concepts regarding the GMS method are briefly introduced. In section III, the usages of the MPIE solver are introduced. In Section IV, the usages of the GMTL solver are discussed. In Section V, the flowchart of the GMS approach combining the GMTL and the MPIE solvers is presented in details. In Section VI, an example is provided to benchmark the GMS approach. Conclusions are presented in Section VII.

## 2. KEY CONCEPTS IN THE GMS METHOD

Some key concepts in the GMS method are introduced in this section. A general understanding of these concepts is necessary to comprehend the flowchart of the GMS method in Section V.

- The scattering of EM waves

  Consider two metal structures: Metal A and B. Time-varying currents flowing on Metal A generate EM waves. These EM waves propagate and are scattered by Metal B around. These scattered EM waves from Metal B again are scattered by Metal A, so on and so forth, until a steady state is reached. Each time EM waves are scattered by one metal structure, electric current increment is induced on that metal structure. The steady state refers to a stage when the current increment is negligible.

- The iteration in the GMS method

  In the proposed GMS method, iteration is used to compensate the interaction between the SP and the RP. From the perspective of physics, this iteration represents the scattering of EM waves bouncing between the SP and the RP. The abovementioned interaction takes place via not only the field couplings, but also the current conducting through the SP/RP junctions. In other words, when currents are excited on the SP due to field couplings from the RP or a lumped source, these excited currents on the SP conduct to the RP through the SP/RP junctions; similarly, the excited currents on the RP due to field couplings from the SP flow to the SP via the SP/RP junctions as well.

- The loading effect

  Though based on different algorithms, the MPIE and the GMTL solvers are both implemented using modified nodal analysis (MNA) [Cheever]. These solvers are built in a way that nodes in the MNA representation share the same definition as

the nodes in the admittance $Y$-matrix [Cheever, Liu, 2013]. Therefore, loadings can be conveniently integrated into the MPIE and GMTL solvers when expressed as $Y$-matrices. When currents are excited on the SP due to field couplings from the RP or a lumped source, the loading effect of the RP is included in the GMTL solver as an admittance matrix $YnP_r$. $YnP$ represents the $n$-port $Y$-parameter. The subscript $r$ stands for the RP. When currents are excited on the RP due to field couplings from the SP, the loading effect of the SP is included in the MPIE solver as an admittance matrix $YnP_s$. The subscript $s$ stands for the SP.

- The impressed current source

  The impressed current source refers to an ideal current source with an infinite impedance in parallel. When currents on the SP conduct to the RP through the SP/RP junctions to excite the RP, these conducting currents are represented using impressed current sources in the MPIE solver. Similarly, when currents on the RP conduct to the SP through the SP/RP junctions to excite the SP, these conducting currents are represented by impressed current sources in the GMTL solver.

- The primary and secondary driving sources

  There are two kinds of sources that drive the iteration process. The initial lumped current source and the field couplings are the primary driving sources, while the conduction currents through the SP/RP junctions are the secondary driving sources. The secondary driving source is a consequence of the primary driving source. Within each iteration, the primary driving sources start the scattering process of EM waves and the secondary driving sources supplement the process. The primary driving sources utilize the GMTL solver and the MPIE solver with $YnP_r$ and $YnP_s$ loaded, respectively. The secondary driving sources use the GMTL solver and the MPIE

solver without loadings. The primary and the secondary driving sources alternatively play a role to obtain the current distribution from the initial state to the final steady state.

## 3. THE MPIE SOLVER

The MPIE formulation is applied to create a full-wave solver in this study. The derivation for the MPIE is well known, and thus is omitted in this paper. For more details, refer to [Liu, 2013] for the wire and surface, and [Wang et al., 2016] for the wire-to-surface junction. Notice that thin wire approximation is used in the MPIE formulation for wires. The thin wire approximation assumes wire current has only longitudinal component and no transverse component. The accuracy of the constructed MPIE solver was validated in [Liu, 2013]. The equation behind the MPIE solver is

$$\begin{bmatrix} j\omega\overline{\overline{C}} & \overline{\overline{\Lambda}}^{T} \\ -\overline{\overline{\Lambda}} & j\omega\overline{\overline{L}} \end{bmatrix} \begin{bmatrix} \overline{\phi} \\ \bar{i} \end{bmatrix} = \begin{bmatrix} -\overline{I}^{e} \\ \overline{V}^{e} \end{bmatrix}. \tag{1}$$

In (1), $\omega$ is the angular frequency. $\overline{\overline{C}}$ and $\overline{\overline{L}}$ are matrices of the distributed capacitance and inductance associated with the meshes that discretize the structure, respectively. $\overline{\overline{\Lambda}}$ is the connectivity matrix that describes the connection relationship of the abovementioned capacitance and inductance. $\overline{\phi}$ and $\bar{i}$ are the electric potential and current that are to be solved. $\overline{I}^{e}$ and $\overline{V}^{e}$ are the external current and voltage source, respectively. The external current source refers to the currents conducting to the RP through the SP/RP junctions. The external voltage source indicates the induced voltage source on the RP due to field couplings from the SP.

When the MPIE solver is employed to solve the current distribution on the RP due to the primary driving source, i.e. the field coupling from the SP, the loading effect of the SP ($YnP_s$) is included as illustrated in Fig. 2. The way to integrate $YnP_s$ into the MPIE

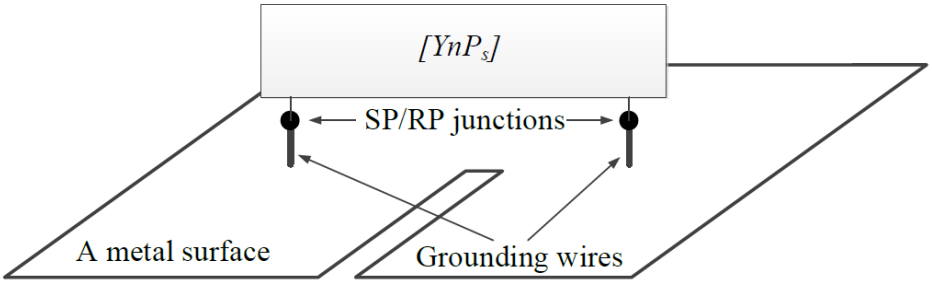


Figure 2. The loading effect of the SP is represented by an admittance matrix $YnP_s$ and integrated into the MPIE solver for the RP. The SP/RP junctions are indicated using dots in this and all the following figures.

solver is to add $YnP_s$ to the corresponding rows and columns of $j\omega\overline{\overline{C}}$, i.e., the capacitance nodes. For example, a two-port $Y$-parameter $Y2P_s$ is connected to the RP at the $p$th and $q$th capacitance nodes. Then $Y2P_s$ is added to the MPIE solver as

$$j\omega \begin{bmatrix} C'_{pp} & C'_{pq} \\ C'_{qp} & C'_{qq} \end{bmatrix} = j\omega \begin{bmatrix} C_{pp} & C_{pq} \\ C_{qp} & C_{qq} \end{bmatrix} + [Y2P_s], \tag{2}$$

where $C_{pq}$ is the element in the $p$th row and $q$th column of $\overline{\overline{C}}$ and $C'_{pq}$ is the modified version of $C_{pq}$ after adding the loading effect. After running the loaded MPIE solver, the current distribution on the RP and the currents conducting through the SP/RP junctions are obtained.

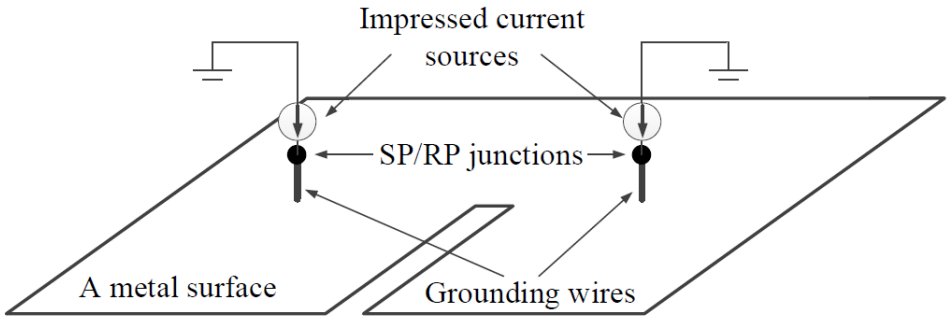


Figure 3. The MPIE solver for the RP is not loaded with $YnP_s$ when impressed currents are applied to mimic currents conducting through the SP/RP junctions from the SP.

When the MPIE solver is used to solve the current distribution on the RP due to the secondary driving source, i.e. the currents conducting to the RP through the SP/RP junctions, the impressed current sources are connected to the SP/RP junctions as shown in Fig. 3. The way to implement the impressed current sources in the MPIE solver is to assign current value to the corresponding rows in $\bar{I}^e$.

Equation (1) is also utilized to extract the loading effect of the RP ($YnP_r$). $\bar{V}^e$ in (1) is set to $\bar{0}$ since the extraction of $YnP_r$ is independent of the external voltage sources. Then (1) is expanded as

$$\begin{cases} j\omega\bar{\bar{C}}\bar{\phi} + \bar{\bar{\Lambda}}^T\bar{i} = -\bar{I}^e \\ -\bar{\bar{\Lambda}}\bar{\phi} + j\omega\bar{\bar{L}}\bar{i} = \bar{0} \end{cases} \tag{3}$$

The second equation of (3) is rearranged as

$$\bar{i} = \frac{1}{j\omega}\bar{\bar{L}}^{-1}\bar{\bar{\Lambda}}\bar{\phi}. \tag{4}$$

Take (4) into the first equation of (3) to replace $\bar{i}$. After some manipulations, the following equation is obtained.

$$\bar{\bar{Y}}_{RP}\bar{\phi} = -\bar{I}^e, \tag{5}$$

where the admittance matrix of the RP is

$$\bar{\bar{Y}}_{RP} = j\omega\bar{\bar{C}} + \frac{1}{j\omega}\bar{\bar{\Lambda}}^T\bar{\bar{L}}^{-1}\bar{\bar{\Lambda}}. \tag{6}$$

One more step is needed to convert $\bar{\bar{Y}}_{RP}$ to $YnP_r$. The procedure is described in [Fan et al., 2003] in great details and thus omitted here. Notice that the SP/RP junctions are treated as the external nodes during the conversion. An external node refers to the outlet node of a network, e.g. an SP/RP junction of the RP.

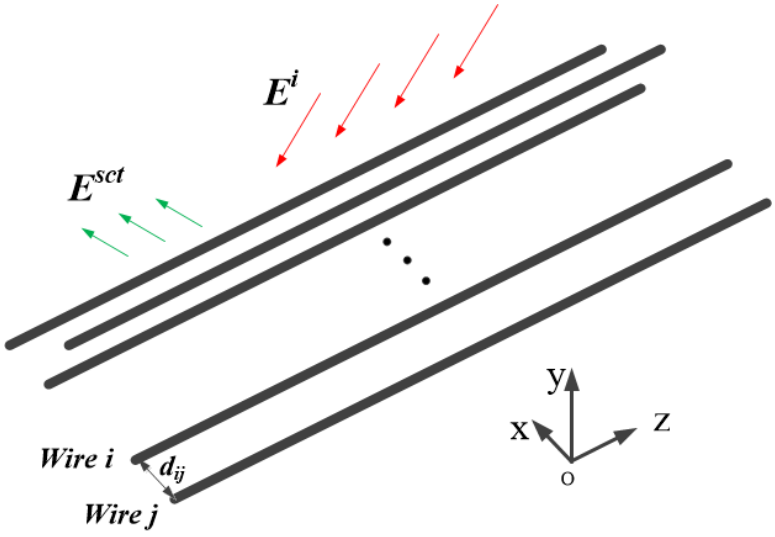


Figure 4. A multi-wire structure illuminated by incident E-field. $E^i$ is the incident field. $E^{sct}$ is the scattered field. $d_{ij}$ is the separation between Wire $i$ and $j$.

## 4. THE GMTL SOLVER

The GMTL solver is developed for the structure shown in Fig. 4. In this figure, a cable harness with multiple wires is illuminated by incident electric field (E-field). The fundamental equations behind the GMTL solver is

$$\begin{cases} \frac{d\overline{\phi}(z)}{dz} + j\omega\overline{\overline{L}}(z)\overline{I}(z) = \overline{E}^i_z(x,y,z) + j\omega D_1\left\{\overline{I}(z)\right\} \\ \frac{d\overline{I}(z)}{dz} + j\omega\overline{\overline{C}}(z)\overline{\phi}(z) = D_2\left\{\overline{I}(z)\right\} \end{cases} \tag{7}$$

In (7), $\overline{\overline{L}}(z)$ and $\overline{\overline{C}}(z)$ are matrices of the per-unit-length (pul) inductance and capacitance for the cable harness, respectively. $\overline{\phi}(z)$ and $\overline{I}(z)$ are the unknown electrical potential and electric current, respectively. $\overline{E}^i_z(x,y,z)$ is the incident E-field. $D_1\left\{\overline{I}(z)\right\}$ and $D_2\left\{\overline{I}(z)\right\}$ are the source correction terms. (7) is solved based on the perturbation theory [Tkatchenko et al., 1995], which includes the retardation delay along the cable harness. Thus, the SP currents obtained by (7) are accurate even if the structure is electrically large. The detailed formulation and validation for the GMTL solver are found in [Wang et al., 2018].

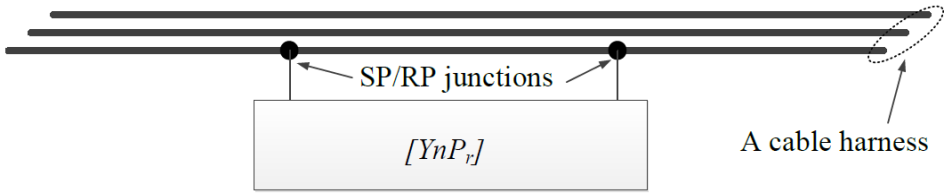


Figure 5. The loading effect of the RP is represented by an admittance matrix $YnP_r$ and integreated into the GMTL solver for the SP.

When the GMTL solver is applied to solve the current distribution on the SP due to the primary driving source, i.e. the field coupling from the RP or a lumped source, the loading effect of the RP ($YnP_r$) is included as illustrated in Fig. 5. Similar to (2), $YnP_r$ is integrated to the GMTL solver at the capacitance nodes. After running the loaded GMTL solver, the current distribution on the SP and the current conducting through the SP/RP junctions are obtained.

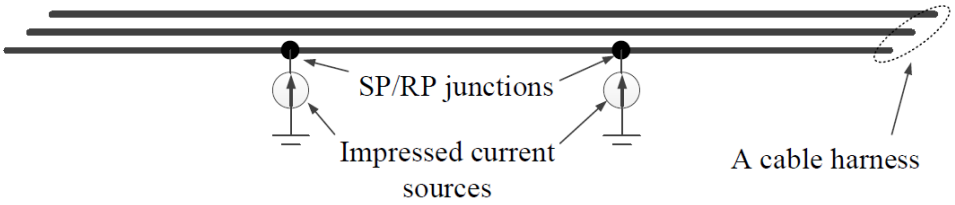


Figure 6. The GMTL solver for the SP is not loaded with $YnP_r$ when impressed currents are injected to the SP/RP junctions from the RP.

When the GMTL solver is used to solve the current distribution on the SP due to the secondary driving source, i.e. the currents conducting to the SP through the SP/RP junctions, the impressed current sources are connected to the SP/RP junctions as shown in Fig. 6.

The GMTL solver is also employed to compute the loading effect of the SP ($YnP_s$) by looking into the SP/RP junctions. The calculation procedure for $YnP_s$ is described as follows. There are $n$ total SP/RP junctions, which are labeled from 1 to $n$. An impressed current source $I_i$ is applied to the GMTL solver through the $i$th SP/RP junction, where $i = 1, 2, \cdots, n$. All the rest SP/RP junctions are left open, which indicates $I_j = 0A$

where $j = 1, 2, \cdots, n$ and $j \neq i$. The converged voltage responses at the $i$th and the $j$th SP/RP junctions are recorded as $V_i$ and $V_j$, respectively. According to the definition of the impedance matrix, the self impedance at the $i$th SP/RP junction is

$$Z_{ii} = \left.\frac{V_i}{I_i}\right|_{I_j=0, j\neq i}, \tag{8}$$

and the mutual impedance from the $i$th to the $j$th SP/RP junction is

$$Z_{ji} = \left.\frac{V_j}{I_i}\right|_{I_j=0, j\neq i}. \tag{9}$$

Sequentially apply the above procedure for $i$ from 1 to $n$. All the obtained impedances constitute the input impedance matrix $ZnP_s$ of the SP. Finally, the input admittance matrix $YnP_s$ is computed by taking the inverse of $ZnP_s$:

$$YnP_s = {ZnP_s}^{-1} = \begin{bmatrix} Z_{11} & Z_{12} & \cdots & Z_{1n} \\ Z_{21} & Z_{22} & \cdots & Z_{2n} \\ \vdots & \vdots & \ddots & \vdots \\ Z_{n1} & Z_{n2} & \cdots & Z_{nn} \end{bmatrix}^{-1}. \tag{10}$$

Notice that the obtained $ZnP_s$ can be directly applied to an MNA solver if the nodes in the MNA representation share the same definition as the nodes in the $Z$-matrix, which is commonly found in partial element equivalent circuit (PEEC) formulation [Cao et al., 2015, 2016, 2017].

Table 1. Notation summary.

| | |
|---|---|
| $YnP_s$ | The input admittance matrix of the SP through the SP/RP junctions, i.e. the loading effect of the SP |
| $YnP_r$ | The input admittance matrix of the RP through the SP/RP junctions, i.e. the loading effect of the RP |
| $I^{src}$ | The initial current source in Norton's model. One of the primary sources. |
| $Z^{src}$ | The source impedance in Norton's model |
| $I_s^{(0)}$ | The initial current on the SP |
| $I_r^{(0)}$ | The initial current on the RP |
| $i$ | The index of iteration, $i = 1, 2, \cdots$ |
| $I_{s2r}^{(0)}$ | The initial current conducting through the SP/RP junctions. Subscript $s2r$ indicating current flows from the SP to RP. One of the secondary sources. |
| $I_s^{(i)}$ | The total current increment on the SP after the $i$th iteration |
| $I_{sr}^{(i)}$ | The current increment on the SP due to field coupling from the RP in the $i$th iteration |
| $I_{ss}^{(i)}$ | The current increment on the SP due to current conducting through the SP/RP junctions in the $i$th iteration |
| $I_r^{(i)}$ | The total current increment on the RP after the $i$th iteration |
| $I_{rs}^{(i)}$ | The current increment on the RP due to field coupling from the SP in the $i$th iteration |
| $I_{rr}^{(i)}$ | The current increment on the RP due to current conducting through the SP/RP junctions in the $i$th iteration |
| $V_s^{(i)}$ | The induced voltage sources on the SP due to field couplings from the RP in the $i$th iteration. One of the primary sources. |
| $V_r^{(i)}$ | The induced voltage sources on the RP due to field couplings from the SP in the $i$th iteration. One of the primary sources. |
| $I_{s2r}^{(i)}$ | The current conducting through the SP/RP junctions in the $i$th iteration. Subscript $s2r$ indicating current flows from the SP to RP. One of the secondary sources. |
| $I_{r2s}^{(i)}$ | The current conducting through the SP/RP junctions in the $i$th iteration. Subscript $r2s$ indicating current flows from the RP to SP. One of the secondary sources. |
| $I_s^{final}$ | The final total current on the SP |
| $I_r^{final}$ | The final total current on the RP |

## 5. FLOWCHART OF THE GMS METHOD

The flowchart of the GMS method is given in Fig. 7. All the employed notations are documented in Table 1. There are eight total steps in the GMS method; note that Steps 3 to 6 constitute one iteration, which is also called one scattering in this paper since each iteration contains one scattering process of EM waves. Details of the flowchart are described as follows.

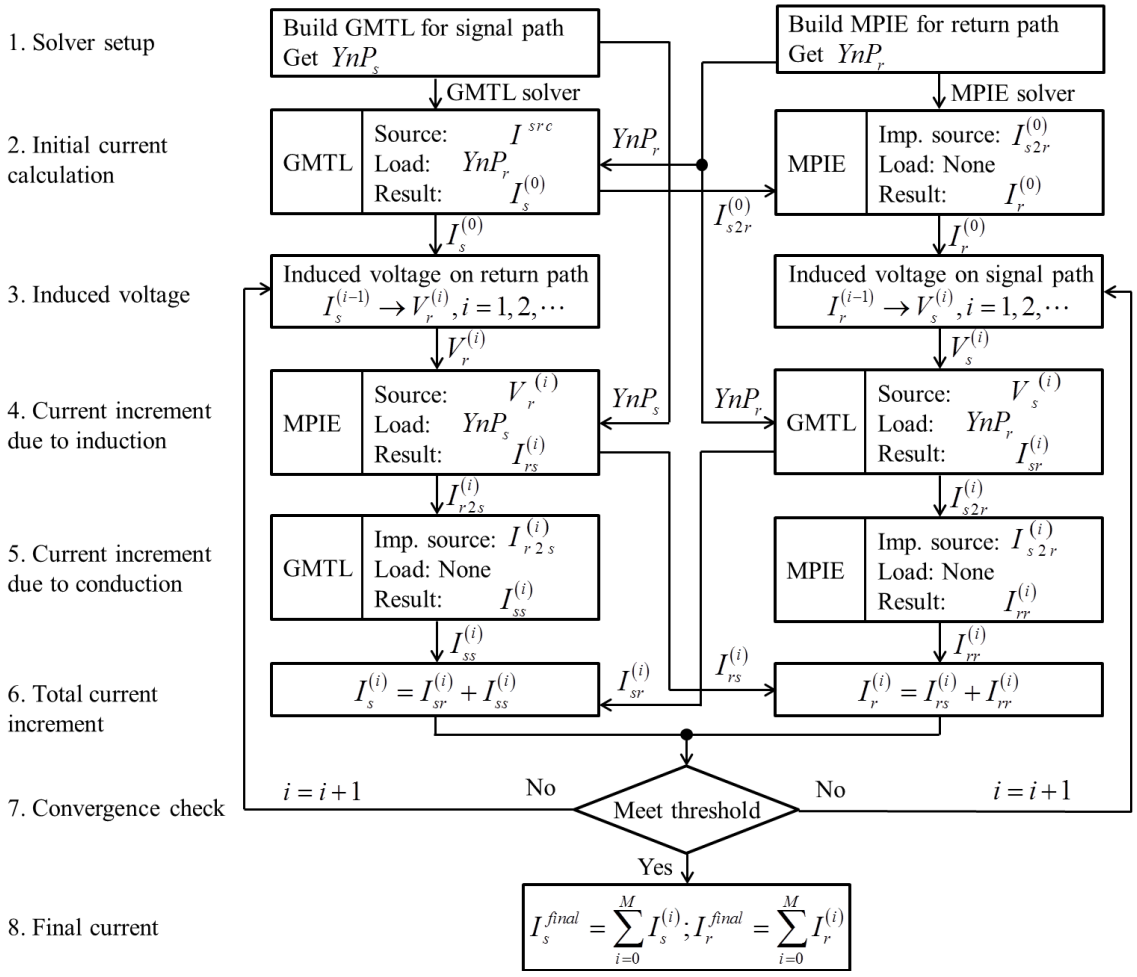


Figure 7. Flowchart of the GMS approach.

Step 1: Solver setup.

Read in the geometry of the structure and set up the GMTL solver for the SP and the MPIE solver for the RP. Obtain $YnP_r$ and $YnP_s$ according to the methods in Section III and IV, respectively.

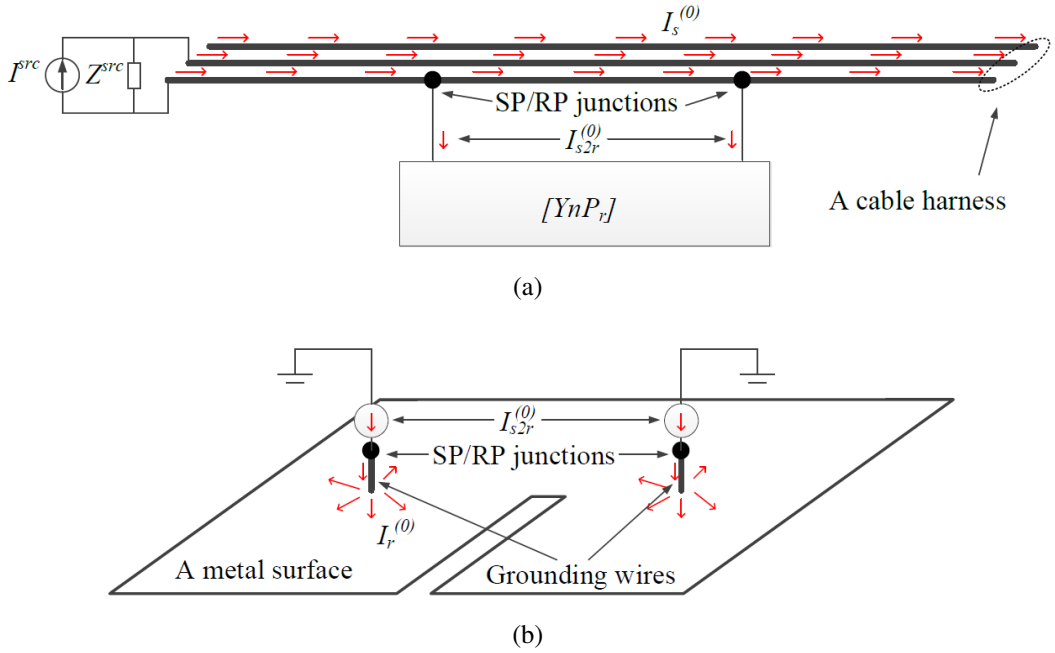


Figure 8. Initial current calculation for (a) the SP and (b) the RP.

Step 2: Initial current calculation.

As shown in Fig. 8 (a), excite the SP by applying the Norton's equivalent source model to the GMTL solver loaded with $YnP_r$. Obtain the initial currents $I_s^{(0)}$ on the SP. Currents conducting through the SP/RP junctions are denoted as $I_{s2r}^{(0)}$, whose subscript indicates currents conducting from the SP to the RP. As illustrated in Fig. 8 (b), these currents excite the RP by applying $I_{s2r}^{(0)}$ to the MPIE solver without loading the $YnP_s$. Obtain the initial currents $I_r^{(0)}$ on the RP.

Step 3: Induced voltage.

Currents on the SP $I_s^{(i-1)}$ cause field couplings to the RP, which further give rise to the induced voltage sources on the RP $V_r^{(i)}$. Similarly, currents on the RP $I_r^{(i-1)}$ lead to field couplings to the SP, which further induce the voltage sources on the SP $V_s^{(i)}$. Notice, $i = 1, 2, \ldots$ indicates the index of iterations. The calculation methods are found in [Wang et al., 2018].

Step 4: Current increment due to induction.

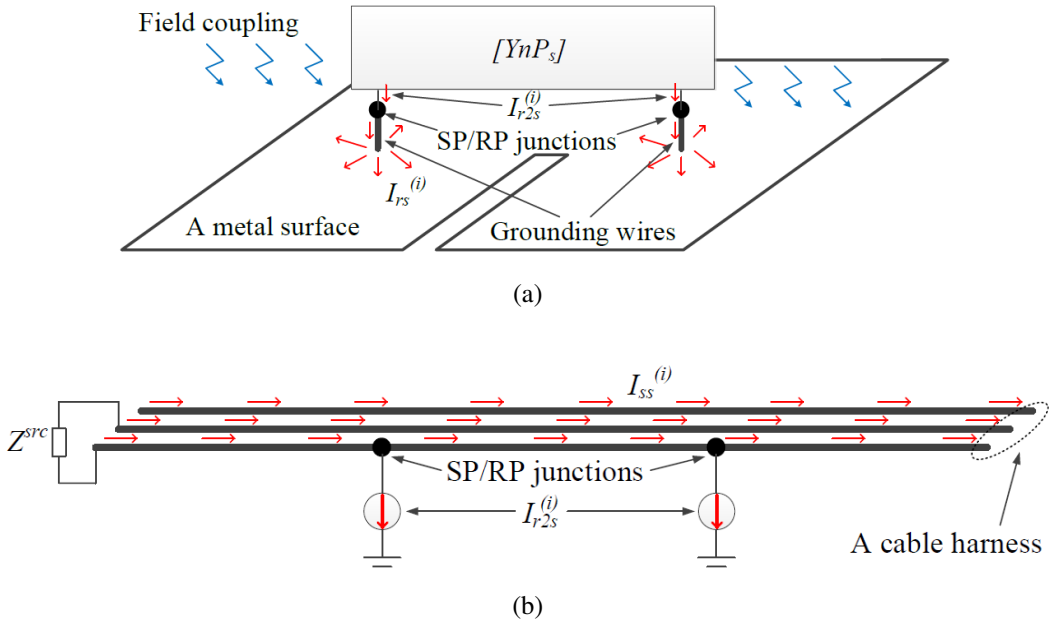


Figure 9. Field couplings from the SP to the RP lead to $V_r^{(i)}$, which further causes (a) currents flowing on the RP $I_{rs}^{(i)}$, and (b) currents conducting to the SP $I_{ss}^{(i)}$.

As shown in Fig. 9 (a), the RP is excited by the field couplings, i.e., applying the induced voltage $V_r^{(i)}$ to the MPIE solver with $YnP_s$ loaded. Obtain the induced currents on the RP $I_{rs}^{(i)}$ and the conduction currents $I_{r2s}^{(i)}$ injected into the SP through the SP/RP junctions. The first $r$ in the subscript of $I_{rs}^{(i)}$ indicates the currents are induced on the RP; the second $s$ in the subscript of $I_{rs}^{(i)}$ indicates the induced currents are caused by the currents on the SP in Step 3.

Similarly in Fig. 10 (a), the SP is excited by the field couplings, i.e., applying the induced voltage $V_s^{(i)}$ to the GMTL solver with $YnP_r$ loaded. Obtain the induced currents on the SP $I_{sr}^{(i)}$ and the conduction currents $I_{s2r}^{(i)}$ injected into the RP through the SP/RP junctions.

Step 5: Current increment due to conduction.

As illustrated in Fig. 9 (b), the obtained $I_{r2s}^{(i)}$ in the previous step conducts to the SP. In order to calculate the current distribution on the SP due to $I_{r2s}^{(i)}$, i.e. $I_{ss}^{(i)}$, apply $I_{r2s}^{(i)}$ to the GMTL solver without loading $YnP_r$. Notice that the first $s$ in the subscript of $I_{ss}^{(i)}$ indicates the currents are defined on the SP and that the second $s$ in the subscript of $I_{ss}^{(i)}$ indicates the obtained currents are originally caused by the currents on the SP in Step 3.

As illustrated in Fig. 10 (b), the obtained $I_{s2r}^{(i)}$ in the previous step conducts to the RP. In order to compute the current distribution on the RP due to $I_{s2r}^{(i)}$, i.e., $I_{rr}^{(i)}$, apply $I_{s2r}^{(i)}$ to the MPIE solver without loading $YnP_s$.

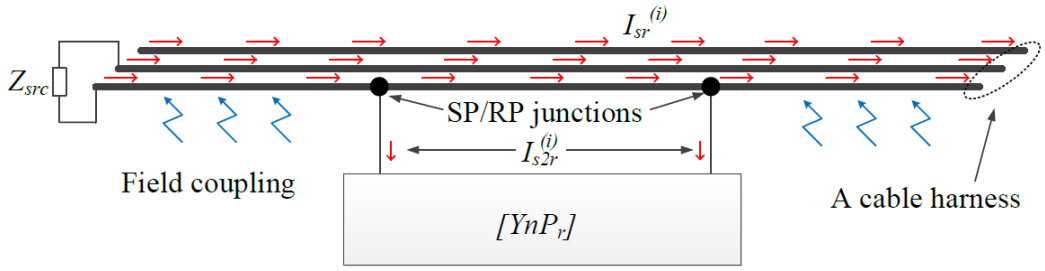


(a)

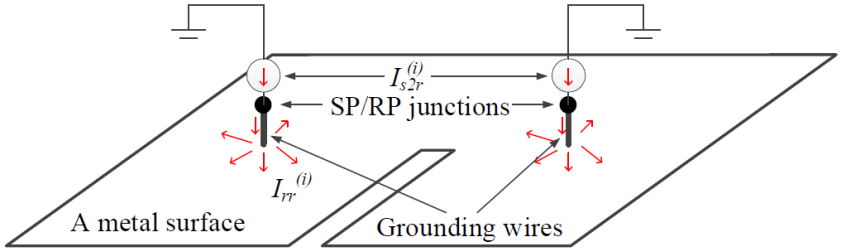


(b)

Figure 10. Field couplings from the RP to the SP result in $V_s^{(i)}$, which further gives rise to (a) currents flowing on the SP $I_{sr}^{(i)}$, and (b) currents conducting to the RP $I_{rr}^{(i)}$.

Step 6: Total current increment.

Combining Steps 4 and 5 during the $i$th iteration, the total current increment on the SP is $I_s^{(i)} = I_{sr}^{(i)} + I_{ss}^{(i)}$; the total current increment on the RP is $I_r^{(i)} = I_{rs}^{(i)} + I_{rr}^{(i)}$.

Step 7: Convergence check.

The total current on the SP after $N$ iterations is $I_s = \sum_{i=0}^{N} I_s^{(i)}$. If the maximal current increment on each wire in the $N$th iteration is less than a certain level (e.g., 5%) of the peak value of the total current on the same wire, the iteration stops and the GMS process continues to Step 8. Otherwise, the GMS process goes on to Step 3 and sets i = i+1. Notice that it is the current increments that are applied to induce $V_r^{(i)}$ and $V_s^{(i)}$ in the following scattering process.

Step 8: Final current.

If it converges after $M$ iterations, the final current on the SP is $I_s^{final} = \sum_{i=0}^{M} I_s^{(i)}$ and the final current on the RP is $I_r^{final} = \sum_{i=0}^{M} I_r^{(i)}$.

## 6. NUMERICAL VALIDATION

To validate the GMS approach on evaluating the current response on a cable harness with ground connections to a nearby metal surface, a test case is created as shown in Fig. 11 with detailed information of geometries, terminations, and excitations. The test case contains four wires and a slotted surface beneath the wire structure. Wire 1 is grounded to the metal surface at two locations on either side of the slot. The cross-sectional view of the whole structure is illustrated in Fig. 11 (b).

Following the flowchart of the GMS approach as described in Fig. 7, the final currents on the cable harness can be obtained. The reference results are computed using the MPIE solver for the whole structure. According to the IEEE standard for validation of computational electromagnetics, computer modeling and simulation [45, 2008], a proper validation can be conducted based on the Feature Selective Validation (FSV) technique

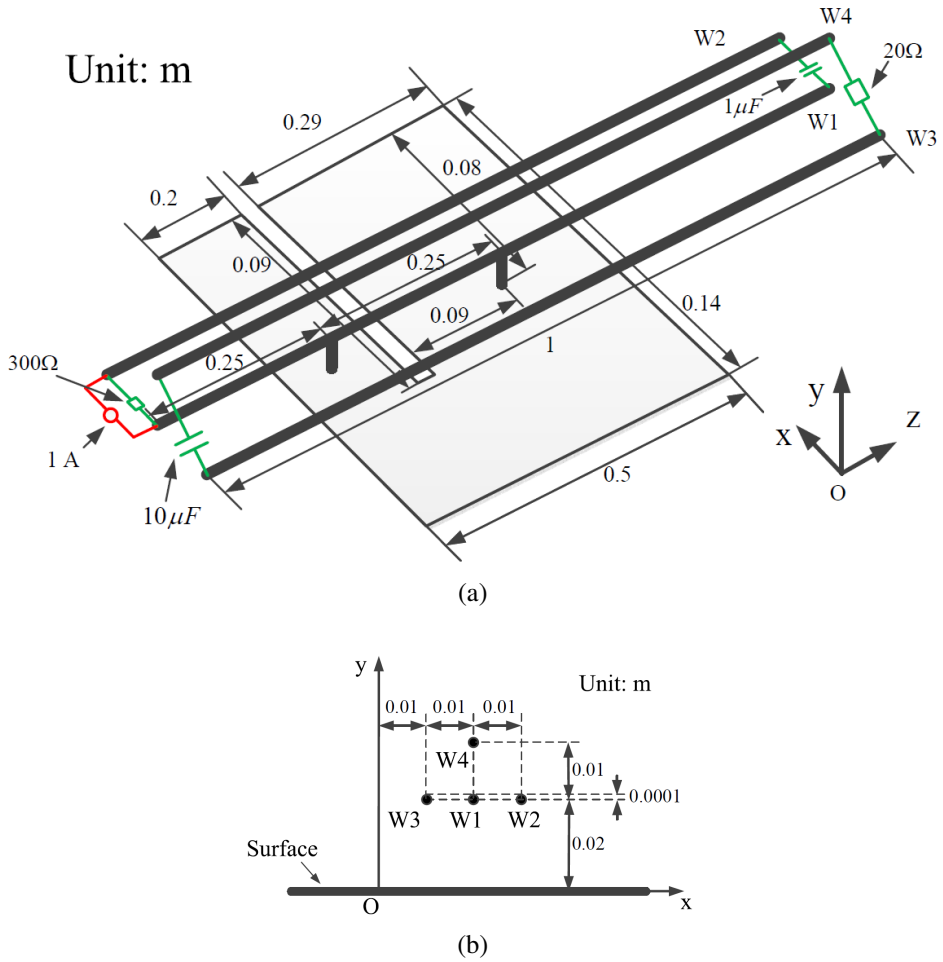


Figure 11. A test case to benchmark the GMS approach: (a) 3-D view with detailed information of geometries, terminations and excitations, and (b) the cross-sectional view. W is short for wire.

[Duffy et al., 2006, Orlandi et al., 2006]. Without the loss of generality, currents on Wire 1, 2, and 3 are compared in Fig. 12 at 800 MHz. From Fig. 12, it is observed that the initial currents without iterations are far different from the reference results. Therefore, it is indispensable to apply the GMS in order to obtain more accurate results. Also from Fig. 12, the computed currents converge after three iterations, and the converged currents match well with the reference results. Abrupt changes of the current distributed on Wire 1 can be found at the locations of -0.25 m and 0 m in Fig. 12 (a) and (b), which are due to the grounding wires. Currents on Wire 1 significantly differ from those on Wire 2, which

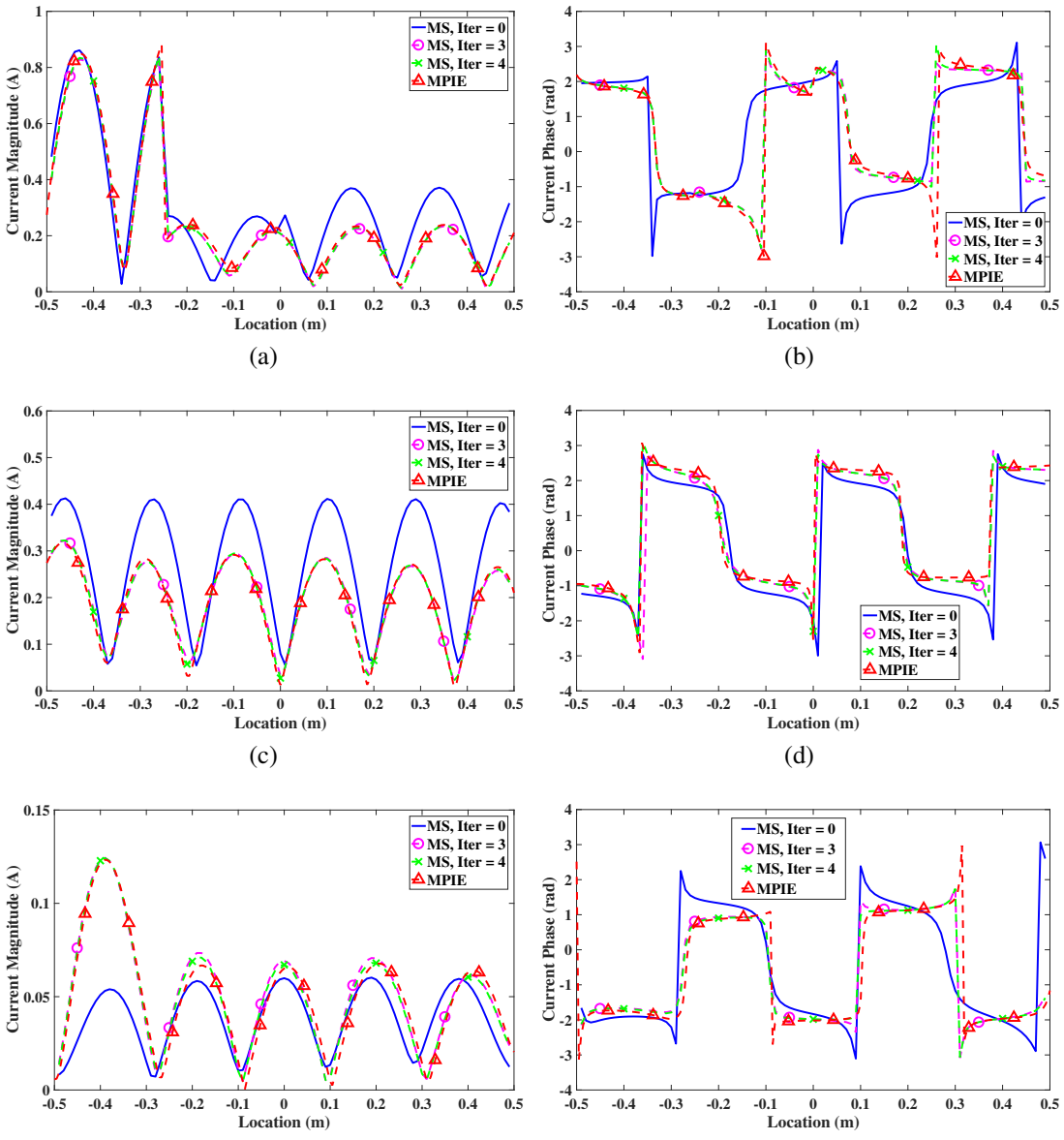


Figure 12. At 800 MHz, (a) magnitude and (b) phase of the currents on Wire 1, (c) magnitude and (d) phase of the currents on Wire 2, and (e) magnitude and (f) phase of the currents on Wire 3.

indicates antenna-mode currents dominating on Wire 1 and 2. The number of mesh cells used in the GMS and the MPIE solvers are listed in Table 2. Less mesh cells are required

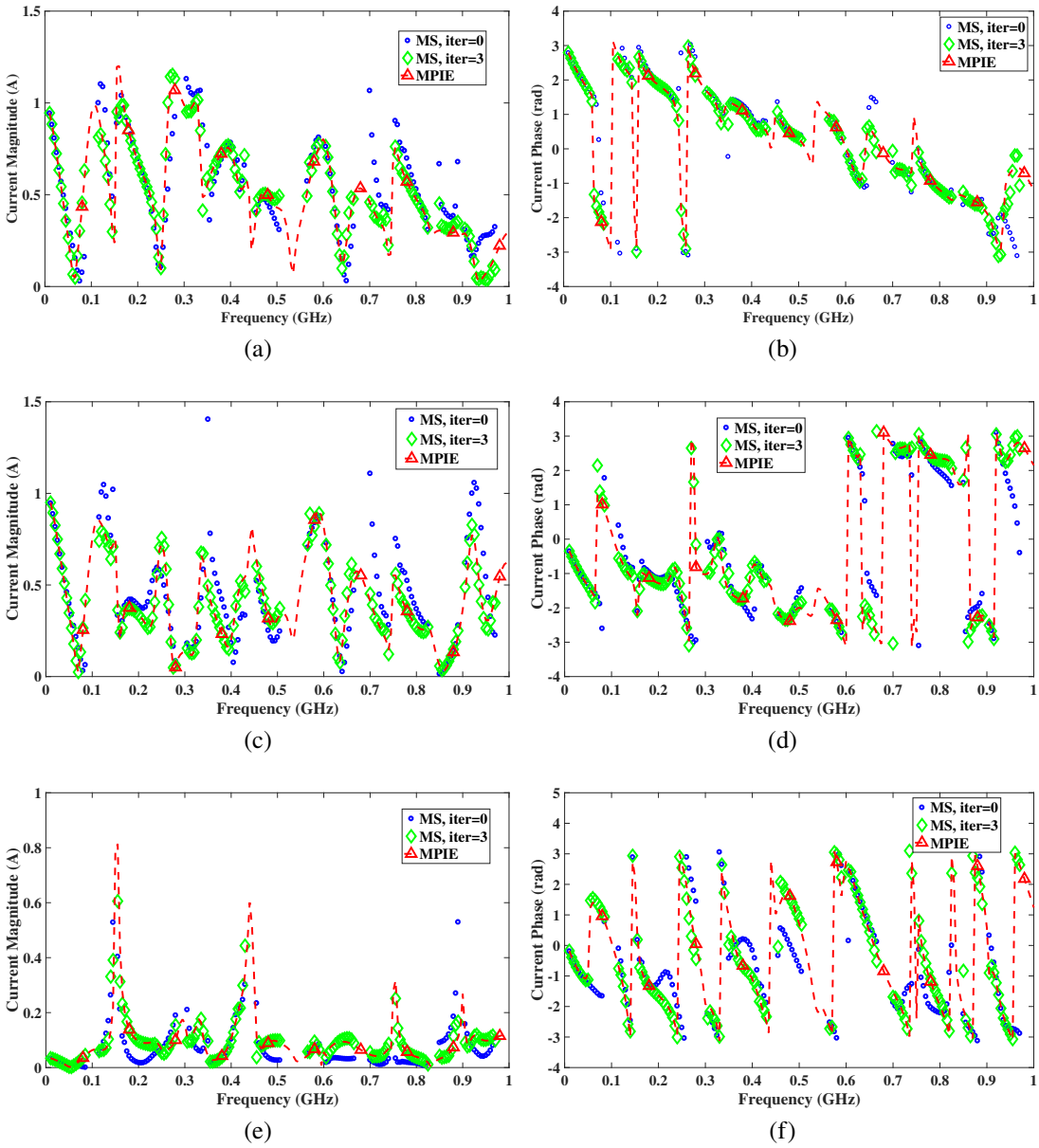


Figure 13. From 10 MHz to 1 GHz, (a) magnitude and (b) phase of the currents at -0.3 m of Wire 1, (c) magnitude and (d) phase of the currents at -0.3 m of Wire 2, and (e) magnitude and (f) phase of the currents at -0.3 m of Wire 3.

in the GMS method to achieve similar accuracy compared to the reference MPIE solver. The reduction in mesh cells will be more phenomenal in cases with more complex wire structures.

Table 2. Mesh cells used in the GMS and the MPIE solvers.

| Mesh cells | SP | RP |
|---|---|---|
| GMS | 400 | 100 |
| MPIE | 840 | 100 |

Current vs. frequency at the location of -0.3 m of Wire 1, 2 and 3 are compared in Fig. 13. The obtained currents by the GMS approach correlate well with the reference results. It should be noted that some frequency points (0.15, 0.3, 0.45, 0.6, 0.75, and 0.9 GHz) are skipped in Fig. 13, since the GMTL method doesn't converge at these frequency points and thus leads to inaccurate results. These frequency points correspond to the natural resonant frequencies of the wires. In other words, when the wire length is a multiple integer of a half wavelength, the GMTL method fails [Bayram and Volakis, 2005]. To resolve the issue in future work, additional loss terms may be added either lumped at the ends of the wires [Middelstaedt et al., 2016] or distributed along the wires [Chabane et al., 2017].

## 7. CONCLUSIONS

In this paper, co-simulation of a cable harness with ground connections to a nearby metal surface is conducted by the GMS method in two parts: the SP and the RP. The SP is solved by the GMTL solver, while the RP is handled by the MPIE solver. Neither the GMTL nor the MPIE solver alone takes into account the mutual interactions between the SP and the RP. To account for these interactions, an iterative scheme is arranged in the GMS method. Each iteration physically represents the scattering process of EM waves. The abovementioned interactions take place via not only field couplings, but also current conducting through the SP/RP junctions. In the studied test case where four wires are set above a slotted surface, only three iterations are required before the currents converge and the converged currents match well with the reference results. This test case validates the

proposed GMS approach for the co-simulation. Although not specifically demonstrated, the GMS approach can be generally applied to cases with more complicated surface structures, since the RP is solved by a mature algorithm, the MoM.

There are some limitations for the proposed GMS method, which essentially result from the limitations of the GMTL solver. First, an upper frequency limit exists for the GMTL solver. Beyond this upper frequency limit, the GMTL solver does not generate an accurate current. This upper frequency may be limited by the maximal wire separation and length. But this requires further investigation. Second, the GMTL solver can only be used to analyze multiple straight thin wires. Future effort is needed to extend the GMTL approach to bent, curved, and arbitrarily oriented wires. For thick wire cases where non-uniform current distribution and proximity effects should be considered, the modal decomposition method [Jin, 2017, Jin et al., 2018] can be employed to extract pul $L$ and $C$. Finally, as mentioned, the GMTL solver fails at wire natural resonance frequencies and future effort can be expended to resolve the issue.

## REFERENCES

IEEE standard for validation of computational electromagnetics computer modeling and simulations. *IEEE Std 1597.1-2008*, pages c1–41, 2008.

I. Badzagua, H. Chobanyan, G. Chikovani, I. Oganezova, E. Yavolovskaya, T. Injgia, A. Gheonjian, and R. Jobava. Effective computational techniques for EMC analysis of cable harness. *Proceedings of the 2010 International Seminar/Workshop on Direct and Inverse Problems of Electromagnetic and Acoustic Wave Theory*, pages 96–102, Sep. 2010.

H. Bagci, A.E. Yilmaz, J. Jin, and E. Michielssen. Fast and rigorous analysis of EMC/EMI phenomena on electrically large and complex cable-loaded structures. *IEEE Trans. Electromagn. Compat.*, 49(2):361–381, May 2007.

Y. Bayram and J. L. Volakis. A generalized MoM-SPICE iterative technique for field coupling to multiconductor transmission lines in presence of complex structures. *IEEE Trans. Electromagn. Compat.*, 47(2):234–246, May 2005.

Y. S. Cao, L. Jiang, and A. E. Ruehli. Distributive radiation and transfer characterization based on the PEEC method. *IEEE Trans. Electromagn. Compat.*, 57(4):734–742, Aug. 2015.

Y. S. Cao, L. Jiang, and A. E. Ruehli. An equivalent circuit model for graphene-based terahertz antenna using the PEEC method. *IEEE Trans. Antenna Propag.*, 64(4): 734–742, Apr. 2016.

Y. S. Cao, P. Li, L. Jiang, and A. E. Ruehli. The derived equivalent circuit model for magnetized anisotropic graphene. *IEEE Trans. Antenna Propag.*, 65(2):948–953, Feb 2017.

S. Chabane, P. Besnier, and M. Klingler. A modified enhanced transmission line theory applied to multiconductor transmission lines. *IEEE Trans. Electromagn. Compat.*, 59(2):518–528, Apr. 2017.

Cheever. All of cheever's MNA pages condensed into one. *[Online]: http://www.swarthmore.edu/NatSci/echeeve1/Ref/mna/MNA_All.html*.

A. G. Chiariello, A. Maffucci, G. Miano, F. Villone, and W. Zamboni. A transmission-line model for full-wave analysis of mixed-mode propagation. *IEEE Trans. Adv. Packag.*, 31(2):275–284, May 2008.

H. Chobanyan, I. Badzagua, T. Injgia, A. Gheonjian, and R. Jobava. Application of hybrid MOM/MTL method to simulation of interaction between cable harness and antennas. *Proceedings of the 2009 International Seminar/Workshop on Direct and Inverse Problems of Electromagnetic and Acoustic Wave Theory*, pages 33–38, Sep. 2009.

A.P. Duffy, A.J.M. Martin, A. Orlandi, G. Antonini, T.M. Benson, and M.S. Woolfson. Feature selective validation (FSV) for validation of computational electromagnetics (CEM). part i - the FSV method. *IEEE Trans. Electromagn. Compat.*, 48(3):449–459, Aug. 2006.

J. Fan, H. Shi, A. Orlandi, J. L. Knighten, and J. L. Drewniak. Modeling DC power-bus structures with vertical discontinuities using a circuit extraction approach based on a mixed-potential integral equation formulation. *IEEE Trans. Adv. Packag.*, 24(2): 143–157, May 2001.

J. Fan, J. L. Drewniak, and J. L. Knighten. Lumped-circuit model extraction for vias in multilayer substrates. *IEEE Trans. Electromagn. Compat.*, 45(2):272–280, May 2003.

S. Jin. Modal based bga modeling in high-speed package. *Ph.D. dissertation, MST, Rolla, MO*, 2017.

S. Jin, D. Liu, Y. Wang, B. Chen, and J. Fan. Parallel plate impedance and equivalent inductance extraction considering proximity effect by a modal approach. *IEEE Trans. Electromagn. Compat.*, (99):1–10.

S. Jin, D. Liu, B. Chen, K. Qiu, J. Lin, R. Brooks, and J. Fan. Analytical equivalent circuit modeling for BGA in high-speed package. *IEEE Trans. Electromagn. Compat.*, 60 (1):68–76, Feb. 2018.

D. Liu. Common mode current estimation for cable bundle inside a vehicle. *Ph.D. dissertation, MST, Rolla, MO*, 2013.

D. Liu, Y. Wang, R. W. Kautz, N. Altunyurt, S. Chandra, and J. Fan. Accurate evaluation of field interactions between cable harness and vehicle body by a multiple scattering method. *IEEE Trans. Electromagn. Compat.*, 59(2):383–393, Apr. 2017.

G. Lugrin, S. V. Tkachenko, F. Rachidi, M. Rubinstein, and R. Cherkaoui. High-frequency electromagnetic coupling to multiconductor transmission lines of finite length. *IEEE Trans. Electromagn. Compat.*, 57(6):1714–1723, Dec. 2015.

A. Maffucci, G. Miano, and F. Villone. An enhanced transmission line model for conducting wires. *IEEE Trans. Electromagn. Compat.*, 46(4):512–528, Nov. 2004.

A. Maffucci, G. Miano, and F. Villone. An enhanced transmission line model for conductors with arbitrary cross sections. *IEEE Trans. Adv. Packag.*, 28(2):174–188, May 2005.

F. Middelstaedt, S. V. Tkachenko, R. Rambousky, and R. Vick. High-frequency electromagnetic field coupling to a long, finite wire with vertical risers above ground. *IEEE Trans. Electromagn. Compat.*, 58(4):1169–1175, Aug. 2016.

J. B. Nitsch and S. V. Tkachenko. High-frequency multiconductor transmission-line theory. *Found. Phys.*, 40(9):1231–1252, 2010.

J.B. Nitsch and S.V. Tkachenko. Complex-valued transmission-line parameters and their relation to the radiation resistance. *IEEE Trans. Electromagn. Compat.*, 46(3): 477–487, Aug. 2004.

A. Orlandi, A.P. Duffy, B. Archambeault, G. Antonini, D.E. Coleby, and S. Connor. Feature selective validation (FSV) for validation of computational electromagnetics (CEM). part ii - assessment of FSV performance. *IEEE Trans. Electromagn. Compat.*, 48 (3):460–467, Aug. 2006.

F. Sabath and H. Garbe. Radiation analysis of PCB layout using a hybrid mom-mtl method. *IEEE Trans. Electromagn. Compat.*, 45(2):424–435, May 2003.

S.V. Tkatchenko, F. Rachidi, and M. Ianoz. Electromagnetic field coupling to a line of finite length: theory and fast iterative solutions in frequency and time domains. *IEEE Trans. Electromagn. Compat.*, 37(4):509–518, Nov. 1995.

D. Topchishvili, R. Jobava, F. Bogdanov, B. Chikhradze, and S. Frei. A hybrid MTL/MoM approach for investigation of radiation problems in EMC. *Proceedings of the 9th International Seminar/Workshop on Direct and Inverse Problems of Electromagnetic and Acoustic Wave Theory*, pages 65–68, Oct. 2004.

A. Vukicevic, F. Rachidi, M. Rubinstein, and S. V. Tkachenko. On the evaluation of antenna-mode currents along transmission lines. *IEEE Trans. Electromagn. Compat.*, 48(4): 693–700, Nov. 2006.

Y. Wang, R. Kautz, N. Altunyurt, and J. Fan. An equivalent circuit model for the wire-to-surface junction based on method of moments. *Proc. 2016 IEEE Int. Conf. Wireless Inf. Technol. Syst. Appl. Comput. Electromagn.*, pages 1–2, 2016.

Y. Wang, D. Liu, Y. S. Cao, R. W. Kautz, N. Altunyurt, S. Chandra, and J. Fan. Evaluating field interactions between multiple wires and the nearby surface enabled by a generalized MTL approach. *IEEE Trans. Electromagn. Compat.*, 60(4):971–980, Aug. 2018.

D. Zhang, Y. Wen, Y. Wang, D. Liu, X. He, and J. Fan. Coupling analysis for wires in a cable tray using circuit extraction based on mixed-potential integral equation formulation. *IEEE Trans. Electromagn. Compat.*, 59(3):862–872, June 2017.

# III. EVALUATING THE CROSSTALK CURRENT AND THE TOTAL RADIATED POWER OF AN ARBITRARY CABLE HARNESS USING THE GENERALIZED MTL METHOD

Yansheng Wang, Ying S. Cao, Dazhao Liu, Richard Kautz, Nevin Altunyurt, and Jun Fan

## ABSTRACT

This paper presents a general formulation of the generalized multi-conductor transmission line (GMTL) method to model an arbitrary cable harness including straight and bent wires. The GMTL equations are solved recursively based on the perturbation theory. This GMTL method facilitates an efficient and accurate evaluation of the current distributed on a cable harness. On top of that, the obtained current in a radiation problem is decomposed into two traveling currents, i.e. the positive-going (PG) and the negative-going (NG) currents, based on the least-square method. With the decomposed currents, the steepest descent (SD) method is further adopted to achieve a fast approximation of the total radiated power (TRP). Last, the capability and the limitations of the GMTL method in terms of the electrical wire separation and length are investigated. The necessity of the recursive corrections is also studied.

**Keywords:** Cable harness, crosstalk, multi-conductor transmission line (MTL), steepest descent (SD) method, total radiated power (TRP).

## 1. INTRODUCTION

Cable harnesses are widely found in modern transportation systems, such as automobiles [Liu et al., 2017], high-speed trains [Zhang et al., 2017], aircrafts [Bagci et al., 2007] and etc. A cable harness is a bundle of wires which serve as the interconnects among

various electronic modules to transmit signals and power. A cable harness needs to be carefully designed and routed in order to meet strict electromagnetic compatibility (EMC) and electromagnetic interference (EMI) requirements.

To evaluate the design and routing of a cable harness, commonly used metrics include the current distribution, the crosstalk current, the total radiated power (TRP) and etc. These metrics can be obtained through either measurements or simulations. However, the measurements are usually inconvenient and costly to realize [Li, 2015, Sun et al., 2007]. Simulation-wise, a cable harnesss is usually modeled using either full-wave methods, like method of moments (MoM) [Wang et al., 2016, Zhang et al., 2017] and partial element quivalent circuit (PEEC) method [Nitsch et al., 2009], or the transmission line (TL) theory [Badzagua et al., 2010, Paul, 2007]. Full-wave methods compute the current distribution on a cable harness with great accuracy but consume large memory and need long simulation time. An alternative approach to model a cable harness is based on the TL theory. The TL theory simplifies the modeling of a cable harness and the computation of the current distribution.

Over the past decades, several TL based methods were developed. [Nitsch and Tkachenko, 2010, 2004] derived the full-wave TL theory that could be applied to a set of thin wires. [Chiariello et al., 2008] described a generalized TL model to study the high-frequency mixed-mode propagation along electrical interconnects. [Tkatchenko et al., 1995] applied a recursive procedure based on the perturbation theory to evaluate the electric currents and potentials on a single wire above a perfect conducting ground. The derivation in [Cooray et al.] accounted for the effects of finitely conducting ground on a single wire. [Lugrin et al., 2015] presented an approach to model the multi-conductor transmission line (MTL) with arbitrary terminations. This approach was still applicable even if the TL approximation conditions no longer held. However, all these proposed methods assume an infinitely large ground plane beneath the wires, which prevents these methods from practical applications since the reference plane beneath the wires inside a modern transportation system, is usually

of irregular shape, limited size, and arbitrary discontinuities such as slots, holes, wedges, etc. The methods discussed in [Liu et al., 2017, Maffucci et al., 2004, 2005, Vukicevic et al., 2006] were not restricted by the reference plane. Nevertheless, these papers only derived TL parameters between two conductors. These derivations are not applicable in real situations where multiple wires exist. The generalized MTL (GMTL) method proposed in [Wang et al., 2018a,b] overcame the abovementioned issues by enforcing all wires to refer to the infinity. However, all the abovementioned TL based methods are only applicable for straight wires. These methods don't support bent cable harnesses. To resolve this issue, this paper presents a general formulation of the GMTL method to cover both straight and bent wires.

With GMTL method, the distributed current on a cable harness is obtained. On top of that, it is of great interest to compute the total radiated power (TRP), which evaluates the radiation capability of a radiator [Cao et al., 2017]. There are several approaches to calculate the TRP of a cable harness. In[Li et al., 2015], the Green's function (GF) method was directly applied to compute the radiated field from the distributed current on a cable harness. An integral of the obtained radiated field led to the TRP. The GF method is straight-forward but inefficient. In [Cao et al., 2015], an efficient TRP calculation method based on the PEEC formulation was presented. However, this method cannot be applied in MTL based formulations. Another approach to compute the TRP was to subtract the ohmic power loss from the input power, which was implemented in EMC studio [EMCoS]. This method requires a good knowledge of the excitations and the terminations. Nevertheless, a cable harness in practice is terminated by complex loading networks that are difficult to characterize. Therefore, this method is not helpful in real applications. In this paper, an accurate and efficient approach based on the obtained current on a cable harness is developed to approximate the TRP. The obtained current is first decomposed into two traveling currents, i.e. the positive-going (PG) and the negative-going (NG) currents, based on the least-square

method. With the decomposed currents, the steepest descent (SD) method [Li and Fan, 2016, Nakamura et al., 1995] is further adopted to facilitate the radiated field and the TRP calculation.

Though the GMTL method has already been applied in previous works [Wang et al., 2018a,b], the capability and limitations of the method are not clear to readers. In this paper, these questions are answered by investigating two parameters, i.e. the electrical wire separation and length. Besides, since the GMTL equations are solved recursively based on the perturbation theory [Tkatchenko et al., 1995], the necessity of the recursive corrections are studied in terms of the accuracy of the crosstalk current and TRP.

The paper is organized as follows. In Section II, a general formulation of the GMTL method is developed to cover both straight and bent cable harnesses. In section III, the TRP from an arbitrary cable harness is approximated based on the SD method. In Section IV, the capability and limitations of the GMTL method are discussed. Conclusions are presented in Section V.

## 2. A GENERAL FORMULATION OF THE GMTL METHOD FOR AN ARBITRARY CABLE HARNESS

In this section, two analytical methods to extract the per-unit-length (pul) inductance (L) and capacitance (C) are presented first. The general formulation of the GMTL method for one bent wire is introduced then. After that, the general GMTL formulation is extended to multi-wire structures.

**2.1. Analytical pul L and C Extraction.** In this paper, the two analytical methods to extract the pul L and C are named 2D static and 2D dynamic pul L and C, respectively.

**2.1.1. 2D Static pul L and C.** The 2D static Green's function between wire #$i$ and #$j$ reads

$$g_{ij}^{static}(\overrightarrow{\rho},\overrightarrow{\rho}') = -\frac{1}{4\pi}\ln\left|\overrightarrow{\rho}-\overrightarrow{\rho}'\right|^2 = -\frac{1}{4\pi}\ln\rho_{ij}^2, \tag{1}$$

where $\vec{\rho}$ and $\vec{\rho}'$ are the locations of the observation and the source points, respectively. As showin in Fig. 1,

$$\rho_{ij} = \left|\vec{\rho} - \vec{\rho}'\right| = \begin{cases} a_i, & i = j \\ d_{ij}, & i \neq j \end{cases} \tag{2}$$

where $a_i$ is the radius of wire #$i$ and $d_{ij}$ is center-to-center separation between wire #$i$ and #$j$.

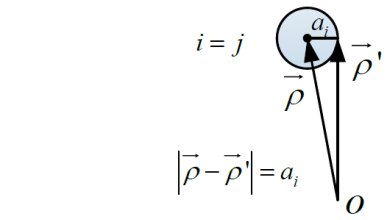


(a)

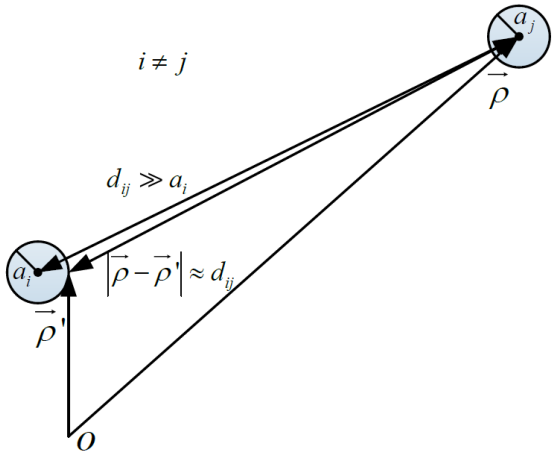


(b)

Figure 1. Cross-sectional geometry for (a) Wire $i$ and (b) Wire $i$ and $j$.

The element in the pul inductance matrix $\overline{\overline{L}}$, i.e. $L_{ij}$, is derived from the magnetic potential as shown below

$$\begin{aligned} A_i\left(\vec{\rho}\right) &= \mu \int_C J_j(\vec{\rho}')\, g_{ij}^{static}(\vec{\rho}, \vec{\rho}')\, ds \\ &= \mu \int_0^{2\pi} \frac{I_j}{2\pi a_j} \left(-\frac{1}{4\pi} \ln \rho_{ij}^2\right) a_j\, d\theta \quad , \\ &= L_{ij}^{static} I_j \end{aligned} \tag{3}$$

where

$$L_{ij}^{static} = -\frac{\mu}{4\pi} \ln \rho_{ij}^2. \tag{4}$$

Notice that a thin wire approximation is used here so that the current $I_j$ flowing on wire #$j$ is uniformly distributed around the wire surface, i.e. the line current density is $J_j(\overrightarrow{\rho}') = \frac{I_j}{2\pi a_j}$.

The pul capacitance matrix $\overline{\overline{C}}$ is the inverse of the pul electric potential coefficient matrix $\overline{\overline{K}}$, i.e.

$$\overline{\overline{C}} = \overline{\overline{K}}^{-1}. \tag{5}$$

The element of $\overline{\overline{K}}$, i.e. $K_{ij}$, is derived from the electric potential as shown below

$$\begin{aligned} \phi_i(\overrightarrow{\rho}) &= \tfrac{1}{j\omega\varepsilon} \int_C \tfrac{dJ_j(\overrightarrow{\rho}')}{dl'} g_{ij}^{static}(\overrightarrow{\rho}, \overrightarrow{\rho}') ds \\ &= \tfrac{1}{j\omega\varepsilon} \int_0^{2\pi} \tfrac{1}{2\pi a_j} \tfrac{dI_j}{dl'} \left( -\tfrac{1}{4\pi} \ln \rho_{ij}^2 \right) a_j d\theta \ , \\ &= \tfrac{1}{j\omega} K_{ij}^{static} \tfrac{dI_j}{dl'} \end{aligned} \tag{6}$$

where $l'$ is the current flowing direction which is perpendicular to the cross-section of the wires and

$$K_{ij}^{static} = -\frac{1}{4\pi\varepsilon} \ln \rho_{ij}^2. \tag{7}$$

**2.1.2. 2D Dynamic pul L and C.** The 2D dynamic Green's function between wire #$i$ and #$j$ reads

$$\begin{aligned} g_{ij}^{dynamic}(\overrightarrow{\rho}, \overrightarrow{\rho}') &= -j\tfrac{1}{4} H_0^{(2)} \left( k \left| \overrightarrow{\rho} - \overrightarrow{\rho}' \right| \right) \\ &= -j\tfrac{1}{4} H_0^{(2)} \left( k\rho_{ij} \right) \end{aligned} \ , \tag{8}$$

where $k$ is the wave number in free space and $H_0^{(2)}(*)$ is the Hankel function of the second kind. Replacing $g_{ij}^{static}(\overrightarrow{\rho}, \overrightarrow{\rho}')$ in (3) and (6) with $g_{ij}^{dynamic}(\overrightarrow{\rho}, \overrightarrow{\rho}')$, the elements in the 2D dynamic pul $\overline{\overline{L}}$ and $\overline{\overline{K}}$ can be obtained as

$$L_{ij}^{dynamic} = -j\frac{\mu}{4} H_0^{(2)} \left( \rho_{ij} k \right) \tag{9}$$

and

$$K_{ij}^{dynamic} = -j\frac{1}{4\varepsilon}H_0^{(2)}\left(\rho_{ij}k\right), \tag{10}$$

respectively.

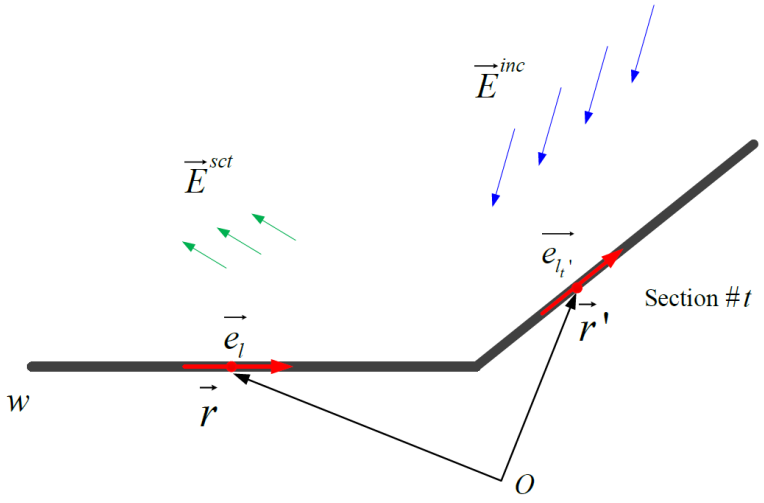


Figure 2. A single wire illuminated by incident E-field.

**2.2. The GMTL Formulation for an Arbitrary Single-Wire Structure.** As shown in Fig. 2, an arbitrary single wire is illuminated by an incident electric field (E-field) $\vec{E}^{inc}$. For a thin wire in MoM, the scattered E-field is

$$\vec{E}^{sct} = -j\omega\vec{A} - \nabla\phi, \tag{11}$$

where the vector magnetic potential $\vec{A}$ and the scalar electric potential $\phi$ are

$$\vec{A}(\vec{r}) = \mu\int_w i(\vec{r}\,')\vec{e_{l'}}g(\vec{r},\vec{r}\,')dr', \tag{12}$$

$$\phi(\vec{r}) = \frac{1}{\varepsilon}\int_w\left(-\frac{1}{j\omega}\frac{d}{dl'}i(\vec{r}\,')\right)g(\vec{r},\vec{r}\,')dr', \tag{13}$$

the free-space Green's function $g(\vec{r},\vec{r}\,')$ is

$$g(\vec{r},\vec{r}\,') = \frac{e^{-jkR}}{4\pi R}, \tag{14}$$

$$R = \left| \overrightarrow{r} - \overrightarrow{r}' \right|, \tag{15}$$

$w$ is the integral domain, $\overrightarrow{r}$ and $\overrightarrow{r}'$ indicate the observation and the source locations, respectively, $l'$ is the local wire direction at the source location $\overrightarrow{r}'$, and $\overrightarrow{e_{l'}}$ is the unit vector along the $l'$-direction at the source location $\overrightarrow{r}'$.

Applying the PEC boundary condition on the locally $l$-directed thin wire leads to

$$E_l^{sct} = -j\omega A_l - \frac{d\phi}{dl} = -E_l^{inc}. \tag{16}$$

The subscript $l$ in (16) indicates the $l$ component of a quantity. After simple manipulations of (13) and (16), the following equations are obtained

$$\begin{cases} \frac{d}{dl}\phi + j\omega A_l = E_l^{inc} \\ \phi + \frac{1}{j\omega} P = 0 \end{cases}, \tag{17}$$

where

$$A_l(\overrightarrow{r}) = \sum_{t=1}^{T} \left( \overrightarrow{e_{l_t'}} \cdot \overrightarrow{e_l} \right) \mu \int_{w_t} i(\overrightarrow{r}') g(\overrightarrow{r}, \overrightarrow{r}') dr', \tag{18}$$

$T$ is the total straight sections constituting an arbitrary cable harness, $t$ indicates the #$t$ straight section, $w_t$ indicates the #$t$ integral domain out of the total integral domain $w$, $\overrightarrow{e_{l_t'}}$ is the unit vector along the $l'$-direction at the source location $\overrightarrow{r}'$ in $w_t$, $\overrightarrow{e_l}$ is the unit vector along the $l$-direction at the observation location $\overrightarrow{r}$, and

$$P(\overrightarrow{r}) = \frac{1}{\varepsilon} \int_w \frac{d}{dl'} i(\overrightarrow{r}') g(\overrightarrow{r}, \overrightarrow{r}') dr'. \tag{19}$$

For clear illustrations, only two straight sections are considered in the structures shown in Fig. 2 and 3.

After adding $j\omega Li$ to both sides of the first equation in (17) and $\frac{1}{j\omega}C^{-1}\frac{d}{dl}i$ to both sides of the second equation in (17), with some manipulations, the following equations are obtained,

$$\begin{cases} \frac{d}{dl}\phi + j\omega Li = E_l^{inc} + j\omega D_1\{i\} \\ \frac{d}{dl}i + j\omega C\phi = D_2\{i\} \end{cases} \tag{20}$$

where

$$D_1\{i\} = Li - A_l, \tag{21}$$

$$D_2\{i\} = \frac{d}{dl}i - CP, \tag{22}$$

and $L$ and $C$ are the analytical pul L and C, respectively, i.e.

$(L, C) \in \left\{\left(L^{static}, C^{static}\right), \left(L^{dynamic}, C^{dynamic}\right)\right\}$.

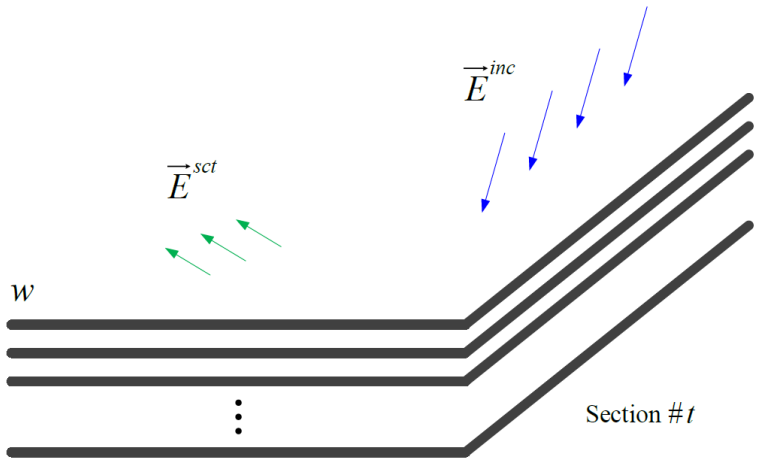


Figure 3. A multi-wire structure illuminated by incident E-field.

**2.3. Extension to a Multi-Wire Structure.** Adopting the extracted analytical pul $\overline{\overline{L}}$ and $\overline{\overline{C}}$, the following equations are constructed to compute the current distribution on an arbitrary wire structure consisting of $N$ wires,

$$\begin{cases} \frac{d}{dl}\overline{\phi} + j\omega\overline{\overline{L}}\overline{i} = \overline{E}_l^{inc} + j\omega\overline{D}_1\left\{\overline{i}\right\} \\ \frac{d}{dl}\overline{i} + j\omega\overline{\overline{C}}\overline{\phi} = \overline{D}_2\left\{\overline{i}\right\} \end{cases}, \tag{23}$$

where the electric potential $\phi$, the current $i$, and the $l$-component of the incident E-field $E_l^{inc}$ in vector format are $\overline{\phi} = \begin{bmatrix} \phi_1 \\ \phi_2 \\ \vdots \\ \phi_N \end{bmatrix}$, $\bar{i} = \begin{bmatrix} i_1 \\ i_2 \\ \vdots \\ i_N \end{bmatrix}$, and $\overline{E}_l^{inc} = \begin{bmatrix} E_{l,1}^{inc} \\ E_{l,2}^{inc} \\ \vdots \\ E_{l,N}^{inc} \end{bmatrix}$, respectively. The source correction terms

$$\overline{D}_1 \left\{ \bar{i} \right\} = \overline{\overline{L}} \bar{i} - \overline{A}_l \tag{24}$$

and

$$\overline{D}_2 \left\{ \bar{i} \right\} = \frac{d}{dl} \bar{i} - \overline{\overline{C}} \overline{P} \tag{25}$$

in (23) are used to compensate the formulation difference between the rigorous MoM and the transmission-line (TL) like method. The $n$th elements in $\overline{A}_l$ and $\overline{P}$ at the observation location $\overrightarrow{r}$ are computed as

$$A_{l,n}(\overrightarrow{r}) = \sum_{t=1}^{T} \left( \overrightarrow{e_{l'_t}} \cdot \overrightarrow{e_l} \right) \mu \int_{w_t} i(\overrightarrow{r}') g(\overrightarrow{r}, \overrightarrow{r}') dr', \tag{26}$$

and

$$P_n(\overrightarrow{r}) = \frac{1}{\varepsilon} \int_w \frac{d}{dl'} I(\overrightarrow{r}') g(\overrightarrow{r}, \overrightarrow{r}') dr', \tag{27}$$

respectively, and $n$ indicates wire #$n$. Notice that the integral domain $w_t$ includes all the $N$ wires in the #$t$ section.

The perturbation theory [Tkatchenko et al., 1995] is applied to solve (23). The beginning ($n = 0$) results $\overline{\phi}_{(0)}$ and $\overline{I}_{(0)}$ are obtained via the following equations

$$\begin{cases} \frac{d}{dl} \overline{\phi}_{(0)} + j\omega \overline{\overline{L}} \bar{i}_{(0)} = \overline{E}_l^{inc} \\ \frac{d}{dl} \bar{i}_{(0)} + j\omega \overline{\overline{C}} \overline{\phi}_{(0)} = \overline{0} \end{cases} . \tag{28}$$

The subsequent ($n \geq 1$) electric potential and current perturbations are then obtained by

$$\begin{cases} \frac{d}{dl}\overline{\phi}_{(n)} + j\omega\overline{\overline{L}}\bar{i}_{(n)} = j\omega\overline{D}_1\left\{\bar{i}_{(n-1)}\right\} \\ \frac{d}{dl}\bar{i}_{(n)} + j\omega\overline{\overline{C}}\overline{\phi}_{(n)} = \overline{D}_2\left\{\bar{i}_{(n-1)}\right\} \end{cases} . \tag{29}$$

The final solutions to (23) are

$$\overline{\phi} = \overline{\phi}_{(0)} + \overline{\phi}_{(1)} + \overline{\phi}_{(2)} + \cdots , \tag{30}$$

and

$$\bar{i} = \bar{i}_{(0)} + \bar{i}_{(1)} + \bar{i}_{(2)} + \cdots . \tag{31}$$

**2.4. A Numerical Test Case.** A numerical test case is created as shown in Fig. 4. The frequency is set to 900 MHz. The equantion (23) is applied to compute the current distributed on the wires. Both the static and the dynamic pul L and C are employed to construct the GMTL equations. Correspondingly, they are referred to as the static and the dynamic GMTL, respectively. The computation results are compared in Fig. 5. The initial result indicates the beginning current obtained by the GMTL method without recursive corrections. The final result refers to the finally converged current obtained by the GMTL method after several recursive corrections. The MPIE result serves as the reference. From Fig. 5, the beginning current on Wire 1 slightly differs from the reference result, and the beginning current on Wire 3 significantly deviates from the reference result. With two recursive corrections, the converged result is obtained. The converged currents on Wire 1 and 3 match well with the reference. The consumed time of different methods at one frequency point is compared in Table 1. According to the tabulated data, the static and the dynamic GMTL are equivalently efficient and both consume much less time than the MPIE method.

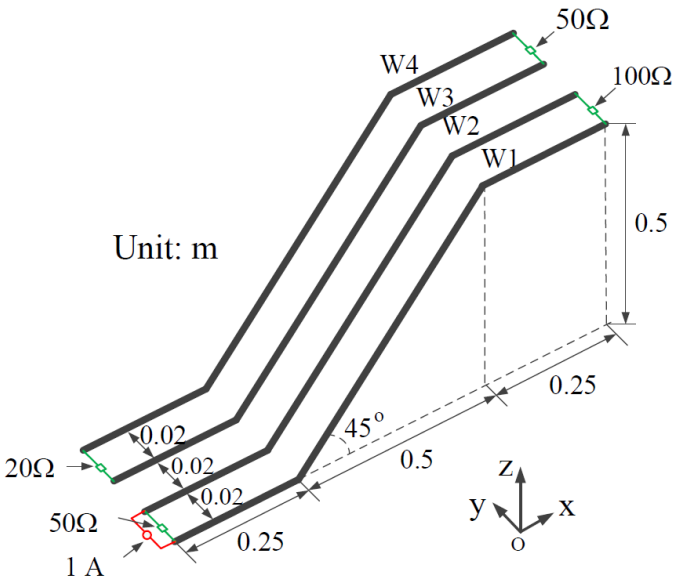


Figure 4. A bent four-wire structure with three straight sections.

Table 1. Time consumption of different methods at one frequency point.

| | Static GMTL | Dynamic GMTL | MPIE |
|---|---|---|---|
| Time (s) | 0.289 | 0.272 | 14.997 |

It can be concluded that the general formulation of the GMTL method is correct, and that both the static and the dynamic GMTL produce accurate results at a high efficiency. Since the static and the dynamic GMTL equivalently reach the accurate results, only the dynamic GMTL is employed in the following discussions.

## 3. TRP CALCULATION BASED ON THE STEEPEST DESCENT METHOD

For TRP calculation, the SD method is superior to the GF method in terms of efficiency [Li and Fan, 2016, Li et al., 2015]. However, there is only limited applications of the SD method for simple structures like a two-wire structure or a single wire above a large ground plane [Li and Fan, 2016, Li et al., 2015]. The limitation is due to a lack of proper methods to decompose the total current on a multi-wire structure with complex termination networks into traveling currents going in opposite directions. In this section,

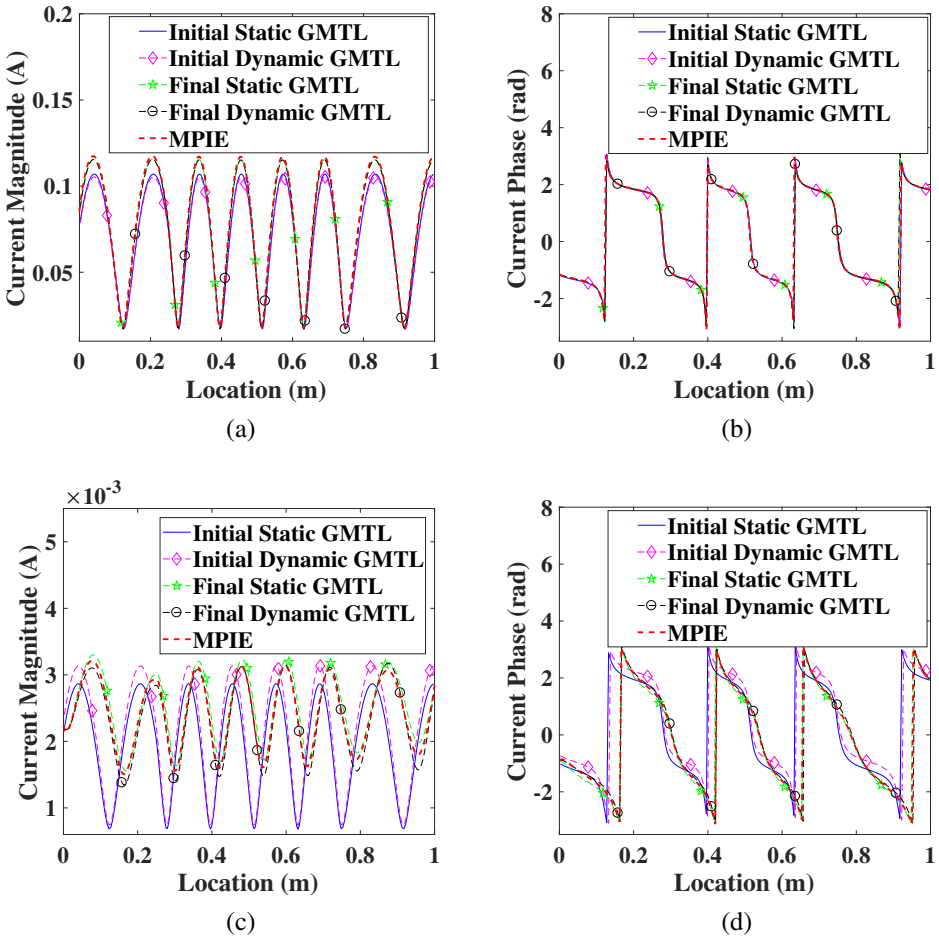


Figure 5. At 900 MHz, (a) magnitude and (b) phase of the current on Wire 1, and (c) magnitude and (d) phase of the current on Wire 3.

a current decomposition method based on the least-square method is proposed first. Next, with the decomposed currents, the radiated field and TRP are approximated using the SD method. A numerical validation follows. In this section, the TRP computed based on the GF method serves as the reference result.

**3.1. Current Decomposition.** According to the SD method proposed in [Nakamura et al., 1995], the total current obtained on each straight section of a wire first needs to be decomposed into two traveling currents: the PG and the NG currents. This can be achieved by the method described below.

The total current $I$ at the position $\overrightarrow{r}'$ of a straight section of a wire can be expressed as the summation of a PG and a NG currents, which reads

$$I\left(\overrightarrow{r}'\right) = I^{+}e^{-j\overrightarrow{\beta}\cdot\overrightarrow{r}'} + I^{-}e^{j\overrightarrow{\beta}\cdot\overrightarrow{r}'}, \tag{32}$$

where $\overrightarrow{\beta}$ is the vector of propagation constant, and $I^{+}$ and $I^{-}$ are the amplitudes of the PG and the NG currents, respectively. (32) holds at all the $m$ source locations, i.e. $\overrightarrow{r_1}'$, $\overrightarrow{r_2}'$,$\cdots$, $\overrightarrow{r_m}'$, on that straight section of the wire. Arrange (32) in the matrix representation, it reads

$$\overline{\overline{T}} \cdot \overline{c} = \overline{I}, \tag{33}$$

where

$$\overline{\overline{T}} = \begin{bmatrix} e^{-j\overrightarrow{\beta}\cdot\overrightarrow{r_1}'} & e^{j\overrightarrow{\beta}\cdot\overrightarrow{r_1}'} \\ e^{-j\overrightarrow{\beta}\cdot\overrightarrow{r_2}'} & e^{j\overrightarrow{\beta}\cdot\overrightarrow{r_2}'} \\ \vdots & \vdots \\ e^{-j\overrightarrow{\beta}\cdot\overrightarrow{r_m}'} & e^{j\overrightarrow{\beta}\cdot\overrightarrow{r_m}'} \end{bmatrix}, \tag{34}$$

$$\overline{c} = \begin{bmatrix} I^{+} \\ I^{-} \end{bmatrix}, \tag{35}$$

and

$$\overline{\overline{I}} = \begin{bmatrix} I\left(\overrightarrow{r_1}'\right) \\ I\left(\overrightarrow{r_2}'\right) \\ \vdots \\ I\left(\overrightarrow{r_m}'\right) \end{bmatrix}. \tag{36}$$

The unknown amplitudes $\overline{c}$ in (33) can be solved using the least-square method, i.e.

$$\overline{c} = \left(\overline{\overline{T}}^{*}\overline{\overline{T}}\right)^{-1}\overline{\overline{T}}^{*}\overline{I}, \tag{37}$$

where $*$ is the conjugate transpose operator.

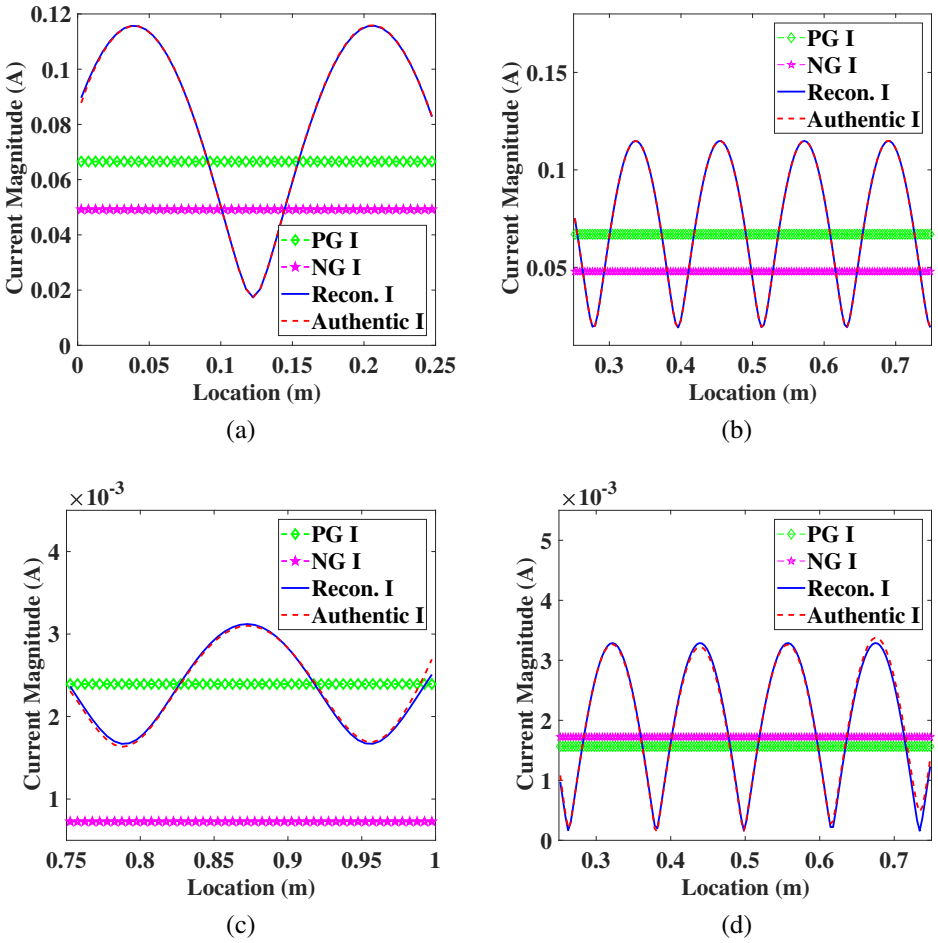


Figure 6. At 900 MHz, magnitudes of the PG current (PG I), the NG current (NG I), the reconstructed current (Recon. I) and the authentic current (Authentic I) are compared in (a) the first section on Wire 1, (b) the second section on Wire 2, (c) the third section on Wire 3, and (d) the second section on Wire 4.

Revisit the test case in Fig. 4. The authentic total current on each section of a wire is decomposed into the PG and the NG currents. The summation of the PG and the NG currents results in the reconstructed total current. All these current quantities are compared in Fig. 6. It can be seen that the least-square method works well to decompose the total current.

**3.2. TRP Approximation Based on the SD Method.** Using the SD method in [Nakamura et al., 1995], the radiated magnetic field $H_{rad}$ at the location of $\overrightarrow{r}$ can be approximated as

$$H_{rad}\left(\overrightarrow{r}\right) \approx \sum_{n=1}^{N} \frac{e^{-jkR}}{4\pi R} U_n \left(A_n + B_n\right), \tag{38}$$

where

$$A_n = \frac{\overrightarrow{e_n} \times \overrightarrow{e_R}}{\beta/k - \overrightarrow{e_n} \cdot \overrightarrow{e_R}} I_n^+ e^{-j\overrightarrow{\beta}\cdot\overrightarrow{r_n}'}, \tag{39}$$

and

$$B_n = \frac{-\overrightarrow{e_n} \times \overrightarrow{e_R}}{\beta/k + \overrightarrow{e_n} \cdot \overrightarrow{e_R}} I_n^- e^{j\overrightarrow{\beta}\cdot\overrightarrow{r_n}'}. \tag{40}$$

In (38), $n$ indicates the $n$th discontinuity point out of the $N$ total discontinuity points, $k$ is the wave number in free space, $R = \left|\overrightarrow{r} - \overrightarrow{r_n}'\right|$ is the distance between the observation point $\overrightarrow{r}$ and the $n$th discontinuity point $\overrightarrow{r_n}'$, and $U_n = \pm 1$ at the starting point and the ending point of the PG current, respectively. The observation points $\overrightarrow{r}$ locate over a sphere with a radius of $r_{sph}$ and centered at the geometric center of the cable harness under investigation. The discontinuity points refer to the bent points and the ends of the cable harness. In (39) and (40), $\overrightarrow{e_n}$ is the unit direction vector of the PG current, $\overrightarrow{e_R}$ is the unit direction vector from the $n$th discontinuity point $\overrightarrow{r_n}'$ to the observation point $\overrightarrow{r}$, and $I_n^+ e^{-j\overrightarrow{\beta}\cdot\overrightarrow{r_n}'}$ and $I_n^- e^{j\overrightarrow{\beta}\cdot\overrightarrow{r_n}'}$ are the PG and the NG currents at the $n$th discontinuity point $\overrightarrow{r_n}'$, respectively.

Further, the TRP is calculated using

$$TRP = \oiint_{\Omega} \frac{r_{sph}^2}{2} \eta |H_{rad}|^2 d\Omega, \tag{41}$$

where $\Omega$ is the solid angle over the whole observation sphere and $\eta$ is the wave impedance in free space.

**3.3. Numerical Validation.** Revisit the test case in Fig. 4. The current distributed on the cable harness is obtained by sweeping the frequency from 5 to 1000 MHz. The SD and the GF methods are applied to the GMTL current to compute the TRP. As a reference,

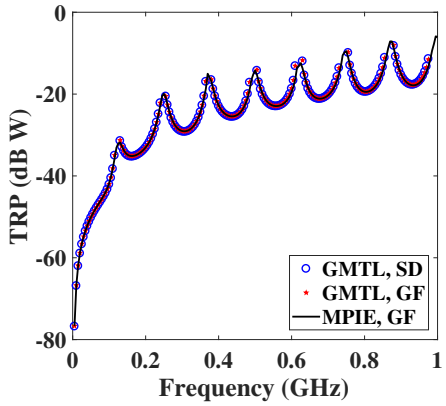


Figure 7. TRP correlation among different methods.

Table 2. Consumed time in TRP calculation using different methods at one frequency point.

| | GMTL, SD | GMTL, GF | MPIE, GF |
|---|---|---|---|
| Time (s) | 0.294 | 2.068 | 1.963 |

the GF method is also employed in the MPIE current to compute the TRP. The obtained TRPs are shown in Fig. 7. TRPs obtained by all these three approaches correlate very well, which validates the SD method. The consumed time in TRP calculation using these three approaches is compared in Table 2. According to the table, the SD method is much more efficient than the GF method.

## 4. THE CAPABILITY AND LIMITATIONS OF THE GMTL METHOD

In this section, the capability and limitations of the GMTL method are investigated through the electrical wire separation and length. Besides, the necessity of the recursive corrections is studied.

**4.1. The Electrical Wire Separation.** The electrical wire separation is defined using the ratio of the maximal wire separation $d$ over the wavelength $\lambda$, i.e. $d/\lambda$. A case is created to investigate how the current distribution and the TRP are affected by the electrical wire separation. Detailed geometry, excitation, and termination of this case are provided in Fig. 8. In this case, the maximal wire separation is 0.6 m, i.e. $d = 0.6$.

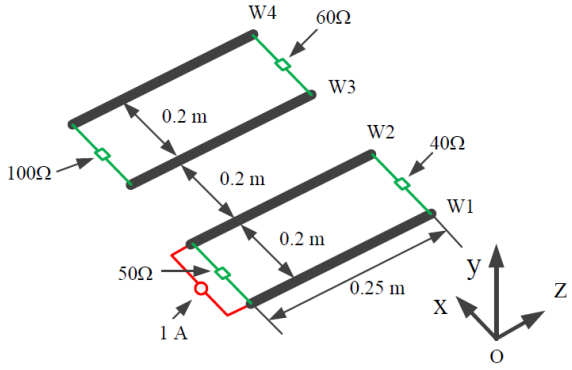


Figure 8. A four-wire case to study the electrical wire separation.

As the frequency is swept, the current magnitudes at the center of Wire 1 and 3 are recorded. The obtained currents are compared in Fig. 9. The legends in these figures are explained as follows. The initial GMTL indicates the GMTL method without any recursive correction. The final GMTL refers to the GMTL method with several recursive corrections to ensure a converged current. The MPIE stands for the reference method. Fig. 9 (b) and (d) each has two curves. The diamond line refers to the absolute current difference between the initial GMTL and the MPIE. The circle line refers to the absolute current difference between the final GMTL and the MPIE.

From Fig. 9 (b) and (d), as the electrical wire separation increases, current by the initial GMTL generally differs from the one by the MPIE. After two recursive corrections, current by the final GMTL matches well with the one by the MPIE. As shown in Fig. 9 (b), the current difference between the initial GMTL and the MPIE on Wire 1 is less than 1 dB, which is negligible. However, the current difference between the initial GMTL and

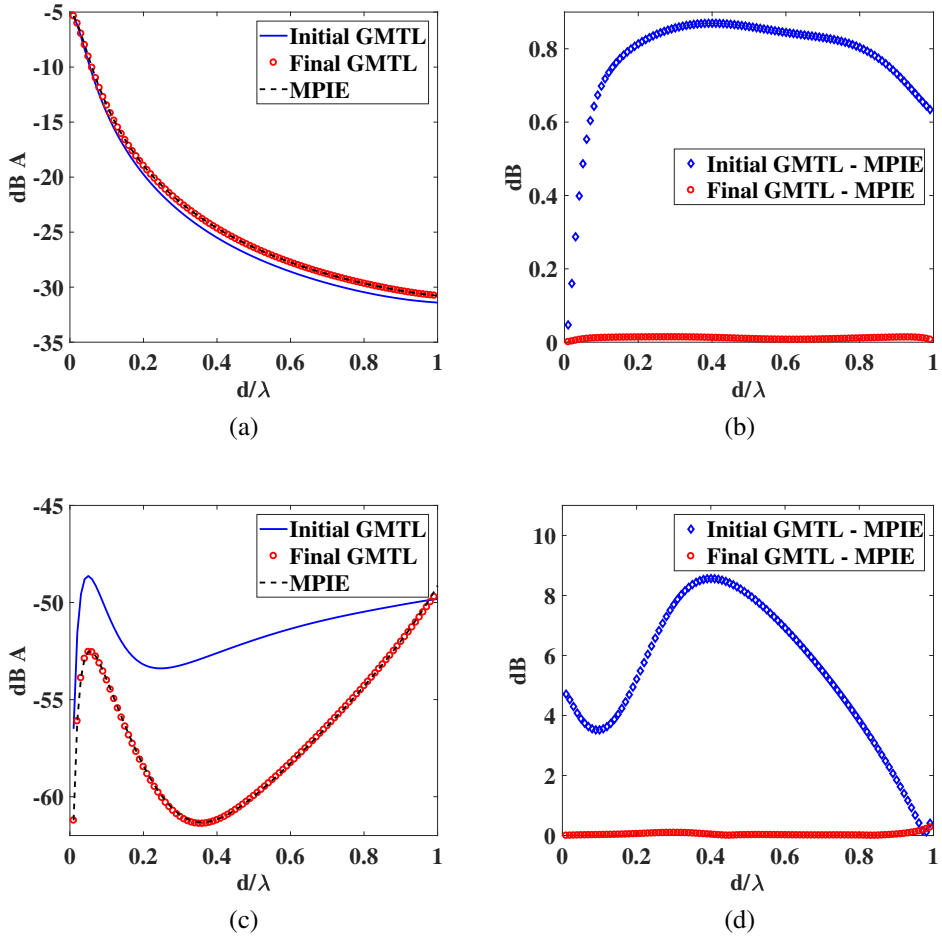


Figure 9. Current magnitude comparison at the center of Wire 1: (a) the absolute value, (b) the difference; Current magnitude comparison at the center of Wire 3: (c) the absolute value, and (d) the difference.

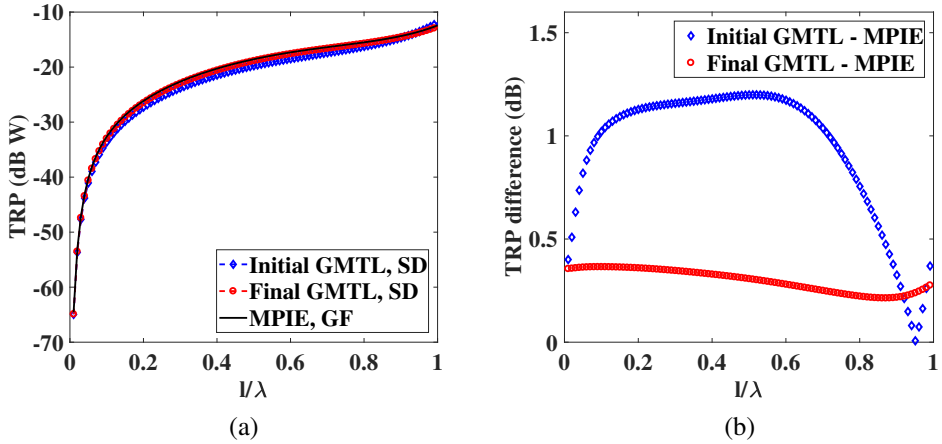


Figure 10. TRP comparison: (a) the absolute value, and (b) the difference.

the MPIE on Wire 3 is mostly larger than 3 dB as shown in 9 (d), which can not be ignored. Therefore, if the crosstalk current is of great interest, the recursive correction is required to reach an accurate result.

From Fig. 10, as the electrical wire separation increases, the TRPs of the initial GMTL and the final GMTL are similar to the reference TRP. The maximal TRP difference is between the initial GMTL and the MPIE and it is less than 1.5 dB, an negligible difference. Generally speaking, if TRP is the major concern, there is no need to conduct recursive corrections.

**4.2. The Electrical Wire Length.** The electrical wire length is defined as the ratio of the wire length $l$ over the wavelength $\lambda$, i.e. $l/\lambda$. A case is created to study how the current distribution and the TRP are affected by the electrical wire length. Detailed geometry, excitation, and termination of this case are provided in Fig. 11. In this case, the wire length is 3 m, i.e. $l = 3$, which equals to 20 wavelengths at 2 GHz. The wire separation is 4 mm, which is less than 1/30 wavelength at 2 GHz. Therefore, the effects due to the wire separation can be neglected.

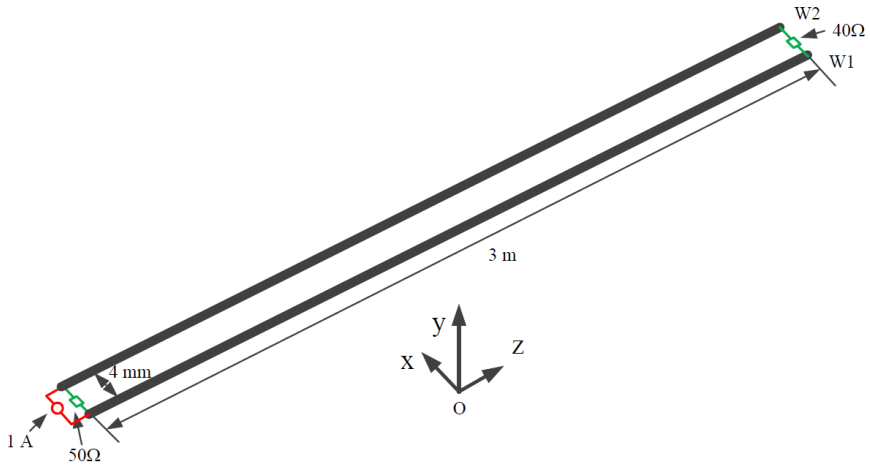


Figure 11. A two-wire case to study the electrical wire length.

As the frequency is swept, the current magnitude at the center of Wire 1 is recorded and illustrated in Fig. 12. Fig. 12 (a) is an overview of the result. Fig. 12 (b), (c), and (d) are the enlarged portions of Fig. 12 (a). From these figures, the current obtained by

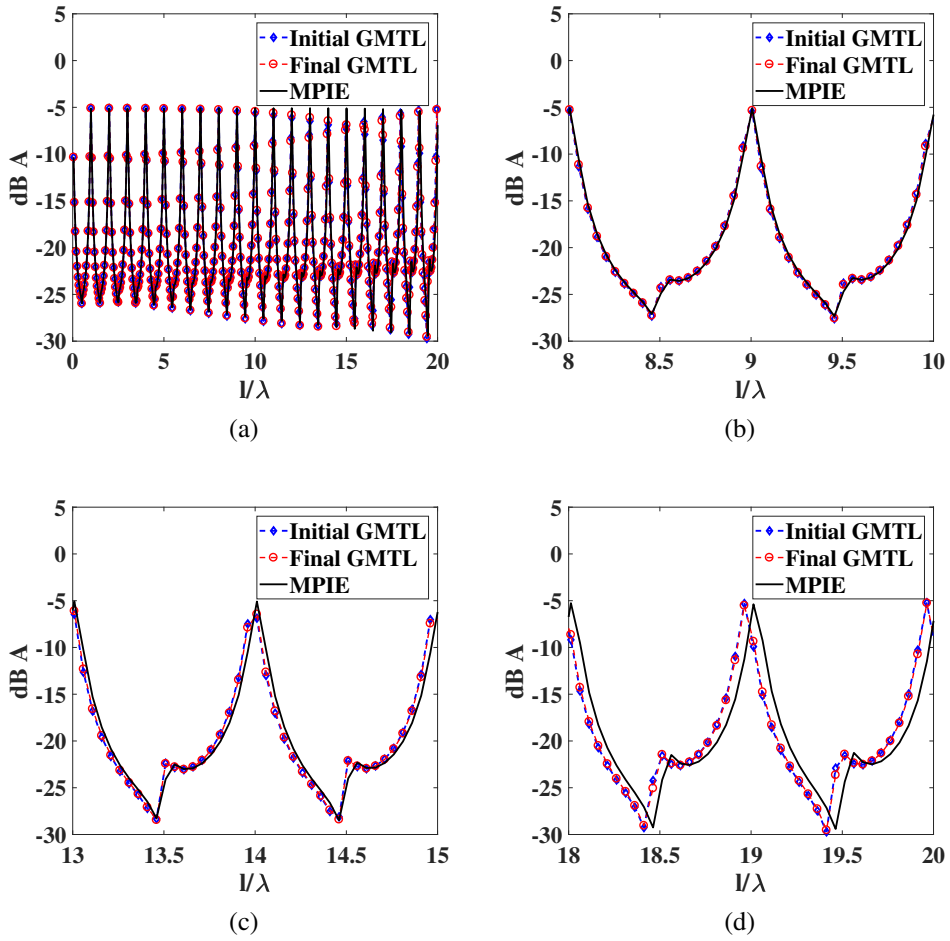


Figure 12. Current magnitude comparison at the center of Wire 1 for different ranges of $l/\lambda$: (a) $0 \leq l/\lambda \leq 20$, (b) $8 \leq l/\lambda \leq 10$, (c) $13 \leq l/\lambda \leq 15$, and (d) $18 \leq l/\lambda \leq 20$.

the GMTL is almost the same as the one obtained by the MPIE when $l/\lambda \leq 15$. When $l/\lambda > 15$, the shift of resonant frequencies can be obviously observed. Similar trend is found in TRP comparison as shown in Fig. 13. When $l/\lambda \leq 15$, the TRP of the GMTL is almost the same as the TRP of the MPIE. However, when $l/\lambda > 15$, the shift of resonant frequencies can be obviously observed. This shifting of resonant frequencies is due to the mesh size differing from the GMTL to the MPIE.

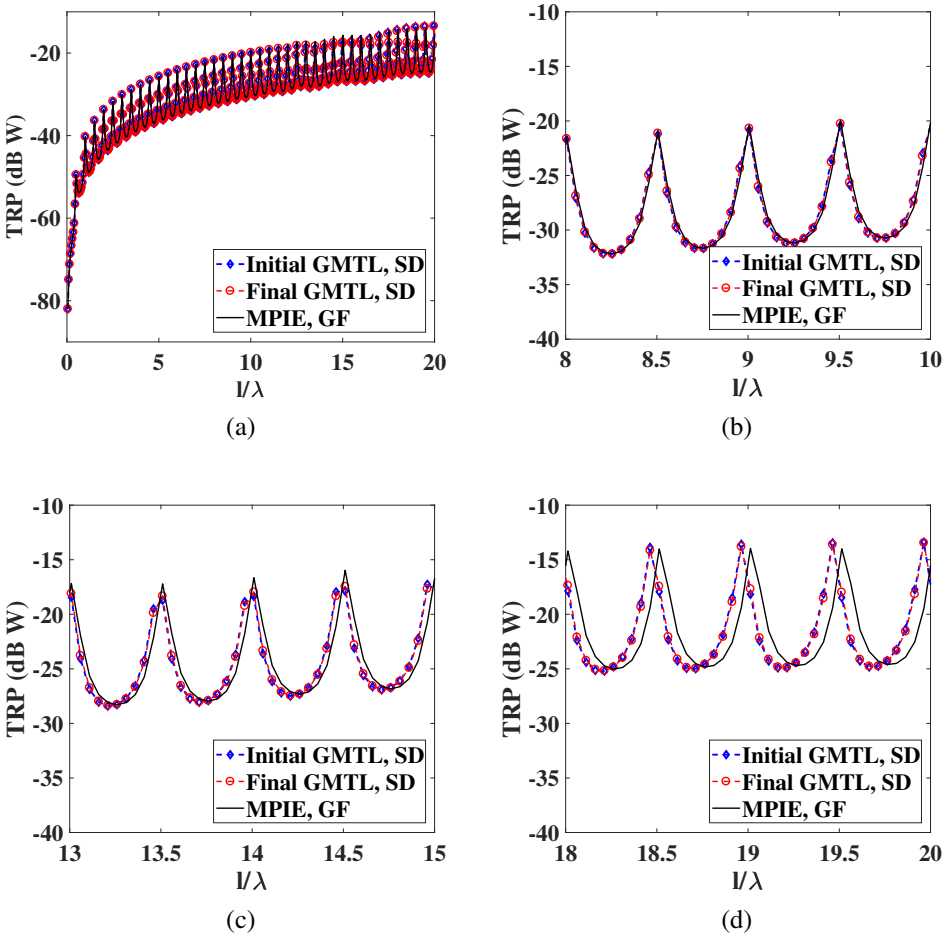


Figure 13. TRP comparison at the center of Wire 1 for different ranges of $l/\lambda$: (a) $0 \leq l/\lambda \leq 20$, (b) $8 \leq l/\lambda \leq 10$, (c) $13 \leq l/\lambda \leq 15$, and (d) $18 \leq l/\lambda \leq 20$.

From Fig. 12 and 13, it can be concluded that along with the increasing electrical wire length, the shifting of the resonant frequencies is becoming more and more severe. However, this is still acceptable within 15 wavelengths. Besides, comparing the final GMTL to the initial GMTL, the result improvement due to the recursive corrections is insignificant.

## 5. CONCLUSIONS

In this paper, a general formulation of the GMTL method is developed for an arbitrary cable harness. The cable harness can be straight or bent. Two analytical methods to extract the pul L and C are derived. Either set of the pul L and C can be used to build the GMTL equations, which produce similar currents. The GMTL equations are solved based on the perturbation theory. Accurate current distribution on a cable harness is obtained after one or two recursions.

Besides, the TRP of a cable harness with complex loading networks can be conveniently evaluated based on the SD method. To be able to apply the SD method, currents flowing on the cable harness are decomposed into the PG and the NG currents using the least-square method. Once the decomposition is achieved, the radiated field in the far field is only contributed by the decomposed currents at all discontinuity points. The SD method is more efficient than the GF method in terms of TRP calculation.

Last, the capability and limitations of the GMTL method are studied in terms of the electrical wire separation and length. It is found that the electrical wire separation doesn't limit the capability of the GMTL method, and that the GMTL method achieves accurate current and TRP as the electrical wire separation varies from 0 to 1. When it comes to the electrical wire length, the GMTL method generally works well. However, as the electrical wire length increases, the shifting of the resonant frequencies is becoming increasingly severe. From this perspective, the GMTL method is accurate up to a limited number of wavelengths. The necessity of the recursive corrections is also investigated. According to the study, recursive corrections are required in order to achieve accurate crosstalk current. However, if the TRP is the major concern, the obtained result is acceptable even if no recursive correction is added.

The GMTL is an extension of the traditional TL theory. Some limitations in the traditional TL theory may still be applicable in the GMTL approach. As is known, the TL theory fails at wire resonances if TLs are left open without terminations. This limitation is

also true for the GMTL approach. To resolve the issue, additional loss terms may be added either lumped at the ends of the wires [Middelstaedt et al., 2016] or distributed along the wires [Chabane et al., 2017]. The present formulation of the GMTL method is based on thin wire assumptions. For thick wire cases where non-uniform current distribution and proximity effects should be considered, the modal decomposition method [Jin, 2017, Jin et al., 2018] can be employed to extract pul $L$ and $C$.

## REFERENCES

I. Badzagua, H. Chobanyan, G. Chikovani, I. Oganezova, E. Yavolovskaya, T. Injgia, A. Gheonjian, and R. Jobava. Effective computational techniques for EMC analysis of cable harness. *Proceedings of the 2010 International Seminar/Workshop on Direct and Inverse Problems of Electromagnetic and Acoustic Wave Theory*, pages 96–102, Sep. 2010.

H. Bagci, A.E. Yilmaz, J. Jin, and E. Michielssen. Fast and rigorous analysis of EMC/EMI phenomena on electrically large and complex cable-loaded structures. *IEEE Trans. Electromagn. Compat.*, 49(2):361–381, May 2007.

Y. S. Cao, L. Jiang, and A. E. Ruehli. Distributive radiation and transfer characterization based on the PEEC method. *IEEE Trans. Electromagn. Compat.*, 57(4):734–742, Aug. 2015.

Y. S. Cao, Y. Wang, L. Jiang, A. E. Ruehli, J. Fan, and J. Drewniak. Quantifying EMI: a methodology for determining and quantifying radiating for practical design guidelines. *IEEE Trans. Electromag. Compat.*, 59(5):1424–1432, Oct. 2017.

S. Chabane, P. Besnier, and M. Klingler. A modified enhanced transmission line theory applied to multiconductor transmission lines. *IEEE Trans. Electromagn. Compat.*, 59(2):518–528, Apr. 2017.

A. G. Chiariello, A. Maffucci, G. Miano, F. Villone, and W. Zamboni. A transmission-line model for full-wave analysis of mixed-mode propagation. *IEEE Trans. Adv. Packag.*, 31(2):275–284, May 2008.

V. Cooray, F. Rachidi, and M. Rubinstein. Formulation of the field-to-transmission line coupling equations in terms of scalar and vector potentials. *IEEE Trans. Electromagn. Compat.*, (99):1–6.

EMCoS. EMC studio, version 8.2. *[Online]. Available: http://www.emcos.com*.

S. Jin. Modal based bga modeling in high-speed package. *Ph.D. dissertation, MST, Rolla, MO*, 2017.

S. Jin, D. Liu, Y. Wang, B. Chen, and J. Fan. Parallel plate impedance and equivalent inductance extraction considering proximity effect by a modal approach. *IEEE Trans. Electromagn. Compat.*, (99):1–10.

S. Jin, D. Liu, B. Chen, K. Qiu, J. Lin, R. Brooks, and J. Fan. Analytical equivalent circuit modeling for BGA in high-speed package. *IEEE Trans. Electromagn. Compat.*, 60 (1):68–76, Feb. 2018.

G. Li. Measurement-based modeling and worst-case estimation of crosstalk inside an aircraft cable connector. *IEEE Trans. Electromagn. Compat.*, 57(4):827–835, Aug. 2015.

J. Li and J. Fan. Radiation physics and design guidelines of high-speed connectors. *IEEE Trans. Electromagn. Compat.*, 58(4):1331–1338, Aug. 2016.

J. Li, Y. Zhang, D. Liu, A. Bhobe, J. L. Drewniak, and J. Fan. Radiation physics from two-wire transmission lines. *Proc. IEEE Symp. Electromagn. Compat. Signal Integrity*, pages 160–164, Mar. 2015.

D. Liu, Y. Wang, R. W. Kautz, N. Altunyurt, S. Chandra, and J. Fan. Accurate evaluation of field interactions between cable harness and vehicle body by a multiple scattering method. *IEEE Trans. Electromagn. Compat.*, 59(2):383–393, Apr. 2017.

G. Lugrin, S. V. Tkachenko, F. Rachidi, M. Rubinstein, and R. Cherkaoui. High-frequency electromagnetic coupling to multiconductor transmission lines of finite length. *IEEE Trans. Electromagn. Compat.*, 57(6):1714–1723, Dec. 2015.

A. Maffucci, G. Miano, and F. Villone. An enhanced transmission line model for conducting wires. *IEEE Trans. Electromagn. Compat.*, 46(4):512–528, Nov. 2004.

A. Maffucci, G. Miano, and F. Villone. An enhanced transmission line model for conductors with arbitrary cross sections. *IEEE Trans. Adv. Packag.*, 28(2):174–188, May 2005.

F. Middelstaedt, S. V. Tkachenko, R. Rambousky, and R. Vick. High-frequency electromagnetic field coupling to a long, finite wire with vertical risers above ground. *IEEE Trans. Electromagn. Compat.*, 58(4):1169–1175, Aug. 2016.

T. Nakamura, N. Hayashi, H. Fukuda, and S. Yokokawa. Radiation from the transmission line with an acute bend. *IEEE Trans. Electromagn. Compat.*, 37(3):317–325, Aug. 1995.

J. Nitsch, F. Gronwald, and G. Wollenberg. *Radiating Nonuniform Transmissionline Systems and the Partial Element Equivalent Circuit Method*. John Wiley & Sons, Ltd., 2009.

J. B. Nitsch and S. V. Tkachenko. High-frequency multiconductor transmission-line theory. *Found. Phys.*, 40(9):1231–1252, 2010.

J.B. Nitsch and S.V. Tkachenko. Complex-valued transmission-line parameters and their relation to the radiation resistance. *IEEE Trans. Electromagn. Compat.*, 46(3): 477–487, Aug. 2004.

C.R. Paul. *Analysis of Multiconductor Transmission Lines, 2nd ed*. Wiley-IEEE Press, 2007.

S. Sun, G. Liu, J. L. Drewniak, and D. J. Pommerenke. Hand-assembled cable bundle modeling for crosstalk and common-mode radiation prediction. *IEEE Trans. Electromagn. Compat.*, 49(3):708–718, Aug. 2007.

S.V. Tkatchenko, F. Rachidi, and M. Ianoz. Electromagnetic field coupling to a line of finite length: theory and fast iterative solutions in frequency and time domains. *IEEE Trans. Electromagn. Compat.*, 37(4):509–518, Nov. 1995.

A. Vukicevic, F. Rachidi, M. Rubinstein, and S. V. Tkachenko. On the evaluation of antenna-mode currents along transmission lines. *IEEE Trans. Electromagn. Compat.*, 48(4): 693–700, Nov. 2006.

Y. Wang, Y. S. Cao, D. Liu, R. W. Kautz, N. Altunyurt, and J. Fan. A generalized multiple-scattering (GMS) method for modeling a cable harness with ground connections to a nearby metal surface. *IEEE Trans. Electromagn. Compat.*, (99):1–10.

Y. Wang, R. Kautz, N. Altunyurt, and J. Fan. An equivalent circuit model for the wire-to-surface junction based on method of moments. *Proc. 2016 IEEE Int. Conf. Wireless Inf. Technol. Syst. Appl. Comput. Electromagn.*, pages 1–2, 2016.

Y. Wang, Y. S. Cao, D. Liu, R. W. Kautz, N. Altunyurt, and J. Fan. Applying the multiple scattering (MS) method to evaluate the current response on a cable harness due to an incident plane wave. *2018 IEEE International Conference on Computational Electromagnetics (ICCEM)*, pages 1–3, 2018a.

Y. Wang, D. Liu, Y. S. Cao, R. W. Kautz, N. Altunyurt, S. Chandra, and J. Fan. Evaluating field interactions between multiple wires and the nearby surface enabled by a generalized MTL approach. *IEEE Trans. Electromagn. Compat.*, 60(4):971–980, Aug. 2018b.

D. Zhang, Y. Wen, Y. Wang, D. Liu, X. He, and J. Fan. Coupling analysis for wires in a cable tray using circuit extraction based on mixed-potential integral equation formulation. *IEEE Trans. Electromagn. Compat.*, 59(3):862–872, June 2017.

# SECTION

# 2. SUMMARY AND CONCLUSIONS

In the first paper, co-simulation of a cable harness consisting of multiple wires and a nearby metal surface is carried out in two parts: the multiple wire part and the surface part. The multiple wire part is modeled by the GMTL approach and solved recursively. A test case demonstrates the accuracy of the recursive GMTL solver. The surface part is handled by the MPIE solver. To account for the mutual interactions between the multiple wires and the metal surface, the MS approach is employed. In the studied test case where four wires are set above a slotted surface, only three scatterings are required before all wire currents converge. And the converged currents match well with the reference results. These test cases validate the proposed recursive GMTL solver and the further MS approach for the co-simulation. Although not specically demonstrated, the MS approach can be applied to cases with more complicated surface structures, since the surface part is purely solved by a mature algorithm, the MoM. One major limitation of the MS method lies in that it can only be applied in cases where the cable harness is not grounded to the metal surface. This issue is resolved by the GMS method in the second paper.

In the second paper, co-simulation of a cable harness with ground connections to a nearby metal surface is conducted by the GMS method in two parts: the SP and the RP. The SP is solved by the GMTL solver, while the RP is handled by the MPIE solver. Neither the GMTL nor the MPIE solver alone takes into account the mutual interactions between the SP and the RP. To account for these interactions, an iterative scheme is arranged in the GMS method. Each iteration physically represents the scattering process of EM waves. The abovementioned interactions take place via not only field couplings, but also current conducting through the SP/RP junctions. In the studied test case where four wires are set

above a slotted surface and one of these wires is grounded to the metal surface through two grounding wires, only three iterations are required before the currents converge and the converged currents match well with the reference results. This test case validates the proposed GMS approach for the co-simulation. Although not specifically demonstrated, the GMS approach can be generally applied to cases with more complicated surface structures, since the RP is solved by a mature algorithm, the MoM. The MS and the GMS methods presented in the first and the second papers, respectively, share some common limitations, which essentially result from the GMTL method. To name a few, the cable harness has to be straight, an upper frequency limit exists for the GMTL method, and etc. Some of these limitations of the GMTL method are studied in the third paper.

In the third paper, a general formulation of the GMTL method is developed for an arbitrary cable harness. The cable harness can be straight or bent. Two analytical methods to extract the pul L and C are derived. Either set of the pul L and C can be used to build the GMTL equations, which produce similar currents. The GMTL equations are solved based on the perturbation theory. Accurate current distribution on a cable harness is obtained after one or two recursions. Besides, the TRP of a cable harness with complex loading networks can be conveniently evaluated based on the SD method. To be able to apply the SD method, currents flowing on the cable harness are decomposed into the PG and the NG currents using the least-square method. Once the decomposition is achieved, the radiated field in the far field is only contributed by the decomposed currents at all discontinuity points. The SD method is more efficient than the GF method in terms of TRP calculation. Last, the capability and limitations of the GMTL method are studied in terms of the electrical wire separation and length. It is found that the electrical wire separation doesn't limit the capability of the GMTL method, and that the GMTL method achieves accurate current and TRP as the electrical wire separation varies from 0 to 1. When it comes to the electrical wire length, the GMTL method generally works well. However, as the electrical wire length increases, the shifting of the resonant frequencies is becoming increasingly severe. From

this perspective, the GMTL method is accurate up to a limited number of wavelengths. The necessity of the recursive corrections is also investigated. According to the study, recursive corrections are required in order to achieve accurate crosstalk current. However, if the TRP is the major concern, the obtained result is acceptable even if no recursive correction is added.

Some work is to be continued in the future to make the GMTL method more and more powerful. First, efforts are needed to resolve the misconvergence issue at natural resonant frequencies of wires. The natural resonant frequencies of wires indicate the frequencies where the wire length is multiple integers of half the corresponding wavelength. The GMTL method is an extension of the traditional TL theory. Some limitation in the traditional TL theory is still applicable in the GMTL approach. One of the limitations is that the TL theory fails at wire natural resonant frequencies if TLs are left open without terminations. This is true for the GMTL method. Since the antenna mode current is included in the GMTL method and no physical terminations can be added between the wires and the infinity, the GMTL method fails at wire natural resonant frequencies. This issue may be resolved by adding addiational loss terms either lumpedly at the ends of the wires [Middelstaedt et al., 2016] or distributedly along the wires [Chabane et al., 2017]. Second, the GMTL method can be extended for thick wire cases where non-uniform current distribution around the wire surface and proximity effects should be considered, the modal decomposition method [Jin, 2017, Jin et al., 2018] can be employed to extract pul $L$ and $C$. Third, stochastic analysis [Wang et al., 2014, 2015, 2016b, 2017a] may be applied in the GMTL formulation to facilitate the statistical study of the cable harness.

# REFERENCES

IEEE standard for validation of computational electromagnetics computer modeling and simulations. *IEEE Std 1597.1-2008*, pages c1–41, 2008.

A. K. Agrawal, H. J. Price, and S. H. Gurbaxani. Transient response of multiconductor transmission lines excited by a nonuniform electromagnetic field. *IEEE Trans. Electromagn. Compat.*, EMC-22(2):119–129, May 1980.

I. Badzagua, H. Chobanyan, G. Chikovani, I. Oganezova, E. Yavolovskaya, T. Injgia, A. Gheonjian, and R. Jobava. Effective computational techniques for EMC analysis of cable harness. *Proceedings of the 2010 International Seminar/Workshop on Direct and Inverse Problems of Electromagnetic and Acoustic Wave Theory*, pages 96–102, Sep. 2010.

H. Bagci, A.E. Yilmaz, J. Jin, and E. Michielssen. Fast and rigorous analysis of EMC/EMI phenomena on electrically large and complex cable-loaded structures. *IEEE Trans. Electromagn. Compat.*, 49(2):361–381, May 2007.

Y. Bayram and J. L. Volakis. A generalized MoM-SPICE iterative technique for field coupling to multiconductor transmission lines in presence of complex structures. *IEEE Trans. Electromagn. Compat.*, 47(2):234–246, May 2005.

Y. S. Cao, L. Jiang, and A. E. Ruehli. Distributive radiation characterization based on the PEEC method. *IEEE International Symposium on APS/URSI*, Jul. 2014.

Y. S. Cao, L. Jiang, and A. E. Ruehli. Electromagnetic characterization for graphene by the PEEC method. *IEEE International Symposium on APS/USNC-URSI*, Jul. 2015a.

Y. S. Cao, L. Jiang, and A. E. Ruehli. Physical interpretation of radiation and transfer characterization based on PEEC method. *IEEE Int. Symposium on Electromagnetic Compatibility*, Mar. 2015b.

Y. S. Cao, L. Jiang, and A. E. Ruehli. Distributive radiation and transfer characterization based on the PEEC method. *IEEE Trans. Electromagn. Compat.*, 57(4):734–742, Aug. 2015c.

Y. S. Cao, L. Jiang, and A. E. Ruehli. An equivalent circuit model for graphene-based terahertz antenna using the PEEC method. *IEEE Trans. Antenna Propag.*, 64(4): 1385–1393, Apr. 2016a.

Y. S. Cao, L. Jiang, and A. E. Ruehli. The equivalent circuit model for non-magnetized and magnetized graphene. *IEEE International Conference on ICWITS-ACES*, Mar. 2016b.

Y. S. Cao, L. Jiang, and A. E. Ruehli. The equivalent circuit model for electrostatic and magnetostatic biased tunable graphene as the absorption material. *The 7-th Asia-Pacific International EMC Symposium*, May 2016c.

Y. S. Cao, L. Jiang, and A. E. Ruehli. The equivalent circuit extraction and application for arbitrary shape graphene sheet. *ACES Express Journal*, 1(5):157–160, May 2016d.

Y. S. Cao, L. Jiang, and A. E. Ruehli. Characteristic analysis for optical antennas: a generalized equivalent circuit model for nanoparticles. *IEEE International Symposium on APS/USNC-URSI National Radio Science meeting*, Jun. 2016e.

Y. S. Cao, L. Jiang, A. E. Ruehli, J. Fan, and J. L. Drewniak. New detailed understanding of the mechanism of radiation in interconnect problems. *25th Conference on EPEPS*, Oct. 2016f.

Y. S. Cao, L. Jiang, A. E. Ruehli, Jun Fan, and James. L. Drewniak. Radiation compatible ports and loads for the *PEEC* method. *25th Conference on EPEPS*, Oct. 2016g.

Y. S. Cao, T. Makharashvili, S. Connor, B. Archambeault, L. J. Jiang, A. E. Ruehli, J. Fan, and J. L. Drewniak. Top-layer interconnect inductance extraction for the pre-layout power integrity using the physics-based model size reduction (PMSR) method. *IEEE Int. Symposium on Electromagnetic Compatibility*, Jul. 2016h.

Y. S. Cao, Y. Wang, L. Jiang, A. E. Ruehli, J. L. Drewniak, and J. Fan. Characterizing EMI radiation physics corresponding to distributive geometry features using PEEC method. *IEEE Int. Symposium on Electromagnetic Compatibility*, Jul. 2016i.

Y. S. Cao, P. Li, L. Jiang, and A. E. Ruehli. The derived equivalent circuit model for magnetized anisotropic graphene. *IEEE Trans. Antenna Propag.*, 65(2):948–953, Feb 2017a.

Y. S. Cao, T. Makharashvili, S. Connor, B. Archambeault, L. J. Jiang, A. E. Ruehli, J. Fan, and J. L. Drewniak. Top-layer interconnect inductance extraction for the pre-layout power integrity. *IEEE Trans. Electromag. Compat.*, 59(4):1339–1346, Aug. 2017b.

Y. S. Cao, X. Wang, W. Mai, Y. Wang, L. Jiang, A. Ruehli, S. He, H. Zhao, J. Hu, J. Fan, and J. Drewniak. Characterizing EMI radiation physics for edge and broad-side coupled connectors. *IEEE Int. Symposium on Electromagnetic Compatibility*, Aug. 2017c.

Y. S. Cao, Y. Wang, L. Jiang, A. E. Ruehli, J. Fan, and J. Drewniak. Quantifying EMI: a methodology for determining and quantifying radiating for practical design guidelines. *IEEE Trans. Electromag. Compat.*, 59(5):1424–1432, Oct. 2017d.

Y. S. Cao, M. Ouyang, Y. Wang, and J. Fan. EMI modeling for a vehicle body using characteristic mode analysis. *Proc. IEEE Symp. Electromagn. Compat. Signal Integrity, 2018*, Aug. 2018a.

Y. S. Cao, Y. Wang, S. Wu, Z. Yang, and J. Fan. EMI edge shielding effectiveness evaluation and design guidelines. *Proc. IEEE Symp. Electromagn. Compat. Signal Integrity, 2018*, Aug. 2018b.

Y.S. Cao and et al. EMI radiation physics using generalized characteristic mode (GCM) analysis with loss for practical structures. *2017 IEEE 26th Conference on Electrical Performance of Electronic Packaging and Systems (EPEPS)*, pages 1–3, 2017.

S. Chabane, P. Besnier, and M. Klingler. A modified enhanced transmission line theory applied to multiconductor transmission lines. *IEEE Trans. Electromagn. Compat.*, 59(2):518–528, Apr. 2017.

Cheever. All of cheever's MNA pages condensed into one. *[Online]: http://www.swarthmore.edu/NatSci/echeeve1/Ref/mna/MNA_All.html*.

B. Chen, M. Ouyang, S. Yong, Y. Wang, and et al. Differential integrated crosstalk noise (ICN) reduction among multiple differential BGA and via pairs by using design of experiments (DoE) method. *Proc. IEEE Int. Symp. Electromagn. Compat. Signal Integrity (EMCSI), 2017*, pages 112–117, Jul. 2017.

B. Chen, J. Wang, Y. S. Cao, M. Ouyang, Y. Wang, S. Jin, X. Liu, X. Peng, and J. Fan. Differential integrated crosstalk noise (ICN) mitigation in the pin field area of serdes channel. *Proc. IEEE Symp. Electromagn. Compat. Signal Integrity, 2018*, Aug. 2018.

A. G. Chiariello, A. Maffucci, G. Miano, F. Villone, and W. Zamboni. A transmission-line model for full-wave analysis of mixed-mode propagation. *IEEE Trans. Adv. Packag.*, 31(2):275–284, May 2008.

H. Chobanyan, I. Badzagua, T. Injgia, A. Gheonjian, and R. Jobava. Application of hybrid MOM/MTL method to simulation of interaction between cable harness and antennas. *Proceedings of the 2009 International Seminar/Workshop on Direct and Inverse Problems of Electromagnetic and Acoustic Wave Theory*, pages 33–38, Sep. 2009.

V. Cooray, F. Rachidi, and M. Rubinstein. Formulation of the field-to-transmission line coupling equations in terms of scalar and vector potentials. *IEEE Trans. Electromagn. Compat.*, (99):1–6.

A.P. Duffy, A.J.M. Martin, A. Orlandi, G. Antonini, T.M. Benson, and M.S. Woolfson. Feature selective validation (FSV) for validation of computational electromagnetics (CEM). part i - the FSV method. *IEEE Trans. Electromagn. Compat.*, 48(3):449–459, Aug. 2006.

EMCoS. EMC studio, version 8.2. *[Online]. Available: http://www.emcos.com*.

J. Fan, H. Shi, A. Orlandi, J. L. Knighten, and J. L. Drewniak. Modeling DC power-bus structures with vertical discontinuities using a circuit extraction approach based on a mixed-potential integral equation formulation. *IEEE Trans. Adv. Packag.*, 24(2): 143–157, May 2001.

J. Fan, J. L. Drewniak, and J. L. Knighten. Lumped-circuit model extraction for vias in multilayer substrates. *IEEE Trans. Electromagn. Compat.*, 45(2):272–280, May 2003.

Y. Han, Z. Yan, Y. Wang, and T. Rahman. A novel EBG structure with embedded meander bridge for broadband suppression of SSN. *Proc. IEEE Asia-Pacific Symp. Electromagn. Compat., 2012*, 2012.

K. Hardin, Ying S. Cao, A. Hosseinbeig, B. Zhao, Nana Dikhaminjia, Zach Kratzer, John Fessler, and James Drewniak. Z-directed component (zdc) technology for power integrity applications. *IEEE Trans. Electromag. Compat.*, (PP):1–9.

C. Huang, B. Zhao, K. Shringarpure, S. Bai, X. Fang, T. Makharashvili, H. Ye, Y. S. Cao, M. Cracraft, M. Cocchini, S. Connor, S. Scearce, B. Archambeault, B. Achkir, E. Li, L. Jiang, A. Ruehli, J. Fan, and J. Drewniak. Power integrity with voltage ripple spectrum decomposition for physics-based design. *IEEE Int. Symposium on Electromagnetic Compatibility*, Jul. 2016.

Q. Huang and et al. Mom-based ground current reconstruction in rfi application. *IEEE Trans. Electromagn. Compat.*, 60(4):1121–1128, Aug. 2018a.

Q. Huang and et al. Desense prediction and mitigation from DDR noise source. *Proc. IEEE Symp. Electromagn. Compat. Signal Integrity, 2018*, Aug. 2018b.

Q. Huang and J. Fan. Machine learning based source reconstruction for RF desense. *IEEE Trans. Electromagn. Compat.*, PP(99).

Q. Huang, L. Li, X. Yan, B. Bae, H. Park, C. Hwang, and J. Fan. MoM based current reconstruction using near-field scanning. *Proc. IEEE Int. Symp. Electromagn. Compat. Signal Integrity (EMCSI), 2017*, pages 549–554, Jul. 2017a.

Q. Huang, F. Zhang, T. Enomoto, J. Maeshima, K. Araki, and C. Hwang. Physics-based dipole moment source reconstruction for RFI on a practical cellphone. *IEEE Trans. Electromagn. Compat.*, 59(6):1693–1700, Dec. 2017b.

Q. Huang, Y. Liu, L. Li, Y. Wang, C. Wu, and J. Fan. Radio frequency interference estimation using transfer function based dipole moment model. *Proc. IEEE Asia-Pacific Int. Symp. Electromagn. Compat., 2018*, May 2018.

C. Hwang and Q. Huang. IC placement optimization for RF interference based on dipole moment sources and reciprocity. *Proc. IEEE Asia-Pacific Symp. Electromagn. Compat., 2017*, pages 331–333, 2017.

L. Jiang, H. H. Zhang, Y. S. Cao, and P. Li. Nonlinear I/O characterization with the time domain electromagnetic simulations. *IEEE International Conference on ICWITS-ACES*, Mar. 2016.

S. Jin. Modal based bga modeling in high-speed package. *Ph.D. dissertation, MST, Rolla, MO*, 2017.

S. Jin, D. Liu, Y. Wang, B. Chen, and J. Fan. Parallel plate impedance and equivalent inductance extraction considering proximity effect by a modal approach. *IEEE Trans. Electromagn. Compat.*, (99):1–10.

S. Jin, Y. Zhang, Y. Zhou, Y. Bai, X. Yu, and J. Fan. Conducted-emission modeling for a high-speed ecl clock buffer. *Proc. IEEE Int. Symp. Electromagn. Compat,. 2014*, pages 594–599, Aug. 2014.

S. Jin, J. Zhang, J. Lim, K. Qiu, R. Brooks, and J. Fan. Analytical equivalent circuit modeling for multiple core vias in a high-speed package. *Proc. IEEE Int. Symp. Electromagn. Compat. 2016*, pages 233–238, Jul. 2016.

S. Jin, D. Liu, B. Chen, K. Qiu, J. Lin, R. Brooks, and J. Fan. Analytical equivalent circuit modeling for BGA in high-speed package. *IEEE Trans. Electromagn. Compat.*, 60 (1):68–76, Feb. 2018.

G. Li. Measurement-based modeling and worst-case estimation of crosstalk inside an aircraft cable connector. *IEEE Trans. Electromagn. Compat.*, 57(4):827–835, Aug. 2015.

J. Li and J. Fan. Radiation physics and design guidelines of high-speed connectors. *IEEE Trans. Electromagn. Compat.*, 58(4):1331–1338, Aug. 2016.

J. Li, Y. Zhang, D. Liu, A. Bhobe, J. L. Drewniak, and J. Fan. Radiation physics from two-wire transmission lines. *Proc. IEEE Symp. Electromagn. Compat. Signal Integrity*, pages 160–164, Mar. 2015.

D. Liu. Common mode current estimation for cable bundle inside a vehicle. *Ph.D. dissertation, MST, Rolla, MO*, 2013.

D. Liu, Y. Wang, R. W. Kautz, N. Altunyurt, S. Chandra, and J. Fan. Accurate evaluation of field interactions between cable harness and vehicle body by a multiple scattering method. *IEEE Trans. Electromagn. Compat.*, 59(2):383–393, Apr. 2017.

G. Lugrin, S. V. Tkachenko, F. Rachidi, M. Rubinstein, and R. Cherkaoui. High-frequency electromagnetic coupling to multiconductor transmission lines of finite length. *IEEE Trans. Electromagn. Compat.*, 57(6):1714–1723, Dec. 2015.

A. Maffucci, G. Miano, and F. Villone. An enhanced transmission line model for conducting wires. *IEEE Trans. Electromagn. Compat.*, 46(4):512–528, Nov. 2004.

A. Maffucci, G. Miano, and F. Villone. An enhanced transmission line model for conductors with arbitrary cross sections. *IEEE Trans. Adv. Packag.*, 28(2):174–188, May 2005.

G. Maghlakelidze, X. Yan, L. Guan, S. Marathe, Q. Huang, B. Bae, C. Hwang, V. Khilkevich, J. Fan, and D. Pommerenke. SNR analysis and optimization in near-field scanning and EMI applications. *IEEE Trans. Electromagn. Compat.*, 60(4):1087–1094, Aug. 2018.

L. Mandache and D. Topan. New treatment of the multiple mutually coupled inductors to improve the modified nodal analysis in harmonic regime. *51st Internationales Wissenschaftliches Kolloquium*, Sep. 2006.

F. Middelstaedt, S. V. Tkachenko, R. Rambousky, and R. Vick. High-frequency electromagnetic field coupling to a long, finite wire with vertical risers above ground. *IEEE Trans. Electromagn. Compat.*, 58(4):1169–1175, Aug. 2016.

T. Nakamura, N. Hayashi, H. Fukuda, and S. Yokokawa. Radiation from the transmission line with an acute bend. *IEEE Trans. Electromagn. Compat.*, 37(3):317–325, Aug. 1995.

J. Nitsch, F. Gronwald, and G. Wollenberg. *Radiating Nonuniform Transmissionline Systems and the Partial Element Equivalent Circuit Method*. John Wiley & Sons, Ltd., 2009.

J. B. Nitsch and S. V. Tkachenko. High-frequency multiconductor transmission-line theory. *Found. Phys.*, 40(9):1231–1252, 2010.

J.B. Nitsch and S.V. Tkachenko. Complex-valued transmission-line parameters and their relation to the radiation resistance. *IEEE Trans. Electromagn. Compat.*, 46(3): 477–487, Aug. 2004.

I. Oganezova, G. Shen, S. Yang, D. Pommerenke, V. Khilkevich, and R. Jobava. Simulation of ESD coupling into cables based on ISO 10605 standard using method of moments. *Proc. IEEE Int. Symp. Electromagn. Compat., 2016*, pages 701–706, Jul. 2016.

A. Orlandi, A.P. Duffy, B. Archambeault, G. Antonini, D.E. Coleby, and S. Connor. Feature selective validation (FSV) for validation of computational electromagnetics (CEM). part ii - assessment of FSV performance. *IEEE Trans. Electromagn. Compat.*, 48 (3):460–467, Aug. 2006.

A. Patnaik and et al. Source isolation measurements in a multi-source coupled system. *Proc. IEEE Int. Symp. Electromagn. Compat. Signal Integrity (EMCSI), 2017*, pages 75–80, Jul. 2017.

C.R. Paul. *Analysis of Multiconductor Transmission Lines, 2nd ed*. Wiley-IEEE Press, 2007.

F. Rachidi. Formulation of the field-to-transmission line coupling equations in terms of magnetic excitation fields. *IEEE Trans. Electromagn. Compat.*, 35(3):404–407, Aug. 1993.

F. Sabath and H. Garbe. Radiation analysis of PCB layout using a hybrid mom-mtl method. *IEEE Trans. Electromagn. Compat.*, 45(2):424–435, May 2003.

G. Shen and et al. Terminal modeling of DC–DC converters with stochastic behavior. *IEEE Trans. Electromagn. Compat.*, PP(99):1–8.

G. Shen, V. V. Khilkevich, D. J. Pommerenke, H. L. Aichele, D. Eichel, and C. Keller. Simple D flip-flop behavioral model of ESD immunity for use in the ISO 10605 standard. *Proc. IEEE Int. Symp. Electromagn. Compat., 2014*, pages 455–459, Aug. 2014.

G. Shen, V. V. Khilkevich, D. J. Pommerenke, H. L. Aichele, D. Eichel, and C. Keller. ESD immunity prediction of D flip-flop in the ISO 10605 standard using a behavioral modeling methodology. *IEEE Trans. Electromagn. Compat.*, 57(4):651–659, Aug. 2015.

G. Shen, V. V. Khilkevich, D. J. Pommerenke, H. L. Aichele, and C. Keller. Terminal model application for characterizing conducted EMI in boost converter system. *Proc. IEEE Int. Symp. Electromagn. Compat., 2016*, pages 576–581, Jul. 2016a.

G. Shen, Q. Liu, V. V. Khilkevich, D. J. Pommerenke, P. Dixon, and Y. Arien. EMI control performance of the absorbing material for application on flexible cables. *Proc. IEEE Int. Symp. Electromagn. Compat., 2016*, pages 30–35, Jul. 2016b.

G. Shen, S. Yang, J. Sun, S. Xu, D. J. Pommerenke, and V. V. Khilkevich. Maximum radiated emissions evaluation for the heatsink/IC structure using the measured near electrical field. *IEEE Trans. Electromagn. Compat.*, 59(5):1408–1414, Oct. 2017a.

P. Shen, Y. Qi, J. Fan, and Y. Wang. The advantages of the RTS method in MIMO OTA measurements. *Proc. IEEE Int. Symp. Electromagn. Compat. Signal Integrity (EMCSI), 2017*, pages 470–473, Jul. 2017b.

S. Shinde and et al. Radiated EMI estimation from DC–DC converters with attached cables based on terminal equivalent circuit modeling. *IEEE Trans. Electromagn. Compat.*, PP(99):1–8.

S. Sun, G. Liu, J. L. Drewniak, and D. J. Pommerenke. Hand-assembled cable bundle modeling for crosstalk and common-mode radiation prediction. *IEEE Trans. Electromagn. Compat.*, 49(3):708–718, Aug. 2007.

EM Software & Systems. FEKO.

T. Tao, H. Ma, C. Huang, Y. S. Cao, J. Drewniak, and E. Li. 'dog-bone' geometry modeling based on peec for package pdn. *IEEE EDAPS Symposium*, Dec. 2017.

C. Taylor, R. Satterwhite, and C. Harrison Jr. The response of a terminated two-wire transmission line excited by a nonuniform electromagnetic field. *IEEE Trans. Antennas Propag.*, 13(6):987–989, Nov. 1965.

Computer Simulation Technology. CST CABLE STUDIO, 2017. *[Online]. Available: http://www.cst.com*.

S.V. Tkatchenko, F. Rachidi, and M. Ianoz. Electromagnetic field coupling to a line of finite length: theory and fast iterative solutions in frequency and time domains. *IEEE Trans. Electromagn. Compat.*, 37(4):509–518, Nov. 1995.

D. Topchishvili, R. Jobava, F. Bogdanov, B. Chikhradze, and S. Frei. A hybrid MTL/MoM approach for investigation of radiation problems in EMC. *Proceedings of the 9th International Seminar/Workshop on Direct and Inverse Problems of Electromagnetic and Acoustic Wave Theory*, pages 65–68, Oct. 2004.

A. Vukicevic, F. Rachidi, M. Rubinstein, and S. V. Tkachenko. On the evaluation of antenna-mode currents along transmission lines. *IEEE Trans. Electromagn. Compat.*, 48(4): 693–700, Nov. 2006.

Y. Wang and et al. Conducted-emission modeling for a switched-mode power supply (SMPS). *Proc. IEEE Symp. Electromagn. Compat. Signal Integrity, 2015*, pages 314–319, Mar. 2015.

Y. Wang, Y. S. Cao, D. Liu, R. W. Kautz, N. Altunyurt, and J. Fan. A generalized multiple-scattering method for modeling a cable harness with ground connections to a nearby metal surface. *IEEE Trans. Electromagn. Compat.*, (99):1–10.

Y. Wang, A. Razmadze, T. Lu, Y. Zhang, J. Chen, and J. Fan. Stochastic modeling of a high-speed signal channel by polynomial chaos method. *Proc. IEEE Int. Symp. Electromagn. Compat,. 2014*, pages 686–690, Aug. 2014.

Y. Wang, S. Penugonda, Y. Zhang, J. Chen, and J. Fan. Studying the effect of drilling uncertainty on signal propagation through vias. *Proc. IEEE Symp. Electromagn. Compat. Signal Integrity, 2015*, pages 365–369, Mar. 2015.

Y. Wang, R. Kautz, N. Altunyurt, and J. Fan. An equivalent circuit model for the wire-to-surface junction based on method of moments. *Proc. 2016 IEEE Int. Conf. Wireless Inf. Technol. Syst. Appl. Comput. Electromagn.*, pages 1–2, 2016a.

Y. Wang, S. Penugonda, S. Jin, J. Chen, and J. Fan. Variability analysis of crosstalk among pairs of differential vias using polynomial-chaos and design of experiments methods. *Proc. IEEE Int. Symp. Electromagn. Compat. 2016*, pages 222–227, Jul. 2016b.

Y. Wang, S. Jin, S. Penugonda, J. Chen, and J. Fan. Variability analysis of crosstalk among differential vias using polynomial-chaos and response surface methods. *IEEE Trans. Electromagn. Compat.*, 59(4):1368–1378, Aug. 2017a.

Y. Wang, S. Wu, Z. Yang, P. Shen, and J. Fan. Studying the effects of location offset on the evaluation of MIMO performance based on the radiated two-stage (RTS) method. *Proc. IEEE Int. Symp. Electromagn. Compat. Signal Integrity (EMCSI), 2017*, pages 464–469, Jul. 2017b.

Y. Wang, Y. S. Cao, D. Liu, R. W. Kautz, N. Altunyurt, and J. Fan. Applying the multiple scattering (MS) method to evaluate the current response on a cable harness due to an incident plane wave. *2018 IEEE International Conference on Computational Electromagnetics (ICCEM)*, pages 1–3, 2018a.

Y. Wang, D. Liu, Y. S. Cao, R. W. Kautz, N. Altunyurt, S. Chandra, and J. Fan. Evaluating field interactions between multiple wires and the nearby surface enabled by a generalized MTL approach. *IEEE Trans. Electromagn. Compat.*, 60(4):971–980, Aug. 2018b.

Y. Wang, S. Wu, Z. Yang, S. Jin, Y. S. Cao, J. Zhang, and J. Fan. Correcting antenna pattern in offset measurements based on equivalent dipole moments. *Proc. IEEE Symp. Electromagn. Compat. Signal Integrity, 2018*, Aug. 2018c.

Y. Wang, S. Wu, Z. Yang, P. Shen, C. Wu, and J. Fan. MIMO performance diagnosis based on the radiated two-stage (RTS) method. *Proc. IEEE Symp. Electromagn. Compat. Signal Integrity, 2018*, Aug. 2018d.

Y. Wang, S. Wu, J. Zhang, Z. Yang, K. Wu, and J. Fan. A simulation-based coupling path characterization to facilitate desense design and debugging. *Proc. IEEE Symp. Electromagn. Compat. Signal Integrity, 2018*, Aug. 2018e.

C. Wu, Y. Wang, L. Li, J. Pan, L. Qu, J. Eriksson, and J. Fan. Estimating the near field coupling from SMPS circuits to a nearby antenna using dipole moments. *Proc. IEEE Int. Symp. Electromagn. Compat., 2016*, pages 353–357, Jul. 2016.

J. Xu, Y. Wang, and et al. A survey on modeling strategies for high-speed differential via between two parallel plates. *Proc. IEEE Int. Symp. Electromagn. Compat. Signal Integrity (EMCSI), 2017*, pages 527–531, Jul. 2017.

X. Yan, Y. Wang, J. Zhou, and J. Fan. A 20 GHz landing probe design based on pogo-pins. *Proc. IEEE Symp. Electromagn. Compat. Signal Integrity, 2018*, Aug. 2018.

Z. Yan, Y. Xiong, W. Yu, and Y. Wang. An improved miniaturized three-layer embedded electromagnetic bandgap structure. *IEEE Trans. Antennas Propag.*, 62(5):2832–2837, May 2014.

Z. Yan, J. Wang, W. Zhang, Y. Wang, and J. Fan. A simple miniature ultrawideband magnetic field probe design for magnetic near-field measurements. *IEEE Trans. Antennas Propag.*, 64(12):5459–5465, Dec. 2016.

Z. Yan, J. Wang, W. Zhang, Y. Wang, and J. Fan. A miniature ultrawideband electric field probe based on coax-thru-hole via array for near-field measurement. *IEEE Trans. Instrum. Meas.*, 66(10):2762–2770, Oct. 2017.

S. Yang, Y. S. Cao, H. Ma, J. Cho, A. Ruehli, J. Drewniak, and E. Li. Pcb pdn pre-layout library for top-layer inductance and the equivalent model for decoupling capacitors. *IEEE Trans. Electromag. Compat.*, PP(99), Nov. 2017a.

S. Yang, E. Li, Y. S. Cao, H. Ma, J. Cho, A. Ruehli, and J. Drewniak. The efficient equivalent model for decoupling capacitors of power distribution network. *IEEE EDAPS Symposium*, Dec. 2017b.

D. Zhang, Y. Wen, Y. Wang, D. Liu, X. He, and J. Fan. Coupling analysis for wires in a cable tray using circuit extraction based on mixed-potential integral equation formulation. *IEEE Trans. Electromagn. Compat.*, 59(3):862–872, June 2017a.

Y. Zhang, Y. Wang, and et al. Estimating the via-plane capacitance for differential vias with shared-antipad based on analytical equations. *Proc. IEEE Int. Symp. Electromagn. Compat. Signal Integrity (EMCSI), 2017*, pages 272–276, Jul. 2017b.

B. Zhao, C. Huang, K. Shringarpure, S. Bai, T. Makharashvili, Y. S. Cao, B. Achkir, M. Cracraft, M. Cocchini, S. Connor, B. Archambeault, L. Jiang, A. Ruehli, J. Fan, and J. L. Drewniak. Transient simulation for power integrity using physics based circuit modeling. *The 7-th Asia-Pacific International EMC Symposium*, May 2016.

B. Zhao, A. Hosseinbeig, N. Dikhaminjia, Y. S. Cao, K. Hardin, Z. Kratzer, J. Fessler, and J. Drewniak. A novel z-directed embedded component for the reduction of voltage ripple on the power distribution network for pcbs. *IEEE Electromagn. Compat. Mag.*, 6(3):91–97, Third Quarter 2017a.

B. Zhao, A. Hosseinbeig, N. Dikhaminjia, Y. S. Cao, K. Hardin, Z. Kratzer, J. Fessler, and J. Drewniak. A novel z-directed embedded component for the reduction of voltage ripple on the power distribution network for pcbs. *Proc. IEEE Int. Symp. Electromagn. Compat. Signal Integrity (EMCSI), 2017*, pages 225–230, Jul. 2017b.

# VITA

Yansheng Wang was born in Henan Province, China. He received the Bachelor of Engineering in Electronic and Information Engineering from Beihang University, Beijing, China in July 2012. He received the Ph.D. degree in Electrical Engineering from Missouri University of Science and Techonology in May 2018.

In August 2012, he started the Ph.D. program at the Electrical Engineering Department of Missouri University of Science and Technology. There, he joined the Electromagnetic Compatibility (EMC) research group. His research interests included radiation and immunity characterization for cable harnesses inside a vehicle shell, method of moments (MoM), multiple-input–multiple-output (MIMO) over-the-air (OTA) testing, source reconstruction based on near-field or far-field patterns, desense measurement and simulation, radio-frequency interference (RFI), broadband E-/H-field probe design, conducted emission modeling, radiated source modeling, stochastic modeling for high-speed channels, and generic model development for PCIe3/4.